UNIVERSITY OF SOUTHAMPTON

FACULTY OF ENGINEERING AND THE ENVIRONMENT

Engineering Sciences

Efficient Human Force Transmission

Tailoring chainrings to a specific cyclist

by

Alexander Purdue

Thesis for the degree of Master of Philosophy

June 2015

UNIVERSITY OF SOUTHAMPTON

ABSTRACT

FACULTY OF ENGINEERING AND THE ENVIRONMENT

Engineering Sciences

Master of Philosophy

EFFICIENT HUMAN FORCE TRANSMISSION

By
Alexander Iain Purdue

The bicycle chainring is extremely efficient (~98%; Spicer et al. (2001)) although the rider interface is subject to noticeable losses. These losses are partly due to the "one size fits all" nature of the circular chainring. A brief visual study of any group of competitive cyclists will show variations in technique and motion, combined with the inherent inter subject variability with relation to muscle make up and activation, this would suggest the ability to maximise the output from any one rider is likely to be held back in some respect. Creating a chainring specifically tailored to a rider could improve efficiency and increase output for a given level of effort. Analysis and modification of the chainring shape has appeared before in the literature, though the analysis and modification was purely theoretical, and any other chainring shape analysis has used non rider specific non-circular chainrings.

Experimental torque data for varying power and cadence is collected, for a competitive cyclist, using a stationary bicycle fitted with instrumented cranks mounted on a trainer, which enables power output to be controlled at varying cadences. Experimental data from the instrumented cranks shows the torque profiles to be asymmetric in nature. This indicates that calibration of the model using experimental data must be carried out. The data also shows a large dependency on the cadence for the "purity" of the torque profile with smoother profiles being produced closer to the optimum cadence. Motion capture data is also collected; this is used to drive the musculoskeletal model used to predict the muscle activity which is occurring for the given motion. With torque data collected a torque model is built based on local cadence. The chain ring shape is then manipulated so as to affect better muscle efficiency in powering the bike. Manipulation is carried out via the motion capture and torque data provided to the musculoskeletal model. Comparisons are made between these results and both circular and production non-circular chainrings.

Two optimised shapes are presented; one a chainring based on a Fourier series expansion, and the other based on an offset ellipse. These shapes both give a reduction in maximum muscle activity of approximately 15% in the musculoskeletal model. Discussion of the specific normalised muscle forces are given, with limitations and ideas for possible future work being given.

Contents

UNIVERSITY OF Southampton

Declaration of Academic Integrity

Please sign to indicate that you have read and accepted the following statements. Your assignment will not be accepted without this declaration.

I confirm that:

1. I have read and understood the University's Academic Integrity Statement, including the information on practice to avoid given in Appendix 1 of the Statement and that in the attached submission I have worked within the expectations of this Statement.

2. I am aware that failure to act in accordance with the Academic Integrity Statement may lead to the imposition of penalties which, for the most serious cases, may include termination of programme.

3. I consent to the University copying and distributing any or all of my work in any form and using third parties (who may be based outside the EU/EEA) to verify whether my work contains plagiarised material, and for quality assurance purposes.

The extent to which I have worked with others is as follows:

Dr Alexander Forrester assisted with the production of the surrogate modelling code and the creation of the initial torque model.

This submission is inadmissible without a written signature below (applies to hard copy only).

Name: Alexander Purdue

Signature: .....

Date: 30/01/2015

Acknowledgements

The author would like to thank Dr Alexander Forrester for his support during this study. He would especially like to thank his fiancée Nichola Barry and his parents, Alan and Liz Purdue, and his sister Kay for their continued support as well.

Chapter 1 Introduction

1.1 Background

1.1.1 Bicycle development

The bicycle is an inline two wheeled human powered vehicle. The ancestor of the modern bicycle is the draisine (see Figure 1-1), a two wheeled vehicle propelled by the person using it by pushing along the ground with their feet and steering the front wheel. It was invented by Baron Karl von Drais and demonstrated in 1817(Hamer, 2005). In the early 1860's two Frenchmen introduced a mechanical crank drive with pedals and an enlarged front wheel; and what most people would now recognise as the penny farthing was invented. By 1885 this design was modified and refined and the "modern bicycle" was born. In the years that followed bicycles were further developed into the equipment we see today on the street and in competitions.

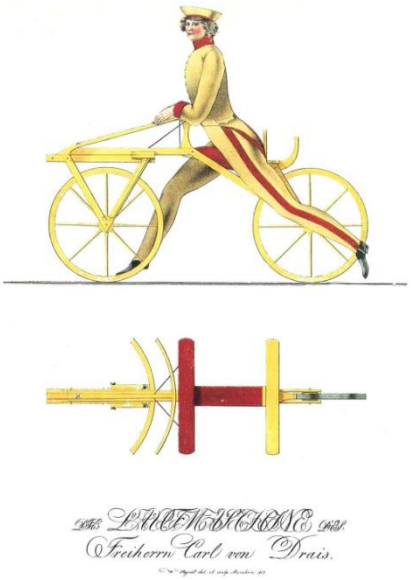

Figure 1-1; A Draisine diagram from the original drawings (Courtesy of commons.wikimedia.org)

With bicycle use being widely popular throughout its existence, the bicycle and the cycling industry have had many socio-economic impacts; influencing the way people live, industrial manufacturing processes, and business and advertising models. At the turn of the 19th century, the bicycle enabled people to live further away from their job locations by commuting. This reduced crowding in inner cities, with people being able to live in the suburbs. Even in the modern day encouraging cycling is seen as a good method for reducing automotive congestion, in developed countries, by introducing cycle lanes and bike sharing initiatives. In developing countries bicycles provide a useful mode of transport to many people who would otherwise

have to walk everywhere. The cycling industry played an important role in the development of more advanced forms of transport, such as cars and aircraft. The manufacturing techniques used and developed for bicycles were used to develop the early cars and planes (the Wright brothers ran a bicycle repair and manufacture business). Other techniques such as mass production, aggressive advertising and mechanisation, taught later industries how to implement these industrial models. However the main lasting impact was that this use of the bicycle acted as a move away from public transport. This made the move to cars easier to achieve, and several recognisable car companies originally started out in the bicycle industry; Rover, Morris Motor and Skoda. All this continued development and customisation has led to improved comfort, faster speeds and specific task specialisation. The bicycle has been an important part of the development of many life changing inventions, and it itself has changed the lives of people.

The continuous development and improvement of bicycles does however point towards one thing, there is still scope for improvement, be it in specialising the bike for a specific task, or just trying to get that little bit extra out of the machine. It is in this mind-set that this project is undertaken; the average bicycle is a versatile and useful invention, but in any specific field there is still room for improvement. While nearly every part of the bicycle has been modified for the varying disciplines of competitive cycling or everyday use, the chain drive itself has been fairly constant; with the front chainrings remaining a circle, despite research and attempts at introducing non-circular chainrings by companies like Shimano. The bicycle chain drive is very effective, though the exact quantitative results of this have not received much publication. Spicer et al (2001) undertook research into this area under the sponsorship of Shimano. This study concluded that analytically the efficiency values should range between 0.97 and 0.99 (see chapter 2 for more detail).

The rider interface however is subject to noticeable losses. These losses are partly due to the "one size fits all" nature of the circular chainring. A brief visual study of any group of competitive cyclists will show variations in technique and motion, combined with the inherent inter subject variability with relation to muscle make up and activation, this would suggest the ability to maximise the output from any one rider is likely to be held back in some respect. Creating a chainring specifically tailored to a rider could improve efficiency, increase output for a given level of effort, or delay the onset of fatigue.

1.1.2 Competitive cycling

The wide use of bicycles means that it is hardly surprising that cycling as a sport has a large following and a great deal of competitiveness associated with it. The International Cycling Union

(UCI) is the association of the National Cycling Federations; it is a non-profit making organisation whose aims include regulating cycling at an international level. Disciplines, according to the UCI, include road, track, and cyclo-cross. These disciplines all use similar regulations and guides and these will be the disciplines targeted for improvement with the research presented here.

Road cycling, as the name suggests, covers competitive cycling which is undertaken outside, on public roads, which are usually closed for the event, or motor racing circuits. This includes individual or team racing and time trials.

Track cycling, usually involves competing in a velodrome which can be internal or external. These velodrome tracks are oval in shape with two straights and two semi-circular sections connecting the straights. Tracks also incorporate banking which can vary both on the same track and from track to track.

In cyclo-cross competitors will complete several laps of a course which is no more than 3.5km in length. The course will contain road, country and forest paths and meadowland. It will also have obstacles that the rider will have to dismount to overcome, though at least 90% of the course must be possible to ride.

There are other disciplines, such as mountain bicycle riding (where the rider may attempt to complete an off road downhill or cross country track in the fastest time) or paracycling (for those with a variety of disabilities, usually similar to track or road cycling) are also organised and managed.

From the outset of their rules the UCI define the "spirit and principle" of the sport with this section:

"Bicycles shall comply with the spirit and principle of cycling as a sport. The spirit presupposes that cyclists will compete in competitions on an equal footing. The principal asserts the primacy of man over machine"(UCI 2012)

This statement gives an overall view of the regulations which is then enforced through the rules that follow. The basis of this is that the competition is about the people and not the machines. Accordingly the rules allow for an amount of variation which in itself is an acceptance that limiting the bicycle to one exact specification would give preference to a rider who is biologically more suited to that setup. As such this variation allows for riders to find the setup which allows for a more efficient transference of biological power to mechanical power. At top levels it is not unusual for riders to use made to measure bike parts such as the frame in their attempts to be

successful in competition. The chainring however is not made to measure, they are always “off the shelf” (production chainrings available for all to buy) and even non–circular ones which give the rider a level of modification with their orientation are still not designed specifically for the rider. It is this we intend to explore. While we will incorporate computational design methods to investigate this, the statement above still lies at the heart of the developments being undertaken.

1.1.3 Anatomy of a bicycle

The subject matter of this work necessitates a reasonable knowledge of the bicycle and its components, with specific attention paid to the chaindrive system. Figure 1-2 shows a labelled diagram of a (mountain) bicycle with the parts shown standard for most varieties of the modern day bicycle. The bike frame is made of three main tubes; the top, down, and seat tube. Attached to the frame are the seat post, head tube, and two seat stays and chain stays. The stays are the smaller tubes which go from the top and bottom of the seat tube to the centre of the rear wheel. At the base of the seat tube is the bottom bracket (not marked) which connects the pedalling mechanism to the frame and allows it to rotate freely. The pedalling mechanism consists of chainrings, a derailleur (front), two crank arms and two pedals mounted on the ends of the crank arms. The chainrings and crank arms are connected to each other so cannot move clockwise (looking at the image from this side) without the other moving. It is however possible to rotate the crank arms anticlockwise without the chainrings moving. The two crank arms are exactly 180° out of phase with each other and both move together. The derailleur controls which of the chainrings the chain is running on and is controlled by the gear controls, usually mounted on the handlebar. The chain runs from the front chainrings to the cogset attached to the rear wheel thereby driving this wheel when the crankarms are rotated in the right direction. The mounting of the rear wheel allows for it to run backwards without moving the cogset and thereby the chain.

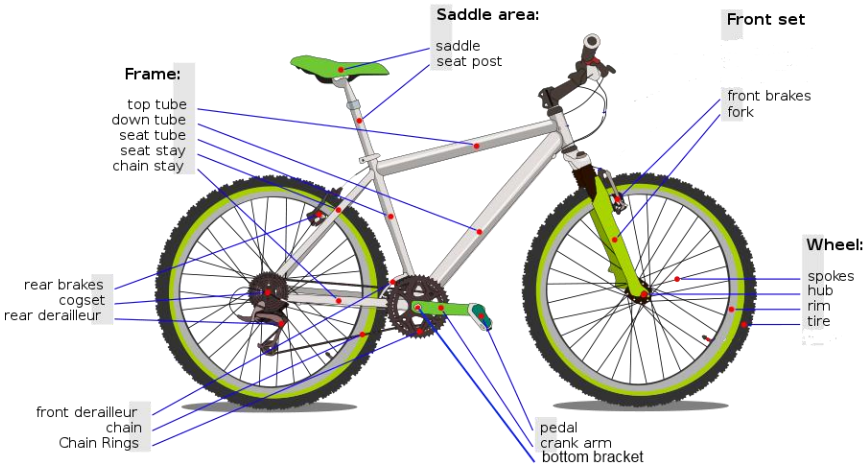

Figure 1-2; Detailed labelled picture of a (mountain) bicycle showing all key parts (Courtesy of commons.wikimedia.org)

1.1.4 An overview of notable non-circular production chainrings

The concept of non-circular chainrings is not a recent one. The three most notable production chainrings are the Shimano Biopace, the Rotor Q-Ring, and the O.Symetric Harmonic (Figure 1-3). The Shimano Biopace is the oldest of the three with production running from the early 1980's until approximately 1993 (Berto et al. 2005) when production was ceased due to a reduction in use. The Rotor Q-Ring and O.Symetric are much more recent and have received high level use very recently. The winner of the Tour de France in 2008, Carlos Sastre, used a Q-Ring and Bradley Wiggins utilised an O.Symetric when he won both the Tour de France and the Olympic Road Time trial gold medal in 2012. These three chainrings are all designed with different design mentalities. The Biopace was designed to smooth the pedalling motion by reducing the chainring diameter when the cranks are horizontal. The design was intended to reduce knee damage by lowering the rate of change of direction of the legs at the top and bottom dead centres. The Q-Rings are designed to imitate human biomechanics and this results in a chainring with a large radius when the leg strength is high and low radius where the leg strength is low (top dead and bottom dead centre, TDC and BDC respectively). It should be noted that the Q-Ring can be mounted in 35 different orientations and to achieve the shape it has been designed for it should be mounted with hole three as the main hole (the mounting hole opposite the crank arm on the side of the chainring). This does mean that the Q-Ring can be mounted in the same orientation to the Biopace but Rotor specifically advise against it as they believe the theory behind that orientation to be flawed(Rotor Q-Ring documentation).

Figure 1-3; Three production non-circular chainrings, from top left going clockwise: Shimano Biopace, Rotor Q-Ring, and O.Symetric Harmonic

Finally the O.Symetric Harmonic is designed in a similar way to the Q-Ring so that the radius varies in proportion to the force produced by the leg, again resulting in a chainring which has a large radius at the points of greatest force and a small radius at the points of least force (TDC and BDC). Figure 1-3 shows the O.Symetric and Q-Ring to be more removed from a circular design than the Biopace, which in passing appears to be circular.

Hansen et al (2009) found blood lactate concentration which was systematically lower with the Biopace. This suggests the Biopace required less muscle activity, which affected muscle fibre recruitment thereby reducing lactate production. While the Biopace has been removed from production, both the Q-Ring and the O.Symetric are still in production and have received some high level success as previously mentioned. This suggests two points which are focal to the research presented here. Firstly, there is an acceptance at the elite level that the circular chainring does not allow the riders to maximise their potential, proven by the use of these non-circular examples. Secondly, these chainrings do not work for everyone as it stands to reason their use would be more widespread if this was true. This suggests that while these designs may work for some riders, others may be finding that they do not, which leads us to the purpose of

this research; can biomechanical modelling and optimisation techniques be used to tailor a chainring to a specific individual for a performance advantage such as increased output or delayed onset of fatigue?

1.2 Project Aim

The aim of this project is to test the proposed method of combining biomechanical modelling with optimisation techniques with the aim of improving a target metric. Rider specific experimental data will be combined with computational models to design a chainring that will lower the amount of force required to provide a set power output. Lower muscle force would reduce the production of lactate and thereby increase the endurance of a cyclist. This study will allow an assessment of whether this method can provide successful results which could be utilised in future studies.

The objectives of this study will be as follows:

- Collect and process experimental data for a given cyclist, allowing for any models produced to more accurately model the cyclist.
- Use experimental data to produce several models of differing complexities for investigations.
- Undertake investigations to assess the effects of variation in bicycle set up including the chainring shape.
- Design and test a chainring shape tailored to the cyclist.
- Assess the effectiveness of this process and the associated feasibility in use and further investigation.

The intended contributions are these:

- Production of a methodology for tailoring a chainring to a specific rider using experimental data.
- An assessment of the effectiveness of the tools used during this investigation for future investigation.

1.3 Thesis outline

This thesis will examine the route this research has taken. Chapter 1 has presented a brief history of the bicycle along with some detail of notable non-circular chainrings. The reasoning behind the undertaking of this research has also been laid out.

Chapter 2 discusses the previous and related research that has been done in the fields that are touched upon by this study. Firstly we consider research about general exercise and then cycling specific research (not including novel chaindrive designs/devices). Experimental techniques are discussed with regard to measurements and performance assessment, and the implications these will have for this research. Musculoskeletal modelling is then covered with an assessment of the methods presented. We then discuss optimisation methods and the relevant literature. Finally we look at prior research that has been done with chainring shape and novel chaindrive devices.

Chapter 3 presents the general methodology that has been used for this research. An overview of the process intended to take the experimental data, process it, and return an optimised design will be shown and explained. We will then discuss the optimisation methods selected for use in detail followed by the biomechanical models that will be utilised and how these have been modified from the repository models.

In chapter 4 we will discuss the experimental data collection. Detailed information will be given about all the equipment and the procedures that were utilised to collect all the preliminary data. A discussion of the equipment and procedures that could be used for experimental assessment of the final design will also be included.

In chapter 5 we will discuss torque models; the data they have been based on, the processing that is used to take the experimental data and provide us with useable profiles. We will also look at how the outputs from these models compares with the original known data.

Chapter 6 will cover the preliminary work undertaken. Optimised designs from basic models will be presented and analysed. Investigations using the Q-Ring shape will be shown and discussed. These designs will then be compared and contrasted. We will also look at other investigations which have been carried out around the design space.

In chapter 7 the final designs will be presented. We will discuss the design decisions, present the optimised designs and take an initial look at the computational results from these designs.

Chapter 8 will cover the detailed computational results of the optimised designs with comparisons to earlier computational experiments. The analysis of these results will then follow.

The final chapter, nine, will cover an overview of the completed research, and the limitations of this research. It will also take a look at the possible future work that could be done in this area, based on this research.

1.4 Summary

In this chapter we have discussed the development of the bicycle from Baron von Drais' invention in 1817 to the modern day versions that can be seen everyday. We have also provided some information on types of competitive cycling, such as road or track cycling, the anatomy of the bicycle, and how efficient the chaindrive mechanism is (~98%). Three notable non-circular chainrings were discussed; the Shimano Biopace, Rotor Q-Ring, and O-Symmetric Harmonic. We described the fundamental design philosophies of these three chainrings; Biopace to smooth pedalling motion, Q-Ring and Harmonic to imitate human biomechanics resulting in a larger radius at the point of largest force production. The competitive success of the latter two chainrings combined with the lack of widespread uptake points to the non-circular chainrings not working for all riders. This idea provides the basis of this study; can we utilise biomechanical modelling and optimisation to tailor a chainring to a specific individual. The Biopace has been shown to reduce the production of lactate and thereby delay the onset of fatigue; we will test the methodology presented here to assess if we can create a chainring which may result in a similar outcome for a specific cyclist. Finally in this chapter we have detailed the structure this thesis will take. Having set out the background and premise of this study we will now discuss the literature around the subject area.

Chapter 2 Literature review

This chapter will present and discuss a sample of the research that has been carried out by other investigators. Related topics discussed include non-circular chainrings, novel pedalling mechanisms, cycling biomechanics, biomechanical modelling, optimisation methods, robust design analysis, and experimental testing theories. The implications the research presented in these papers is also discussed. The structure of this literature review will roughly be as follows:

- Exercise; aerobic and anaerobic, basic anatomy
- Cycling related research;
    - Cadence
    - Power production
    - Kinetics; assumptions and methods of measuring
- Experimental techniques;
    - Data collection methods
    - Performance assessment methods
- Musculoskeletal modelling
- Optimisation
- Robust design
- Previous chainring shape alterations
- Other novel ideas for pedalling mechanism modification

2.1 Exercise

Exercise is defined as "a displacement of the homeostasis of rest elicited by muscle contractions resulting in movement and increased energy expenditure" (Scheuer & Tipton 1977) or more simply "activity requiring physical effort, carried out to sustain or improve health and fitness" (Oxford Compact English Dictionary 1996). While in prehistoric times exercise was a way of life and essential (ACSM 2005) it has now become more of a recreational pastime. There are exceptions to this trend though such as professional and full time athletes using exercise as a full time job and primary source of income (some athletes are not paid a salary so are not classed as professional; instead they earn their money from sponsorship).

There are two types of exercise; aerobic and anaerobic (with and without oxygen respectively) with the differences occurring at a cellular level. The energy expenditure required for exercise involves the muscle cells converting biochemical energy into useable energy (adenosine triphosphate, ATP), by the process or respiration (either aerobic or anaerobic). Anaerobic respiration occurs when the cells require ATP faster than it can be produced aerobically due to

the necessary oxygen supply being insufficient. This results in the cells creating lactate as a by-product and this is transferred into the blood stream to be cleaned out by the liver. There is effectively a transition phase, based on exercise intensity, from solely aerobic respiration to a large amount of anaerobic respiration. The anaerobic threshold (AT) is the exercise intensity at which lactate starts to accumulate in the blood stream due to it being produced faster that it can be metabolised in the liver. This point identifies the switch from aerobic exercise to anaerobic exercise. Typical aerobic exercises are low intensity such as endurance cycling with anaerobic exercises being short, high intensity activities, such as sprinting or weightlifting.

Performance assessment during exercise can use a plethora of different methods, such as distances covered, or time taken to cover certain distances. It is also possible to look at biological/physiological measurements to assess how the body has responded to the exercise that has been undertaken. One method is to measure the amount of lactate in the blood stream. The idea of maximal lactate steady state (MLSS) is defined as "the highest blood lactate concentration and work load that can be maintained over time without continual blood lactate accumulation"(Billat et al. 2003). As such it allows for the use of MLSS as an identifier for AT (Aunola & Rusko 1992). Several measurements of blood lactate can therefore give empirical evidence of whether the exercise is fully aerobic and maintainable or is resulting in a build-up of lactate. Another method is to use breath analysis equipment, to assess ventilator parameters. Obviously with the respiration in the muscles requiring oxygen, the body naturally tries to increase the oxygen supply by increasing the rate of breathing when the oxygen demand from the muscle increases. Breath composition also changes, allowing for several different readings to act as reliable measurements. Previous research has shown ventilation (VE) (Yamamoto et al. 1991), ventilator equivalent for oxygen (VE/VO_2)(Amann et al. 2004), respiratory exchange rate (RER) (Solberg et al. 2005), and respiratory rate (RR) (Carey et al. 2005), to all agree with MLSS.

Another way of measuring exercise effects is to utilise the perceived effort (RPE) scale by Borg(Borg 1998). The numbers on the Borg scale start at 6 and go up to 20, are effectively based on heart rate (with the numbers being divided by 10). The starting point of 6 is based on the average resting heart rate of an adult which is 60bpm (beats per minute). Some of the numbers have verbal anchors designed to aid the subject in identifying the correct number; no exertion at all, through somewhat hard, to maximal exertion. General validation of the scale is achieved due to the linear nature of both the scale and linearly increasing growth function between RPE, VO_2 and HR (heart rate).

Later in this chapter specific muscles will be mentioned, we will also be discussing in depth how specific muscles are reacting to changes in designs according to the musculoskeletal modelling.

Along with the anatomy a knowledge of the terminology about the body, biological planes, and specific types of motion will be of use to the reader. While some of the terms that follow will not be used they are provided to give a more complete understanding.

Directional terms:

- Anterior/posterior: The anterior and posterior (or ventral and dorsal) refer to the front and back of the human body (with the exception of the head). Relatively if something is closer to the front than something else, it is in the anterior direction and can be referred to as anterior.
- Superior/inferior: These relate to up and down on the body; superior is higher, inferior is lower.
- Lateral/medial: In the third axis the directions are slightly different to the other directions as lateral can refer to either left lateral or right lateral direction. The medial direction actually points towards the median, i.e. the middle point of the body.
- Proximal/distal: Due to the ability of limbs to move relative to the body it is necessary for another convention when discussing limbs. Proximal describes where the limb joins the body and distal is used for the point furthest from the point of attachment to the body.

There are three main body planes (Figure 2-1); sagittal plane, coronal plane, and transverse plane. A sagittal plane (or lateral plane) separates the left and right sides, the midsagittal plane or median plane is used to describe a sagittal plane that passes through the median. A coronal plane (or frontal plane) divides the body into posterior and anterior portions. Finally a transverse plane divides the body into superior and inferior sections. Another set of terminology that the reader will find of use is the terminology or kinesiology, i.e. human movement, so we will also list those that may be of use in the remainder of this document.

Movement terms:

- Flexion/extension: These terms relate to the angle between bones at a joint. Flexion means the angle is decreasing, whereas extension means the angle is increasing.
- Adduction/abduction: These terms refer to a movement that brings a part of the anatomy closer/away from the middle sagittal plane of the body.

- Medial rotation/lateral rotation: These terms refer to rotation towards and away from the centre of the body. Also referred to as internal and external rotation.
- Plantarflexion/dorsiflexion: These terms refer to the movement of the foot and are special versions of flexion/extension. Plantarflexion increases the angle between the top of the foot and the shin, whereas dorsiflexion decreases this angle.
- Eversion/inversion: These terms again relate to the foot and describe movement of the sole of the foot away/towards the median plane respectively, with rotation occurring at the subtalar joint.

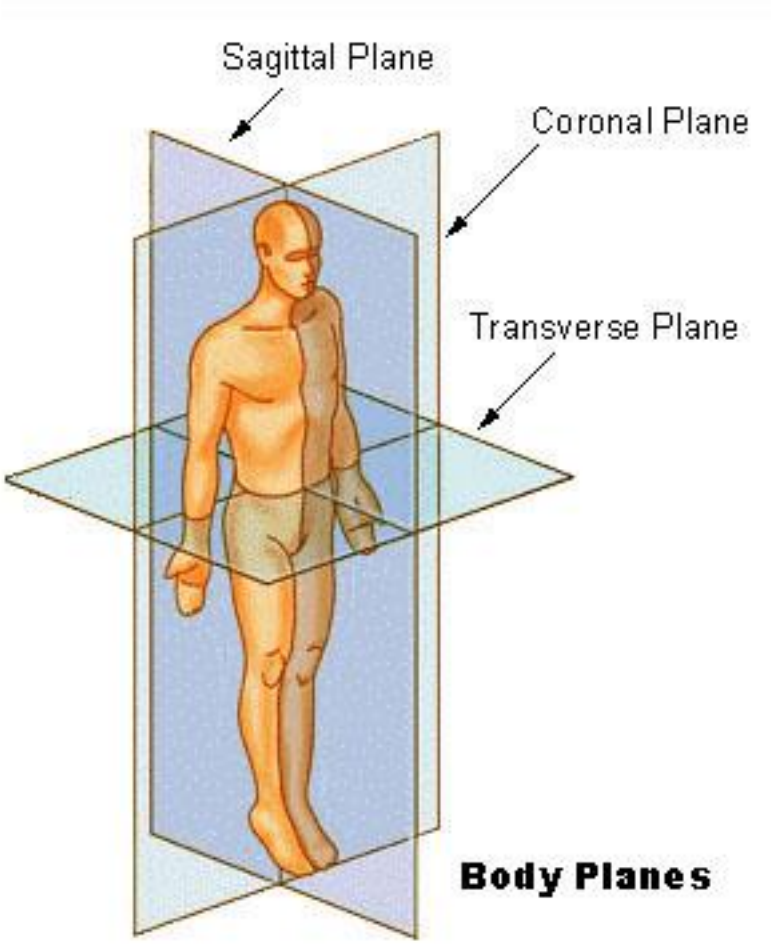

Figure 2-1; Image showing the body planes; sagittal, coronal, and transverse (Courtesy of commons.wikimedia.org)

2.2 Cycling related research

In the previous section we considered the basic principles of exercise and the methods which can be used to assess performance and physiological responses to changes. We also gave an overview of the terminology related to discussing the human body. We will now consider work that has utilised these techniques, among others, to increase the knowledge base of cycling such as torque and power effects.

The Borg scale, mentioned in section 2.1, was utilised by Bertucci et al. (2007) when they undertook an investigation into the differences between laboratory and outdoor cycling. Crank torque was also assessed using an SRM Training system Powermeter (scientific model; SRM, Schoberer, Germany). In the lab a Monark ergometer (818 E; Monark, Verberg, Sweden) was used while a race bicycle (10.2kg) equipped with clipless pedals was used on the road. This provides one point of error in this research due to the differences in both feel and performance between an ergometer and an actual bicycle mounted on a treadmill or rollers. One major difference is with the ergometer flywheel crank inertial load registering 5.2kg*m^2 compared with values ranging from 21.8 – 137.2 kg*m^2 on the outdoor testing. Torque values were collected at 0°, 45°, 90°, 135° and 180° corresponding to the left leg pedal power phase (the segment of the rotation where the left leg is producing the power by pushing down on the pedal). With modern systems it is now possible to collect torque values at a higher frequency therefore giving a better torque profile which will be advantageous for this investigation. Laboratory tests were carried out at 60, 80 and 100 rpm, with level outdoor tests at 80 and 100 rpm and uphill outdoor tests at 60 and 80 rpm. All tests were carried out at maximal aerobic power (MAP) which was assessed prior to the testing. Results showed a large variation in the torque profiles; peak torque and torque range was +7.7% and +9.4% respectively from laboratory at 60 rpm to outdoor uphill at 60 rpm, and greater perceived effort levels in the lab.

The mechanical differences between laboratory and outdoor conditions may have impacted the results as crank inertial load has been shown to affect crank torque profile(Hansen et al. 2002). The difference in perceived exertion could be due to the cycling in the laboratory being viewed as an aversive task(Rejeski 1981), though this is difficult to ascertain as they do not describe the laboratory environment. The final point to consider is their choice of cadences. A generally accepted natural cadence is 90 rpm so the exclusion of this value is odd, and the values selected appear arbitrary with no reasoning presented. Research has also shown that individuals are naturally suited, and will naturally select a specific cadence if given no incentives(Hansen & Smith 2009). An investigation to find the preferred cadence of the riders could be undertaken prior to a similar investigation to Bertucci; then a comparison could be done between riders with similar preferred cadences. While there are certain procedural improvements that could be made with this study, the overall conclusion that testing outdoors using an actual bicycle is better than testing in a laboratory using an ergometer should still remain true. As such planning of procedure for testing the final design should consider whether outdoor testing is either feasible or desirable in this instance.

Hansen & Smith (2009) present an overview of the factors affecting cadence choice. They mention the "cadence paradox"(Kohler & Boutellier 2005); the curious situation whereby oxygen uptake and energy expenditure are better at relatively low cadences, yet any given subject will naturally select a higher cadence. They list the factors as age, MAP, power output, gradient, crank inertial load, drafting (the act of directly following another cyclist thereby reducing profile drag), and duration of cycle. While the effects of these various factors are assessed the answer to the cadence paradox is not found as lower cadences are again found to be more effective. They conclude that further research is necessary.

Cadence variation is an important part of research in this area, and so it features heavily in the majority of papers which are presented here. It is also one of the easiest to adjust so the level of investigation is not surprising.

The power production of the bicycle is due to the torque being produced by the legs pushing on the pedals. While pushing down on the pedal, on the downstroke, the leg is generating the torque which is driving the bicycle. It is also, however, having to work against the other leg which, unless trained to lift, is causing a torque reduction (which they refer to as negative work)(R R Neptune & van den Bogert 1998); the leg on the upstroke is usually just resting on the pedal so the driving pedal must overcome this as well. While this force is not great it is a reduction in the torque production of the pedalling. Neptune and Herzog investigated how this torque reduction varied with cadence. By measuring pedal forces at different cadences for different riders they were able to assess this variation (R R Neptune & W Herzog 1999) with the result being that a minimum torque reduction was found at 90 rpm. This matches neatly with the generally preferred cadence, though whether this is a factor or merely a side effect of the competitive cyclists being used is unanswered. If this cadence was their preferred cadence then it stands to reason that any length of time pedalling at that cadence will have resulted in a gradual increase in torque production efficiency at that rate. Again it would be of interest to identify the riders preferred cadence and include this in the assessment of "negative work".

Many studies have been carried out involving cycling cadence and actual cycling technique as this is an area of great interest to competitive cyclists and those interested in cycling research. Ettema et al investigated how cadence impacted the phases of joint power, crank power, force and force effectiveness(Ettema et al. 2009). Tests were undertaken in a laboratory using an I-magic ergometer (Tacx, The Netherlands) and at 72% of the VO_{2max} of each participant. The results show that cadence has an impact on the different mechanical variables with each showing different time lags, implying the cadence is having an impact on the technique itself.

This effect is supported by a study showing that the gastrocnemius and soleus muscles operate differently at different cadences(Sanderson et al. 2006). Sanderson et al. kept the power output constant at 200W and increased cadence in intervals of 15 rpm starting at 50 and finishing at 110. Measurements were taken once the HR was considered stable, variation no more than 2 beats per minute (BPM) for 1 minute. As the cadence was increased the knee became less extended and the ankle more plantarflexed (angle between top of foot and shin increased). These were accompanied by a decrease in range of motion of both muscles and an increase in velocity range. The bicycle used in this investigation was not configured for each rider, which is anomalous when compared with other investigations as it means the participants may not have been accustomed to the exact set up and this may have impacted results. A similar investigation where participants were allowed to configure the bike would be of interest. They conclude that the research may have important implications as an increase in cadence is changing when the muscle power is generated, partially due to a change in technique, again the implications for not allowing specific rider alteration are not taken into account. It is also pointed out that this may be partly to do with preferred cadence.

Cannon et al (2007) carried out an investigation in a similar field looking into the effect on muscle activity and cycling gross efficiency (mechanical efficiency, physiological efficiency, energy costs) that variation of the ankle angle produced. Eleven trained cyclists were given verbal cues on changing the ankle angle during pedalling and then given a week to practice pedalling with those positions. It is unclear whether this amount of time is enough for proficiency to be acquired and the level of proficiency acquired by the test subjects is not mentioned. The cyclists were tasked with learning two pedalling positions, one with more plantarflexion and one with more dorsiflexion (angle between foot and shin decreased). These were both tested on the same day; so it is questionable as to how proficient the participants were able to become in two different techniques. It may have been advisable to test separately with the participants able to practice only one new technique in the week leading up to the test. Results suggest that introducing more dorsiflexion into the pedalling technique increases gastrocnemius muscle activity and decreases gross mechanical efficiency (how effectively the muscle force is used), suggesting cyclist natural technique may be most effective.

The papers which have been presented previously have only involved level cycling, with the exception of one paper(Bertucci et al. 2007). In competitive cycling hill climbing can be an important factor, shown by some of the recent winners of the major cycling events such as the Tour de France excelling on the hill climb sections. There is not much information on the subject

of uphill cycling, possibly due to the difficulty of collecting on hill data or simulating a hill in the lab effectively. We will now discuss two papers which involve research into uphill cycling. Caldwell et al. (1998) investigated the pedal and crank kinetics in uphill cycling. The uphill condition was simulated by securing the ergometer to a standard exercise treadmill and raising the angle this way. This did mean that the bike was laterally secure and this may impact the results as the riders did not need to balance the bike when in the standing position. No significant difference in pedal and crank kinetics was noted between level and uphill cycling with a difference identified from sitting to standing. This is unsurprising as standing removes the support of the saddle and adds another gravitational component to the system; the legs must now hold the body up as well as powering the bicycle. The question of whether the lateral stability affects results is answered by the resulting data which agrees with previous non constrained hill climbing data(Álvarez & Vinyolas 1996), though that study only utilised one subject so further investigation with more subjects would be useful to the knowledge base.

Bertucci et al.(2005) investigated the effects on the crank torque profile when changing pedalling cadence in level ground and uphill road cycling. They use a similar methodology to their previous paper which was mentioned. Four tests were used; level ground at 80 and 100 rpm, and uphill at 60 and 80 rpm. If a test was failed due to the subject not meeting the requirements then another test was run. A 5 minute break was given between tests, though it is not stated if this allowed for subjects to recover properly from the reasons for failing tests or even the previous test. For a better comparison more cadences should have been used on both level and uphill tests, although there was similarity at 80 rpm. Variations in the torque profile were found between the level ground at 100 rpm and the uphill tests, with only a slight change between level and uphill at 80 rpm. Crank torque profile varied with cadence. Mean torque at 80 rpm was 25% lower than at 60 rpm. A conclusion is presented that limiting cadences to close to 80-100 rpm will constrain variations in muscular activity patterns. The result from both this paper and the paper by Caldwell (1998) is that there is a negligible difference between level and uphill cycling if posture is kept constant.

There has been some interest in attempting to identify optimum parameters in cycling; Hull M.L, 1989 carried out a parameter study in 1989. Five variables were investigated; cadence, crank arm length, seat tube angle, seat height, and foot position on pedal. Free body diagrams were constructed with equations of motion used to calculate a joint moment based cost function, with some discussion also carried out as to how the rider anthropometry affects the outcome. Some kinematic data (angular position, velocity, and acceleration of both the crank and foot link

relative to the crank) and force data was collected for both pedals while the kinematic data was being collected. The force data was scaled to give a power output of 200W. Sensitivity analysis was carried out by normalising the cost function to a reference value (90 rpm, 0.17m crank arm length, 73° seat tube angle, 0.784m seat height, 0.125m for longitudinal foot position). Cost function was plotted against each variable that had also been normalised. The results of the sensitivity analysis gives cadence and crank arm length as the most sensitive, with foot position on pedal as being the least sensitive, though the results suggest investigation into all variables except foot position on pedal is warranted based on sensitivity.

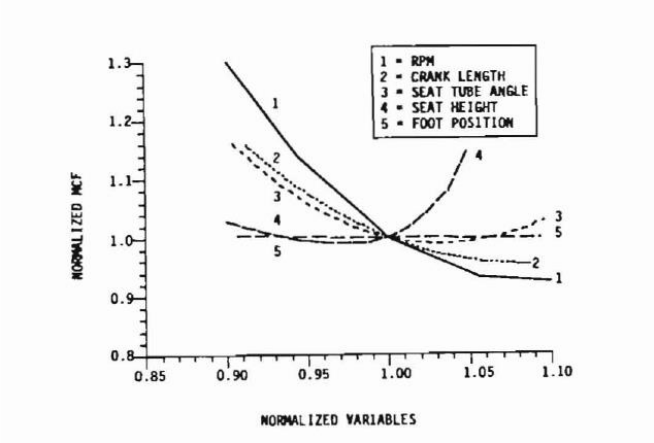

2-2; Normalised variables vs. normalised moment cost function at the original reference point. Curves indicate relative sensitivity of the cost function to the five biomechanical variables. (Hull, 1989)

Optimisation results vary between 98 rpm and 124rpm depending on anthropometric considerations and number of variables optimised, with crank arm length varying between 0.14 and 0.15m. As crank arm length increases cadence decreases. Conclusions about sensitivity and variable interaction seem logical though the discrepancy between results suggested and "industry standard" is curious, though may be due to the methodology used which is simplistic. Since then there have been other papers which have investigated variables such as (Too D., 2000); who investigated the effect of pedal crank arm length on joint angle and power production. Five different crank arm lengths (110, 145, 180, 230, and 265mm) were trialled with the peak power being produced at 180mm; this value is closest to the value of 170-175mm which is "industry standard"(based on a survey of available lengths from a major retail outlet) and agrees with general cycling knowledge. The power plots were parabolic with 180mm being the top, though the decision to have such large gaps between lengths could be rectified and re-trialled. Having a 35mm gap is quite large, and not using the "industry standard" of 170mm is curious so retesting with much smaller intervals may give the maximal power at a different length.

2.3 Cycling movement measurement

Cycling movement is quite unique to each rider. The combination of exact bicycle configuration, exact cyclist biometrics, and same technique, will be extremely rare, if not unique. This does mean that when modelling a cyclist their specific kinematics should be used for the model to be as accurate as possible. The following papers will focus on measurement of these kinematics with particular interest paid to the hip movement.

The reason for the interest in the hip movement is that a common assumption made when modelling cycling is that the limb movement is entirely planar (in the sagittal plane). This assumption has been tested (Umberger & Martin 2001) for ergometer cycling. 4 cameras were used to capture the motion which was used to run a 2D and a 3D model. The results were that maximum ankle eversion occurred at 36% of the pedal cycle later in the 2D model. There are also discrepancies in the hip between the two models which could have been due to the method of defining the hip in the 2D model. Discrepancies in frontal plane ankle joint motion require the use of a 3D model. The conclusion is that if possible the planar assumption should not be used. The sample size used was however quite small (4 subjects) and intersubject variability was low so repeating the test with more varied subjects would provide more concrete proof.

Neptune and Hull have published two papers in which they investigate the methods of determining hip (HJC) movement in seated cycling(Neptune & Hull 1995; Neptune & Hull 1996). As the earlier of their papers only used one subject, the latter repeats most of the testing done in their 1995 paper with more test subjects, to assess if the results found in 1995 could be applied to more cyclists.

The four methods(Neptune & Hull 1995) used were as follows; standard method (STD), trochanter method (TRO), new method (ASIS), and fixed hip method (FIX). The standard method utilised an intracortical pin, with a triad of markers attached, which was threaded 2cm into the lateral iliac crest. The TRO method used a spherical marker placed over the superior aspect of the greater trochanter (see Figure 2-3) and assumed this to be the HJC.

The ASIS method determined HJC using a video marker placed over the anterior superior iliac spine. A vector of fixed magnitude and orientation in the sagittal plane was established based on the vector between the average anterior-superior iliac spine and the trochanter coordinates. This method assumes no rotation in the sagittal plane of the pelvis. Finally the FIX method assumes the HJC is fixed throughout the cycle, and was based on measurements taken when the cyclist was stationary.

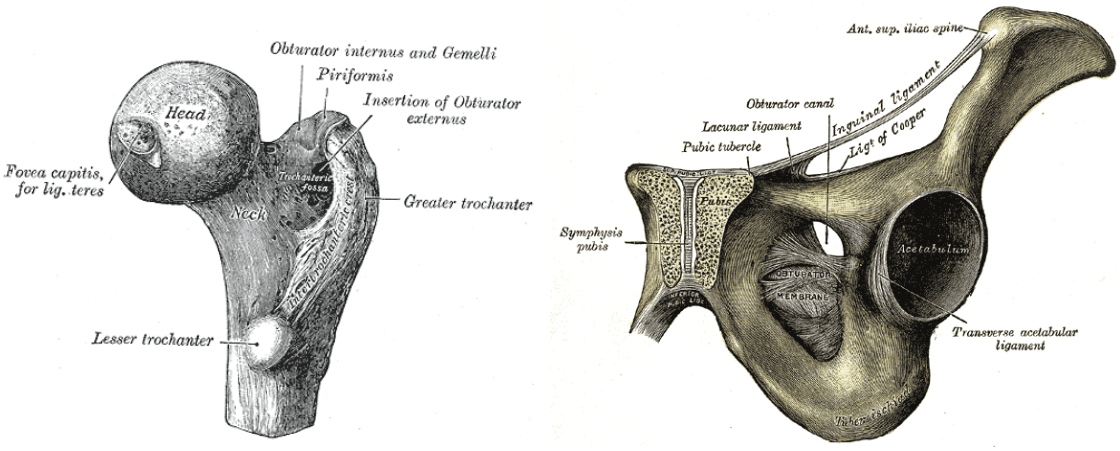

Figure 2-3; Notated images of the upper part of the femur (left) and left part of the pelvic bone (r) (Images courtesy of Gray's Anatomy)

All four methods were measured from the same test; i.e. all markers were placed on the rider and one test was carried out. These methods were used to collect the motion data and these data were then fed into a model, a five bar linkage system in plane motion, to assess effects of the different methods. The first conclusion is that the FIX method is more prone to error, though this was countered with it also being the most accurate over all work rates and pedalling rates. ASIS allowed for more accurate computation of the hip joint power, and also indicated the hip movement with less error than the TRO method. The final conclusion is that the STD method is always more accurate but as it is an invasive technique it is not reasonable to use this for a large proportion of research. An assumption is made that the STD method has had no impact on the cycling technique. This is an interesting assumption to make as any variation in what the cyclist feels will affect their technique and screwing a pin into the pelvis would logically result in something the cyclist would feel and have some impact on this technique. Another study with the same rider and excluding the STD method would give a better idea as to whether this effect was significant.

Their 1996 paper repeats the tests, with no STD test, on another 7 cyclists. The results in this case showed that ASIS produced significantly different hip joint movement patterns than TRO, resulting in very different power and work calculations. They find that at naturally preferred pedalling rates (~90 rpm) and lower work rates (<225W) hip joint movement was minimum and as such, in these conditions it is adequate to use the FIX method as it is least prone to error(Neptune & Hull 1996).

2.4 Musculoskeletal modelling

Musculoskeletal modelling is a complex task, partly due to the inherent redundancy in the body and the inability to accurately measure what occurs when the body undertakes a task. In this

section we will attempt to give the reader an understanding of how musculoskeletal modelling works and the variations and limitations that can arise from using it.

2.4.1 General musculoskeletal modelling

Before the widespread uptake of computers and the growth of musculoskeletal modelling, analysis tended to be done representing sections of limbs as segments and working out joint torques(Hull & Gonzalez 1989). This can lead to incorrect interpretations of muscle function(Fregly & Zajac 1996; Raasch et al. 1997) and shows that it is necessary to treat the body as the more complex system it is. The use of musculoskeletal modelling is therefore of great importance in the area of understanding how the body reacts to different activities/situations without the necessity of constant human subjects.

The redundancy we mention is due to the human body containing more actuators (muscles) than it actually needs to carry out any given movement. This causes a fundamental issue with modelling as the issue of which muscles are recruited for a given moment and how much force they must each exert is in most cases impossible to measure. This again is a complex issue with musculoskeletal modelling as such procedures as EMG can only monitor surface level muscles, while invasive procedures can cause discomfort and affect movement being, by definition, invasive. It is not possible to measure muscle forces non-invasively(Komi 1990; Gregor & Abelew 1994). To this end it is a difficult task to use subjects to test products, movements etc. This paves the way for computational musculoskeletal modelling which allows researchers/product developers etc. to predict the effects or impacts without using physical subjects. This is highly useful where many designs are being trialled as this can be done on a computer in a much faster way than using people. It is this point which makes musculoskeletal modelling useful to this research; the ability to quickly trial many modifications without the need for a cyclist present is invaluable.

Musculoskeletal modelling can be done in one of two ways; forward dynamic or inverse dynamics (Figure 2-4). Forward dynamics is associated with the chain from muscle activation through to motion. Inverse dynamics on the other hand takes the motion as its starting point and working back to the muscle activations(Pandy 2001). This leads to both methods involving a different type of optimisation. While forward dynamics is a dynamic optimisation, which solves on optimisation problem for the whole movement, inverse dynamics is a static optimisation, solving for each instant of the movement. To perform an optimisation for muscle force we can use both approaches; with forward dynamics it is necessary to incorporate a goal of the motor task and then loop the whole forward dynamics loop until an optimum muscle force criteria is

met which fulfils the motor task successfully. This means that from a computational effort point of view the two are very different; the time required to run forward dynamics is much greater than that for inverse dynamics.

There are downsides to the use of inverse dynamics however; primarily the dependency on the motion and the accuracies associated with these. This was discussed in section 2.3 so the reader should have an idea as to the issues that can arise. The issue of redundancy is overcome by the use of optimisation approaches such as the min/max criterion(J Rasmussen, M Damsgaard & Voigt 2001). The min/max criterion is the muscle recruitment algorithm used in the AnyBody software and as such we will leave a more detailed discussion until the next subsection.

The next issue we will discuss is the makeup of the model itself, i.e. how the bones and muscles are modelled. Typically the bones are modelled as rigid bodies(Damsgaard et al. 2006) so we will now focus on the method for modelling the muscles. The most common muscle model is the Hill type model(Hill 1970) and a modified version is frequently used(Zajac 1989). The model (see Figure 2-5) is based upon several assumptions which include:

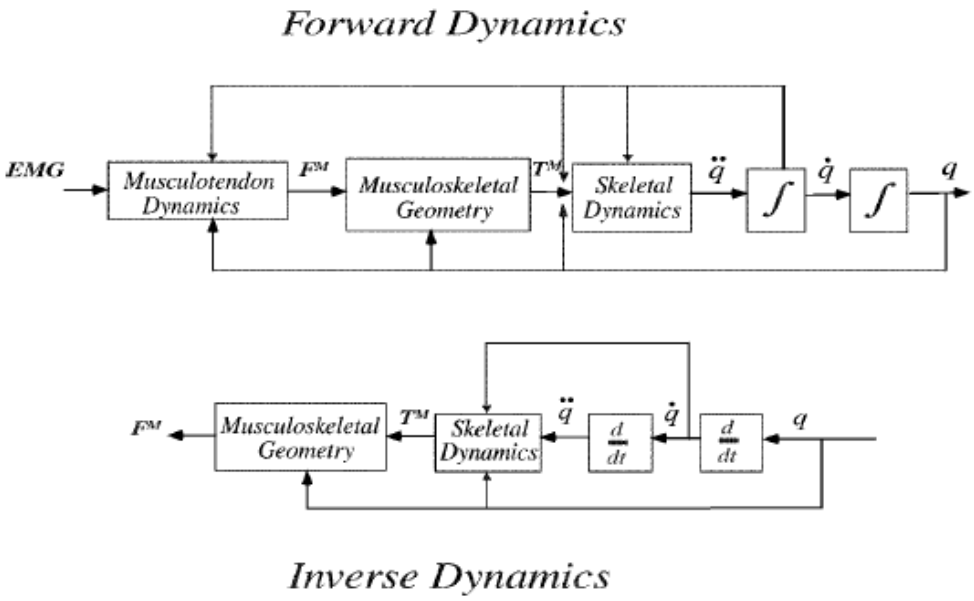

Figure 2-4; Comparison of forward and inverse dynamics methods commonly used to determine muscle force; (TOP) Muscle excitations are the inputs and body motions are the outputs in forward dynamics. Muscle forces (F^M) are an intermediate result. (BOTTOM) Body motions are the inputs and muscle forces the outputs (Pandy 2001)

- The muscle may give a tension force
- The muscle cross-sectional area and volume remains constant
- No damping is included in the model for the contractile element (CE)
- No fatigue mechanism is included

- No activation dynamics are included

There are other, more complex models(Hatze 1977; Huxley 1957),based on cross-bridge mechanisms. These however are less suited to numerical implementation since they involve solution of differential equations, of quantities that are not directly related to the mechanical function of the muscle. In the Hill-type model, the force producing properties are described by four parameters: a muscle's peak isometric force, corresponding fiber length, pennation angle, and the intrinsic shortening velocity of muscle. These data are nearly always based on the literature, which is usually from cadaver dissections. This means we can model the image shown in Figure 2-5 by a single, nonlinear differential equation that relates musculotendon force, musculotendon length, musculotendon shortening velocity, and muscle activation to the time rate of change in musculotendon force. This can be integrated numerically to find musculotendon force at the next instant. Another shortcoming of this model is the inability to involve muscle history as this has been shown to have an impact on force production(Herzog 2004). While this could prove useful it is very rarely used and not involving it in the investigation keeps complexity to a minimum.

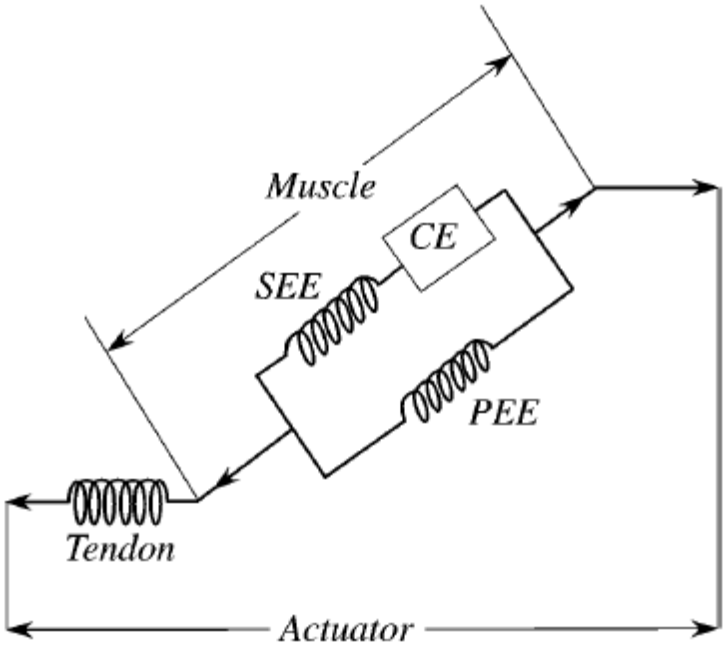

Figure 2-5; Model used to simulate muscles. Made up of three elements in series with an elastic tendon. The mechanical behaviour is modelled by a Hill-type contractile element (CE), a series-elastic element (SEE), and a parallel-elastic element (PEE) (Courtesy of Pandy, 2001)

While musculoskeletal modelling is a very useful tool, the complexity of the body and the amount of unknown information means that human subjects still do, and probably always will, hold an important role in these investigations.

2.4.2 AnyBody

The AnyBody Modelling System utilises inverse dynamics to carry out its musculoskeletal modelling. It was designed with the following aims(Damsgaard et al. 2006):

- It should be a modelling system; i.e. a tool that allows users to construct models from scratch or use or modify the existing models to suit different purposes
- The system should facilitate model exchange and cooperation on model development, and it should allow models to be scrutinised
- If possible, it should have sufficient numerical efficiency to allow ergonomic design optimisation on inexpensive computers
- The system should be capable of handling body models with a realistic level of complexity

The program uses the Hill-type model described above along with a tailored muscle recruitment algorithm to solve the redundancy issue. It consists of two applications; a windows GUI (graphical user interface) and a console application which are both meant to run the models created in the software in the same way and produce the same results. The console application is intended for the use with third party software, but only has the ability to load and run models which have been created and modified by using the GUI.

The first paper we will mention (Damsgaard et al. 2006) provides a good overview of the AnyBody software. A brief explanation is given to the muscle model, as described in the previous subsection, and a description of how the software is used by the user is also given the same treatment. The final description they give is a condensed version of another paper(Rasmussen et al. 2001) and describes the muscle recruitment algorithm that the software uses. Linear optimisation is favoured over non-linear techniques due to the ease with which they can be implemented and the efficiency with which they run. While a polynomial criteria is popular, for powers higher than one it leads to non-linear optimisation problems which are computationally demanding to solve. The min/max (minimise the maximum muscle activity) criterion they suggest is equivalent to the polynomial criteria of a very high power, both mathematically and qualitatively. This is thereby used in an iterative process whereby when a muscle is determined uniquely during a step it is removed and the reduced problem is then solved. A downside to this criteria is that it does require a tailored algorithm though, whereas a polynomial criteria can be solved with standard optimisation methods.

The AnyBody software has been used to carry out a wide variety of investigations, some of which have been published, while others are available to look at but have not been published in a peer

reviewed manner. The first piece we will look at falls into the second of those two categories. The investigation looked into the role of elastic energy stored in the tendons during cycling(Rasmussen et al. 2001). They show that tendon elasticity does not have a beneficial impact on cycling efficiency (force input to power output) and this also gives basis for bicycle frames being as rigid as possible. They conclude that tendon elasticity is associated with a loss of energy in cycling. While this is not directly useable in this research it does show that there are losses in cycling which are inherent and cannot be removed. Therefore it is important to minimise those that can if overall efficiency is to be maximised. The next paper(Rasmussen et al. 2002)involves utilising the software for design optimisation and was published in a peer reviewed journal. It introduces the idea of using the software to perform optimisation. It initially describes the algorithm and the process the software takes while solving a motion for a specific design variable, before using that knowledge to optimise the design of a hand saw. For this example internal optimisation algorithms are used to search the design space. A discussion is provided about the model used and the resulting design. It is pointed out that it is unlikely the optimised design is actually best due to the simplifications in the model, such as absence of wrist rotation, and the planar motion of the sawing arm. However while this design may not be optimum the process of using musculoskeletal modelling, specifically AnyBody, in design optimisation is valid, as long as the model used provides an accurate enough representation. Since this paper the software has been used for several optimisation investigations, such as optimising swimming arm stroke(Nakashima et al. 2012), designing a pedalling mechanism for paraplegics(Rasmussen et al. 2004), and ergonomic optimisation of a bicycle crank mechanism(Rasmussen et al. 2005). Based on this work the AnyBody software looks to be a good basis for undertaking this research.

2.5 Optimisation

The analysis of a function in computational engineering to find a specific value, usually a maximum or minimum, is referred to as optimisation. Methods for optimisation will generally fall into one of two categories; global search, or local search. In a global search the optimisation searches the entire design space to try and find the optimum value, whereas in a local search only a certain area is searched. Both have their advantages and disadvantages; a global search may not uncover the overall optimum value, especially if it believes the value to lie in a different place. A local search on the other hand is more likely to find the optimum value if it is close (i.e. a local optima) but will not produce good results if the value is not within its search region.

The ability to computationally model projects, such as wing designs or structures, and then perform analysis on them without the need to manufacture and physically test them has greatly

improved and accelerated the design process. It is now possible to trial hundreds of examples in computational fluid dynamics (CFD) or finite element analysis (FEA) in the same time it would take to manufacture and test just one design. However the computational time is highly dependent on the complexity of the design being tested etc. and while time reductions have been found it is still infeasible to trial every possible design, especially when the design contains multiple variables. As such the use of surrogate (or meta-) modelling is of great use in computational design. The premise being that a computationally expensive cost function (design metric) can be represented in a simpler way allowing for faster searching of the design space with lower requirements on number of actual samples needed. The basic idea is that an initial (computationally affordable) sample is taken of the design function and statistical inference is then used to predict where the best results lie.

The starting point of any surrogate model is the sample, gathered by using a sampling plan. There are several different methods, such as full factorial and Latin hypercubes. The full factorial is the most simple and samples the design space by means of a uniformly distributed rectangular distribution of points. While this gives a good coverage of the design space it can be very computationally expensive, especially with complex functions, to take the measurements at each point. For this reason sampling plans based around a Latin square can be used. A Latin square is a grid where each vertical and horizontal line has one measurement point in it.

1	2	4	3
3	1	2	4
4	3	1	2
2	4	3	1

Figure 2-6; Example of a Latin square; no number is repeated in the same row or column

In Latin hypercubes this theory extends in however many more dimensions they contain. Each of these “lines” is referred to as bins; so each bin contains one sampling point. The first starting point is the random Latin hypercube, whereby the only criteria is that there is only one point in each bin. While this is straightforward, the sampling plan created cannot guarantee a good sample of the design space; a diagonal sample for example fulfils the criteria but obviously does not provide a good sample of the space. We need to use a space filling metric (such as suggested by Morris and Mitchell(Morris & Mitchell 1995)) to ensure the sampling plan will provide an adequate view of the design space. This can then be joined with evolutionary operation(George E P Box 1957)which generates “offspring” by combining two of the points already sampled and adding a slight mutation (see genetic algorithms after). The “offspring” and “parents” are then

compared to find the best criteria (Morris-Mitchell) value (manually searching for best Morris-Mitchell values would be very time consuming). This combination gives the best Latin hypercube method(Forrester et al. 2008) which will act as the base for the optimisation we undertake here.

Once we have a sample, we can either search the design space (this is not surrogate modelling however), or we can build a surrogate model which we can then search.

The wide range of methods for surrogate modelling means that it would be inefficient to describe them all here. Instead we will focus on two cases initially; polynomials and radial basis functions. The polynomial method effectively uses a truncated Taylor series expansion(Hastie et al. 2009; George E.P. Box & Draper 1987) and can be ideal for uncertainty analysis in certain cases. However they can be unsuitable for highly non-linear, multimodal, or multidimensional landscapes. They are also limited in that, once constructed they give little indication of where to sample the design space to find an optimum value.

In radial basis functions a complicated function is represented as a weighted sum of simple functions. This allows for predictions to be made by predicting from the simple functions and combining these using the weights. This means that as well as the value at each sample point there is also a basis function term centred on each point. They are easy to implement and control the flexibility of (Hastie T., 2001).These provide the foundations of other methods such as Kriging.

Kriging was first developed in 1951(Krige 1951) by a South African mining engineer (Danie Krige) and started to be used in engineering design following work to apply the method to the approximation of computer experiments(Sacks et al. 1989). In addition to the tuned basis functions of other methods, Kriging has a statistical interpretation that "allows one to construct an estimate of the potential error in the interpolator"(Jones D.R., 2001). This ability to estimate the error means that Kriging is very useful tool for global optimisation and will therefore be used to create the surrogate models used in this document. A detailed description of the Kriging method, along with others, can be found in "A taxonomy of global optimization methods based on response surfaces" (Jones D.R., 2001).

Within surrogate modelling code it is necessary to use optimisation algorithms to calculate where to take the next sample point. A genetic algorithm (GA) is one good candidate for this. Genetic algorithms are based around a few principles; fitness, parents, offspring, mutation, and elitism. The idea is that an initial sample is given and each of these points has a fitness value; i.e. a normalised function value. The greater the fitness value the better that point is. A genetic

algorithm does not stop at that point though. It “mates” two of the initial sample points (“parents”) to create a new sample point; an “offspring”. The “offspring” configurations are controlled by the “parents” and the cross-over point which was used to mate them; this can either be predefined or random. The “offspring” are then given fitness values and this process continues until either the number of specified generations, or a convergence criteria has been met. There are two modifications which can be applied to a GA; mutation and elitism. Mutation means that when the “mating” is done there is a chance for a random change in the “offspring” which is not dependent on either of the “parents”. The other is elitism whereby the “parent” with the best fitness value is guaranteed to survive to the next generation i.e. one of the “offspring” will be a clone of that point.

The optimisation process we will use will use a sampling plan utilising a space filling metric, and surrogate modelling involving Kriging, and genetic algorithms. More details about the optimisation code and process will be given later in the document.

2.6 Bicycle chaindrive modification

As has been previously stated there have been previous work and research into modification of the bicycle chainring. In this subsection we will discuss the work involving non-circular chainrings, both theoretical and practical, and we will look at other novel work involving the chaindrive mechanism.

2.6.1 Non-circular chainring research

The first modifications we will consider involve changing the shape of the chainring; as this is the aim of this research it is an area of great interest. As we have previously discussed several notable production non-circular chainrings we will first look at research that has utilised these.

Firstly we will look at one piece of research(Hansen et al. 2009) which looked into the effects of chain wheel shape on crank torque, freely chosen pedal rate, and physiological responses during submaximal cycling. To analyse these effects, participants were asked to perform some cycling tests using a Biopace chainring, and a circular chainring. The results were that the chainring shape had no significant effect on peak and minimum torque, or pedal rate, or crank angle of peak torque. Most physiological responses also showed little difference between chainring shapes, with the exception of blood lactate concentration which was systematically lower with the Biopace. As stated in chapter 1 this suggests the Biopace reduced muscle force necessary affecting muscle fibre recruitment thereby reducing lactate production. In the appendix of this paper the plausibility of their reasoning behind the lower lactate level is tested using the AnyBody software, with the results showing slightly lower activations for the Biopace shape.

The Q-Ring mentioned in section 1.1.4 claims scientific backing in its advertising (www.rotorbikeusa.com). This scientific backing is in the form of an unpublished report by Martinez et al, at the University of Valladolid in Spain(Cordova Martinez et al. 2004). Blood samples taken several days before the test were compared with blood samples just before and after a maximum effort test. A reduction in lactic acid (lactate) (9.1%) was found with the Q-Rings when compared with the normal chainrings. They match this with the cyclists lasting longer at 90% maximal power, and also being able to release more power (W) during sprints (+0.6-6.6%). The length of time the cyclists lasted with the Q-Rings is not quantified as testing was ceased once the rider had achieved 8 minutes more than the previous test. Interestingly before testing the riders' optimum Q-Ring rotation was worked out. It is not stated how this was calculated and the research would be more thorough if multiple orientations had been tested. This would also prove this optimum orientation procedure to be accurate. While performance improvement is found it is not specified which orientation each rider was using and so comparison is not as clear cut. Nevertheless performance improvement was found, and when this is combined with the top level success the Q-Ring has achieved, mentioned in chapter 1, it is clear non-circular chainrings have something to bring to the sport.

A second study using Q-Rings was undertaken to assess the variation between circular chainrings and Q-Rings with regard to performance and physiological variables(O'Hara et al. 2012). An initial test was carried out using a circular chainring before Q-Rings were fitted and the subjects trained and raced with these and were subject to the same test every week for the next four weeks. Finally in the last week the circular chainrings were refitted and the test was again repeated. The testing involved submaximal exercise tests followed by a 1km time trial. There were significant improvements in performance with the Q-Ring (reduction in time, increased average speed, increased average power). Oxygen consumption and heart rate were significantly lower with the Q-Rings during submaximal testing. Two other points of note are the improvements in performance occurred after just one week with the Q-Ring and that with the final test using the circular chainrings the values returned to pre-Q-Ring test values. They point out that this means the improvements were only evident while using the Q-Rings. They also point out that the majority of the physiological measures do not equivocally support the notion of an adaption period being necessary contrary to Rotor's guidelines. Again, this suggests non-circular chainrings can provide performance improvement.

One investigation(Ratel et al. 2004) looked at the physiological responses during cycling with noncircular harmonic and circular chainrings. In this instance a harmonic chainring (Samovedi

S.A.M., Monaco) can be described as a skewed ellipse where the major and minor axes are not perpendicular. The O.Symetric mentioned in chapter 1 is a good example of a harmonic chainring. Two incremental sessions were completed, one using the harmonic chainring and one using the circular chainring; this was randomly assigned. Physiological measures taken were ventilation (V_E), oxygen uptake (VO_2), CO_2 output (VCO_2), heartrate (HR). No significant difference was found at submaximal and maximal rates between the two chainrings. While the submaximal exercise levels are detailed the maximal ones are not so confirmation of those results would not be possible. There are two noticeable flaws in this investigation. Firstly the gear wheel was chosen freely during the first session, be that with the harmonic or circular chainring, and this choice was then imposed on the second session. It would be interesting to see if the chainring shape had any impact on the choice of gearwheel as no data on the chosen gearwheels is presented. Another issue is the recurring theme of acclimatisation; the cyclists in this study were just given the chainring and the study carried out. Considering Rotor suggest a month long acclimatisation to the Q-Ring, the lack of practice with this chainring may have had an impact on results.

Having considered the testing of production chainrings we will now discuss work set out to design the shape of the chainring itself(Kautz & Hull 1995; Rankin & Neptune 2008). This work is highly relevant to the research done here as we intend to design the shape of the chainring so any discoveries or lessons that can be derived from these papers may be important for our own work.

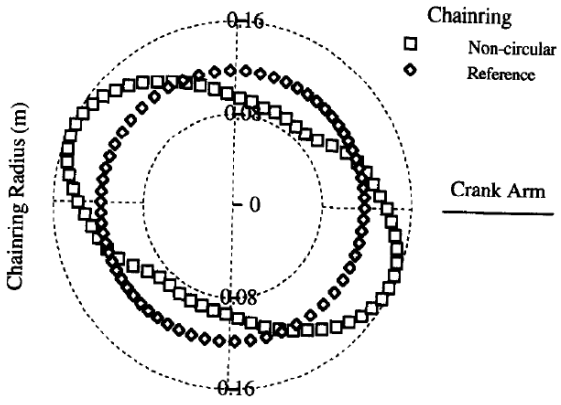

Figure 2-7; The circular and optimised chainring shapes from Kautz et al (1995). The cranks are horizontal for this image.

The chainring shape found by Kautz et al (see Figure 2-7) was not the primary purpose of their paper. They present a dynamic optimisation analysis for equipment setup problems in endurance cycling. This optimisation method is tested on the chainring shape and it is this reason

that a new chainring shape is designed. We will not discuss the optimisation method itself here but will focus on the produced design and its effects and limitations. The basic model was a five bar linkage system; one bar representing the thigh, one the shank, one the foot, one the crank, and one the crank to thigh link (the bicycle saddle post). The forces in the leg are then resolved using moments about each joint in the system. The result of this optimisation is a chainring shape which claims to be an improvement. This improvement however is irrelevant due to the chainring design being physically impossible due to two main reasons. Firstly the chainring caused a substantial increase in muscle activation specifically when joint velocity was high. The increase in muscle activation results in a 25% peak increase in torque at the knee, which is a physiological impossibility. The other flaw is the presence of cusps in the design. Experimentally these would not act as the design intended as the nature of the chain would mean this shape was not followed exactly. It may be of interest in future work to use the optimisation method used here with a more complex model, such as the AnyBody software, to discover if this method is capable of producing physically possible improved shapes.

In the second example Rankin et al set out to find an optimal chainring shape which would maximise crank power during isokinetic pedalling. The use of the term isokinetic here may be slightly misleading as they use it referring to maximal cycling and not just steady speed cycling. They utilised the musculoskeletal modelling software SIMM (Musculographics Inc., U.S.A) whereby they controlled the muscle excitations (forward dynamics) and chainring parameters to simultaneously optimise both using a simulated annealing algorithm(Goffe et al. 1994). Their work was intended to build upon Kautz et al, though the results they found were significantly different. Rankin found an elliptical chainring with eccentricity dependent on cadence; 1.35 for 60 rpm, 1.29 for 90 rpm, and 1.24 for 120 rpm. The chainring was orientated 60° out of phase with Kautz' chainring and had a 36% higher eccentricity on average. The algorithm proved to be robust; with similar shapes for all chainrings irrespective of starting parameters. It should be noted that the elliptical nature, while slowing the pedal during the power phase to allow for more force to be transferred, also increases torque reduction. This may explain the decrease in eccentricity as cadence was increased as torque reduction is more prominent at higher cadences(Neptune & Herzog 1999). They conclude that experimentation validation is necessary to test if these computed variations transfer into actual effects.

While Rankin et al use a different approach, utilising forward dynamics and specifying muscle excitations, there are some limitations which can be taken and considered for our own research. They use a Hill type model(Zajac 1989) with no history dependence(Abbott & Louvain 1952).

While history dependence can have a noticeable impact on muscle strength it is difficult to incorporate into a musculoskeletal model and would cause variation in results. This does mean that it is logical to acknowledge the effects but not take these details into account. Assuming no history dependence allows for the average conditions to be modelled in a more straight forward way. No drivetrain dynamics were modelled and while drivetrain efficiency is very high(Spicer et al. 2001) crank inertial load may have some impact on results. The final limitation is the use of the fixed hip assumption which has been shown to introduce errors and decrease accuracy in modelling(Neptune & Hull 1995).

2.6.2 Novel chaindrive ideas

The non-circular chainrings presented in the previous subsection are not the only research which has been undertaken to modify the drivetrain mechanism to change performance. Other papers have fundamentally changed the pedal-crank-chainring system.

One such investigation(Zamparo et al. 2002) looked at the mechanical efficiency of using a novel pedal-crank prototype. An incremental test on a stationary ergometer was undertaken using a sun and sun-wheel configuration which allows the effective length of the crank to vary depending on whether the driving leg is acting on it (see Figure 2-9). This should increase output in the power production phase and also reduce torque reduction in the upstroke as the moment arm length has been changed. Testing was carried out at 60 rpm, as discussed earlier higher cadences, specifically 90 rpm, would have been of interest. There was a significant variation in aerobic capacity of the subjects with 3 of the 7 terminating the test at 200W, and only 2 of the 7 reaching the 300W mark aerobically (assessed via ventilator parameters). More subjects should be used so that variation within aerobic capacities could be better assessed.

VO_2 was significantly lower with the proposed pedal crank and this matched with a reduction in the work needed to accelerate the limbs with the cranks. These results translated into a negligible difference below 250W between the two cranks but at higher powers the improvement with the proposed crank could be up to 2% improvement. A theoretical 1hr test was run with the proposed cranks outperforming the standard cranks. Differences were more prominent in taller riders who were able to get more out of the longer cranks. This is certainly interesting research however with competitive cyclists wanting to maintain a low weight bicycle mechanisms like this which add weight and complexity are unlikely to find much use.

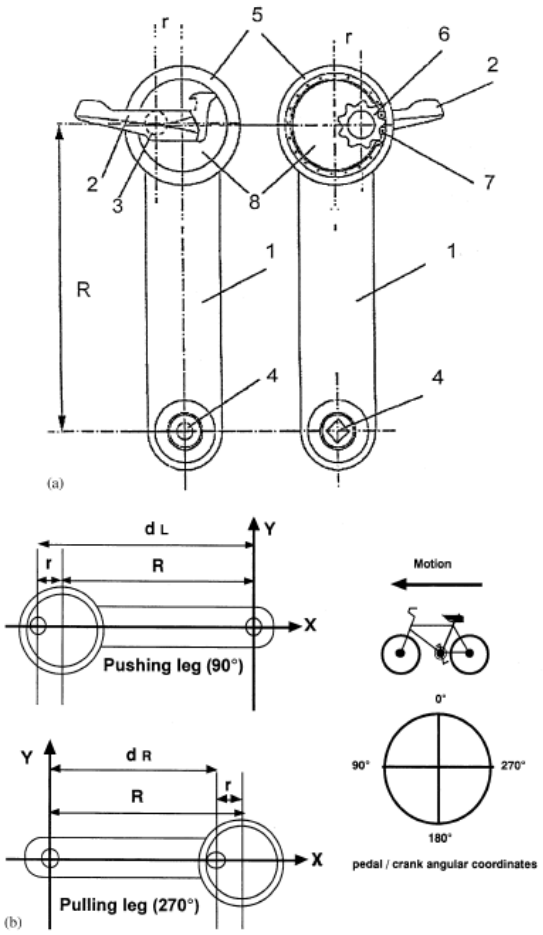

Figure 2-9; Schematic of the pedal crank designed by Zamparo et al. Front view is on the left, rear on the right. (1) Crank, (2) pedal, (3) pedal pivot, (4) bottom bracket, (5) sun-wheel, (6) sun, (7) roller bearings, (8) open enclosure. Pedal-crank length varies between R-r and R+r

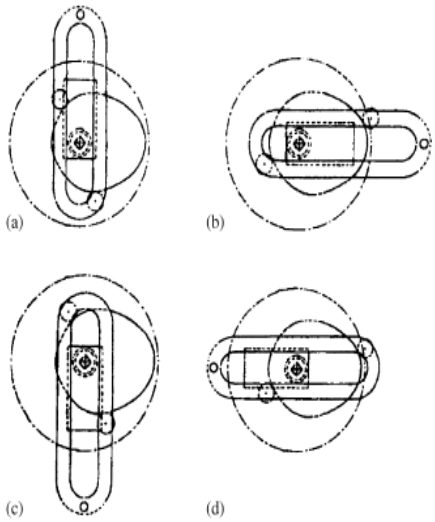

Figure 2-8; Novel crank mechanism by Hue et al . (a) crank arm length is 175mm similar to the arm length of circular chainrings. (b) at 90 degrees maximum length is 200m. (c) crank arm length returns to 175mm. (d) crank arm length is down to 150mm

The idea to shorten the crank arm during the upstroke and lengthen it during the downstroke has also been investigated(Hue et al. 2001; Hue et al. 2007). These two investigations utilised the same crank mechanism (see Figure 2-8) but involved slightly different protocols and subjects. In both cases they use two crank arms which slide into each other and are controlled by an elliptical cam inside the circular chainring; this varied the crank arm length between 150mm and 200mm. Both investigations utilised a two trial system. The first trial was an incremental test using an ergometer and the crank mechanism. The second trial varies slightly between the two; in the 2001 investigation two "all out" 1km sprints were undertaken with a one hour rest between. One test used the normal system, one used this novel mechanism. Both were done on the participants own bicycle which was mounted to a home trainer. In the 2007 investigation again two "all out" 1km sprints were done but there was a day's rest between the tests and they were carried out on a velodrome track. Interestingly, while both investigations showed very little physiological differences between the cranks, a performance improvement was seen in the first investigation but not in the second one. The second investigation used 17 year old subjects, whereas the first investigation used adults aged 18-26. Perhaps this difference, and the difference of laboratory testing versus velodrome testing (added tasks of trajectory and change in position) could explain the difference in results. Another point which is not discussed in these papers is acclimatisation time; the participants have not had any experience with the crank mechanism. While there is some suggestion that this is necessary most research does not tend to involve it, but it may be of interest to see if results varied with a period of acclimatisation involved in the investigation.

The issue of "negative work"(torque reduction)(Neptune & Herzog 1999) is such that some riders have trained themselves to pull the non-driving pedal up so as to remove any torque reduction occurring. Böhm et al investigated whether short-term training with SmartCranks (SmartCranks GmbH, Zug, Switzerland) had any effect on power output(Böhm et al. 2008). These cranks are very different to normal cranks, in that they are able to rotate independently of each other, but they cannot work together. The suggestion is that using these cranks will train a rider to pull up the non-driving pedal therefore removing torque reduction. Two groups were given 5 weeks to train, with one using the SmartCranks and one using normal cranks. Results showed no significant difference with peak power values remaining similar between the two groups. There was, however, a reduction in work during the downward stroke when having trained with the SmartCranks; possibly due to the removal of recovery phase of the gastrocnemius which was acting in both directions.

Figure 2-10; SmartCranks training system; both cranks can move independently of each other but only one can drive the chainring at a time

All of the papers in this subsection have tried to reduce torque reduction with little success. It is still, however a point of interest for researchers and so further work is to be expected in the future.

2.7 Summary

This chapter has covered the literature review which was carried out for this study. Exercise has been defined as "activity requiring physical effort, carried out to sustain or improve health and fitness", and the two types aerobic and anaerobic have been discussed and how lactate build up signifies the difference between the two. The anaerobic threshold is the point at which exercise becomes anaerobic. Methods of measurement such as blood lactate levels, breath composition, and respiratory rate can be used to monitor performance levels, with the latter two shown to agree with MLSS (maximal lactate steady state), the value of the anaerobic threshold. Use of the Borg scale is another option which attaches numbers to give a perceived effort scale.

After discussing exercise the focus moved on to cycling related research. Testing outdoors using an actual bicycle is highlighted as preferential over laboratory testing though the feasibility of this may not be possible depending on necessary test equipment. Cyclists have a preferred cadence which tends to be around 90rpm despite oxygen uptake and energy expenditure being better at relatively low cadences. The idea of “negative work” or torque reduction has been raised, with a minimum identified at a cadence of 90rpm. Cadence is shown to have an effect on the actual cycling technique; knee extension and ankle plantarflexion is shown to alter with cadence which naturally affects how the muscles are behaving during the motion. Cyclist natural technique is suggested to be most effective. Negligible difference in torque profile is discovered between level and uphill cycling if posture is kept constant. A parameter study identified

cadence and crank arm length as having the largest impact on cost function of the five variables used (cadence, crank arm length, seat tube angle, seat height and foot position on pedal).

Due to the intention to use motion capture for this study we next considered research around the subject of cycling movement measurement. Cycling movement is unique to each rider and there has been particularly interest in hip movement in previous papers; this is due to a common assumption when modelling cycling that the limb movement is entirely planar. The researchers identify an intracortical pin to be the best method of measurement though its invasive nature make it unfavourable. They conclude that the method of fixing the hip in a stationary position is suitable for cadences around 90rpm and power outputs of less than 225W as hip movement was minimal in these conditions and this method was least prone to error.

The next topic covered is musculoskeletal modelling, first in general principles and secondly with relation to the musculoskeletal modelling software AnyBody. The inherent redundancy in the body and the inability to accurately measure how muscles are behaving makes musculoskeletal modelling a complex task. The redundancy is due to the human body containing more muscles than it actually needs to carry out any given movement. Musculoskeletal modelling can be done by either forward or inverse dynamics. Forward dynamics takes muscle activations and follows those through to the production of a movement (with muscle force being calculated on the way. Inverse dynamics starts with the motion and solves to find muscle activations (again muscle force is found in this process). Inverse dynamics is preferential as it is a static optimisation process unlike forward dynamics which is a dynamic optimisation so has a higher computational effort cost. However inverse dynamics is heavily reliant on the accuracy of the motion description as previously discussed. The model features bones as rigid bodies with the muscles being described by a modified Hill type model. The AnyBody software features a min/max criterion to overcome the inherent redundancy; the maximum normalised muscle force is minimised throughout the motion. This is equivalent to a polynomial criteria of a very high power but does require a tailored optimisation algorithm instead of standard optimisation methods.

Optimisation was the next subject to be considered. The benefits of surrogate modelling to represent a more computationally expensive cost function have been explained. Combining latin squares with a space filling metric and an evolutionary methods are used to find the best Latin hypercube method. Radial basis functions are utilised by Kriging to create the initial surrogate model which is then searched using genetic algorithms.

Finally we investigated previous research relating to bicycle chaindrive modification. The effect of chainring shape on crank torque, freely chosen pedal rate and physiological responses were investigated, with the Biopace chainring reducing lactate production by lowering necessary muscle force and affecting muscle fibre recruitment. In a separate study performance improvements were found using the Q-Ring. Also oxygen consumption and heart rate was found to be lower using the Q-Ring. The results of both of these non-circular chainrings points toward performance improvements being possible by altering the standard circular chainring. Previous chainring shape optimisation has been discussed with one design being both physically infeasible due to high torque increase at the knee and the presence of cusps in the design. Another study used forward dynamics and an elliptical shape and found a design 60^{o} out of phase with the previous result, with eccentricity decreasing with increased cadence. It will be of interest to see how these results compare to our own designs. Some attention is given to some novel chaindrive ideas. Two papers attempted to increase crank arm length during the drive phase. The first investigation showed a reduction in VO_2 and a theoretical 2% improvement on a one hour test. The second investigator used similar mechanism but with two different age groups and in different situations. Little physiological difference was shown in this case but a performance improvement was seen in the first investigation and not the second. A novel mechanism to train riders to pull up to reduce torque reduction was also examined though no significant peak power difference was found.

Having covered the literature around the subject matter we are studying here we will now discuss the general methods used throughout this study.

Chapter 3 General methods

In this chapter we will discuss the general methods that are applied throughout the document. We will start by outlining the process intended and then give more details as to the specifics of the surrogate and biomechanical models.

3.1 Outline of process

As stated in the chapter 1 we will be testing a methodology of optimising a chainring shape using a computational musculoskeletal model. To do this we will modify the chainring shape using a surrogate model calibrated with experimental data. The method utilised is shown in Figure 3-1. Design of experiments will be carried out for both computational and experimental data points. The experimental data points will provide torque data which will be utilised to infer torque profiles for new chainring shapes. The design of computer experiments will provide the chainring shapes that will be used for the sampling which the normalised muscle force surrogate model will be based upon. The chainring shapes will be combined with torque profiles based on the experimental data and fed into the AnyBody software which will return a value for maximum

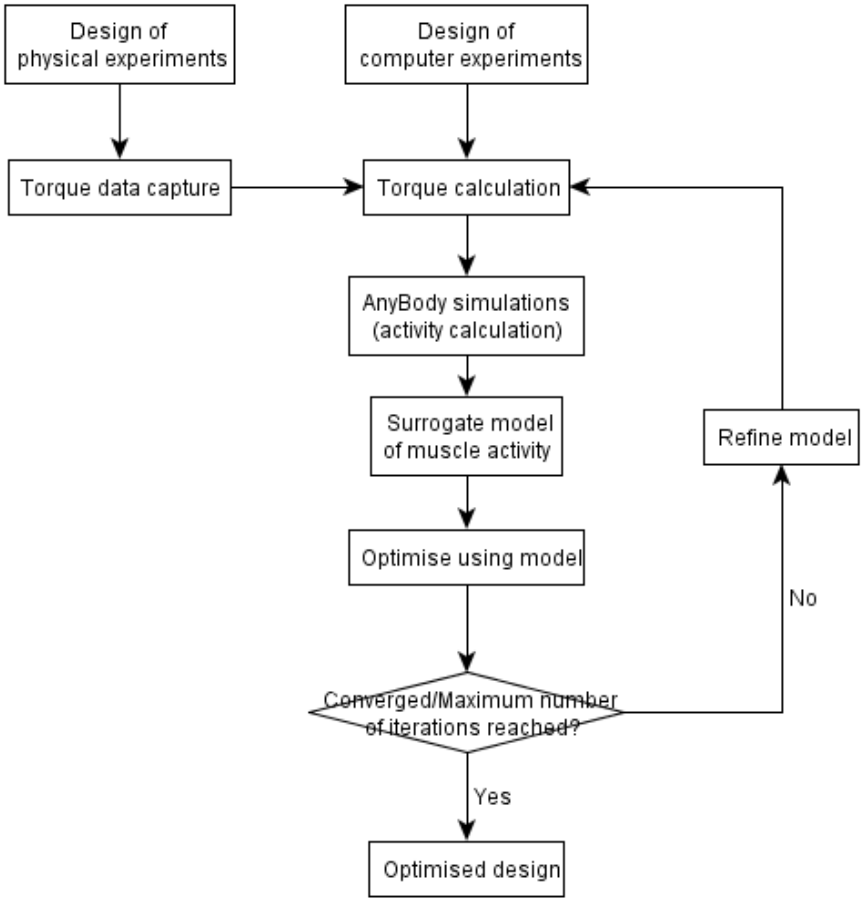

Figure 3-1; Flow chart of optimisation process

muscle activity. This is the metric targeted for optimisation and is the value of the normalised

muscle force. From this point on we will refer to this metric as the normalised muscle force to avoid confusion with actual muscle activity. These data will then populate a surrogate model of the normalised muscle force which will then be used to suggest an improved shape. This shape will then be run through the AnyBody software and these data will be used to refine the surrogate model. This loop will continue until the convergence criteria is met or the maximum number of iterations is reached.

3.2 Optimisation methodology

This section will look in detail at the optimisation methodology and the details behind the methods being used which have not already been covered in the literature review. As we have already stated the sampling plan will be made using a space filling metric, and the data will have a surrogate model based on Kriging fitted to it enabling the use of likelihood to search the design space .Genetic algorithms will be used to search the likelihood. We will also be using expected improvement to select our new data point location, and using imputation to handle infeasible results which occur. As expected improvement and imputation have not been covered yet they will be detailed here.

The method of improving the surrogate model used here is a search and infill strategy, whereby a new point is predicted as an improvement, and then the actual value of this point is used to improve the surrogate model. As such the method of selection for an infill point is quite important, especially as number of infill points can be limited due to computational cost. One way is to utilise the probability of improvement

$$P[I(\mathrm{x})] = \frac{1}{\hat{s}\sqrt{2\pi}} \int_{-\infty}^{0} e^{-\frac{[I-\hat{y}(x)]^2}{2s^2}} dI$$

Where $P[I(\mathrm{x})]$ is the probability of improvement at x, $\hat{s}$ is the RMSE (root-mean-square-error), I is the improvement, and $\hat{y}(\mathrm{x})$ is the prediction of the function at that point. We know that the global optimum will eventually be discovered as $P[I(\mathrm{x})] = 0$ when $\hat{s} = 0$. This zero probability of improvement at an already sampled point means sampling will eventually become dense, leading to the optimum being found. We can improve on this method though by also looking at the amount of improvement we expect to find, the expected improvement. This is given by

$$E[I(\mathrm{x})] = \begin{cases} (y_{min} - \hat{y}(\mathrm{x}))\boldsymbol{\Phi}\left(\frac{y_{min} - \hat{y}(\mathrm{x})}{\hat{s}(\mathrm{x})}\right) + s\phi\left(\frac{y_{min} - \hat{y}(\mathrm{x})}{\hat{s}(\mathrm{x})}\right) & if\ s > 0 \\ 0 & if\ s = 0 \end{cases}$$

where $\boldsymbol{\Phi}(.)$ and $\phi(.)$ are the cumulative distribution function and probability density function respectively. Again, for the same reasons as the predicted improvement, the expected improvement will also always find the global optimum.

The second of these two details which we will look at is the use of imputations to handle infeasible results. In a design space there is the potential for areas of infeasibility, areas where the combination of variables results in a failed simulation for one reason or another. When this occurs during surrogate modelling it is important to handle these results in the correct way. One method is to use a basic penalty function whereby a failed simulation is given an arbitrarily high value (if you are searching for a minimum) to mark that simulation out as infeasible. The downside of this is that in can drive the search away from the surrounding area and the feasible results which are there. An imputed value should serve to divert the search to the feasible region by reducing the expected improvement $E[I(\mathrm{x})]$ at that point to zero. As we move away from an area of feasible designs

$$\|\mathrm{x}^{(n+1)} - \mathrm{x}^{i}\| \to \infty$$

$$\psi^{(i)} \to 0$$

$$\hat{y}\left(\mathrm{x}^{(n+1)}\right) \to \hat{\mu}$$

I.e., predictions are higher than optimum. If functions have a low modality ($\hat{\theta}$), updates are drawn to the surrounding area of infeasibility. If we instead use $\hat{y} + \hat{s}^2$,

$$\|\mathrm{x}^{(n+1)} - \mathrm{x}^{i}\| \to \infty$$

$$\hat{y}\left(\mathrm{x}^{(n+1)}\right) + \hat{s}^2\left(\mathrm{x}^{(n+1)}\right) \to \hat{\mu} + \hat{\sigma}^2$$

and

$$\|\mathrm{x}^{(n+1)} - \mathrm{x}^{i}\| \to 0$$

$$\hat{y}\left(\mathrm{x}^{(n+1)}\right) + \hat{s}^2(\mathrm{x}^{(n+1)}) \to y(x^{i})$$

Using $\hat{s}^2$ instead of s keeps the surrogate model smooth when imputations are located close to feasible points. By using imputation we can continue the searching of the model even when results fail.

The process of the code works like this:

1. Produce sampling plan

2. Sample design space
3. Construct surrogate based on successful points
4. Impute failed points based on surrogate model
5. Construct surrogate based on successful and imputed points
6. Search surrogate for improvement
7. Take new infill point
8. Repeat steps 3-7 until convergence criteria has been met or maximum number of iterations has been reached

For this investigation the target function for optimisation, in this case minimisation, will be the normalised muscle force (maximum muscle activity in AnyBody) for all muscles, as such we will only concern ourselves with the peak value of all the muscles at once. Details on sample sizes and number of iterations will be defined by each investigation.

3.3 Biomechanical Model development

The AnyBody software is provided with a repository which contains an assortment of models, some produced by the company, and others by users which are validated before inclusion, for different purposes and with varying levels of complexity. These include an arm curl model, several gait models, and three cycling models of increasing complexity. Two of these models have been used in this work, while one of the gait models has been modified for use also.

The three cycling models are as follows; a two dimensional (2D) model, a three dimensional model (3D), and a full body model. The full body model is not utilised as it produces the same lower limb results as the 3D model while taking more computational time due to the addition of the upper body muscles. These models are all set up to model one revolution of the chainring; to do this they take in the values for the cadence (in revolutions per minute), and the power

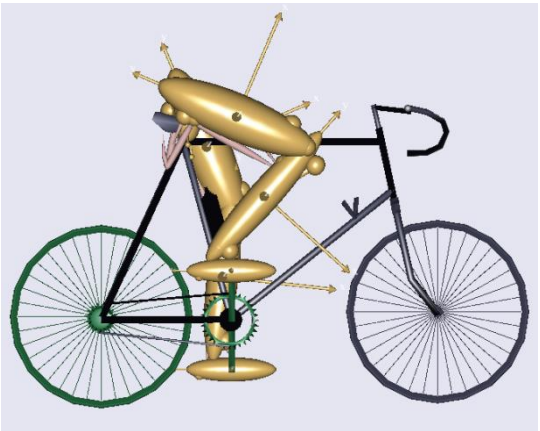

Figure 3-2; 2D bicycle model from the AnyBody repository (Model 1)

output (in watts), along with bike setup specifics such as pedal arm (crank) length and width (in mm), and seat position height and lateral position (in mm). The model then performs an inverse dynamic analysis, as explained earlier, to solve this movement and calculate the muscle forces required to complete. All three models use the same bicycle model with the differences all being in relation to the human part of the model.

The first model used was the "2D" model which can be seen in Figure 3-2. This model is not actually two dimensional, but the name convention works to identify this version as the simplest cycle model available. Going forward we will refer to this as Model 1. 8 muscles are included in each leg of the model; the hamstring, biceps femoris, gluteus maximus, rectus femoris, vastus, gastrocnemius, soleus, tibialis anterior. This is a very simple leg model which takes approximately 5 seconds to load and run.

The second model is the 3D model as seen in Figure 3-3. The model contains the upper part of the body not including the shoulders and arms. Some lower torso muscles are also included and the leg and foot muscles are much more detailed than the previous model. There are approximately 42 muscles per leg, which gives the model a load and run time of approximately 45 seconds. Going forward we will refer to this model as Model 2.

The initial conditions of the human component are all defined in the body component files, these

Figure 3-3; 3D bicycle model from the AnyBody repository (Model 2)

are in a separate file to the application files, as they can be utilised by all application files. These conditions were left at the default values, which have been set up using the literature. The final model used was based on a gait model (called GaitLowerExtremity) in the repository which was altered. Force plates that were present in the initial model were removed and a crank/crank arm model was introduced. The lower body model in this instance is the most advanced and complex

body model we will use. This human model is referred to as Twente Lower Extremity Model (TLEM), and consists of 159 muscles and 6 joint degrees of freedom. The model based on recently published work in Clinical Biomechanics(Klein Horsman et al. 2007), is still being completed but an almost complete model is used here. As such this model is similar to the 3D model, but with more muscle groups included to enable more detailed investigation into specific muscle responses and activation. This model will be referred to as Model 3.

Name/description	Reference name	Number of muscles	Run time (approx.)
2D model	Model 1	16	5 seconds
3D model	Model 2	84	45 seconds
GaitLowerExtermity (modified)	Model 3	159	360 seconds

Table 1; AnyBody model summary

It should be noted that none of the biomechanical models discussed here consider the effect of frictional losses associated with the chaindrive. We have mentioned some of the alterations that were necessary with the most complicated model, but other alterations were necessary for all the models. The system needed to be modified so that investigations using rider torque data and user defined chainring shapes could be undertaken. The torque in the cycle models was originally calculated at each time step depending on the stage of the revolution; this was changed to a lookup table based on experimental data which the model interpolated between depending on the time step. The next stage was control of the chainring shape which we will discuss in the next section. The calibration of the final model will be discussed in the next chapter where we will cover the data collection and its uses.

3.4 Chainring shape modification

A circular chainring should give a constant angular velocity, assuming the rider is pedalling uniformly, so it stands to reason that changing this velocity is the same as increasing or decreasing the local radius at that time. This is achieved by modifying the angular position of the crank during the cycle; a lower angular velocity when the chainring is slower representing an increase in local radius and a higher angular velocity when the chainring is faster representing a decrease in local radius.

Once a chainring shape has been identified by the surrogate model the shape is translated into a local cadence profile. With this cadence profile we can then extrapolate the inputs we need to drive the musculoskeletal model. For Models 1 and 2 this takes the form of adjusting the angle of the right crank arm at a given timestep so that the cadence during the timestep is correct. For

Model 3 a similar procedure is done; although in this case we interpolate the motion capture data to accelerate or decelerate the motion of all of the markers as required.

One of the primary ways in which the shape was defined was by use of a Fourier series expansion. The use of a Fourier series expansion gives a level of control over the shape while keeping the number of variables required to describe the shape to a low easily manageable number. The Fourier series used here is defined as:

$$f(\theta) = a_0 + \sum_{n=1}^{5} [a_n \cos(n\theta) + b_n \sin(n\theta)] \quad (1)$$

a_0 is the point at which the expansion fluctuates which in this instance is set to 90 (i.e. 90rpm). By summing this equation between $n = 1$ and $n = 5$ we generate 10 coefficients to change; $a_1$to a_5 and b_1 to b_5. $\theta$is the rotation point of the chainring, with 0 representing the right crank arm at 90°. This expansion allows for a good approximation of any smooth periodic function. By increasing the number of terms the level of detail is increased; for simple functions this requires only a couple of variables, with more required as complexity increases. For description of the chainring the approximation was expanded to eleven terms; starting point plus ten sinusoidal terms. This value was decided on as it provided a decent level of control over the shape while still allowing for acceptable computational time for optimisation.

3.5 Summary

This chapter has discussed the general process, optimisation methodology, biomechanical model development, and the chainring shape modification. The general process utilises both a design of physical experiments and a design of computer experiments. These feed into a torque calculation for a designed chainring shape which is used to drive the biomechanical model which in turn returns a value of normalised muscle force which is identified as the target metric. Surrogate modelling is used to search the design space until an optimised design is found. Kriging is used to predict the design space not covered by data points. Genetic algorithms are used to search the likelihood, while imputation is used for non-feasible data points to allow for data close to these points to be considered.

Three biomechanical models are detailed; Model 1 (2D model), Model 2 (3D model), and Model 3 (modified GaitLowerExtremity model). Each of these models has increased level of complexity over the model before allowing for higher fidelity results to be collected. This increased complexity results in higher run times which have been detailed. The models do not consider frictional losses associated with the chaindrive.

Finally we have discussed modification of the chainring shape which has been achieved by increasing/decreasing the local angular velocity (local cadence). For Model 1 and 2 this was achieved by modifying the crank angle at a given timestep while for Model 3 the motion capture data was interpolated to accelerate/decelerate the local angular velocity as necessary. The primary shape definition used here was a Fourier series expansion with 10 coefficients. Having detailed the general methods we will now move on to the data collection which provided the data used in the models discussed in this chapter.

Chapter 4 Data collection

To computationally model a cyclist, and hence design a tailored chainring, actual data is required. To this end it is necessary to ask the cyclist to cycle in an environment where we can monitor them, using equipment to measure and record specific data. This chapter will discuss the equipment and experimental protocols which have been utilised to achieve these goals.

4.1 Equipment used

The computational model is calibrated using experimental data from a specific rider. These data are collected via a variety of equipment. The equipment used is as follows:

- Bicycle ergometer
- Bicycle
- Instrumented crank arms
- Motion capture equipment
- Data logger
- Breath analyser
- EMG electrodes

The bicycle ergometer used is the Tacx Cycleforce i-magic (as used by(Ettema et al. 2009). This claims to be able to recreate the resistances of rolling, air and incline, while also being able to make the cyclist feel like they are riding on different surfaces. The resistance control is done using an electromagnetic brake, which allows for the power output of the bike to be controlled via the system. This means the resistance is raised if the cadence of the cyclist decreases to maintain the power, and vice versa, enabling data collection to be done at a constant power

Figure 4-1; Tacx Cycleforce i-magic cycle ergometer. An electromagnetic brake allows for simulating resistance of rolling, air, and incline.

output. The ergometer also holds the bike vertically so that the study can be carried out with non mobile equipment.

The bike used to carry out data collection is a Specialized S-Works Roubaix with Shimano Dura-Ace components. It is an off the shelf bicycle designed for endurance road cycling.

The instrumented crank arms used are part of the SRM Science power meter system. This has strain gauges built into the crank arms which enable high density data collection throughout the revolution, including both total torque and power output. Cadence is also measured though this is only calculated once per revolution so does not measure local cadence, i.e. the specific cadence at that point during the revolution. The specific model used is the Octalink Shimano which quotes an accuracy measurement of +/-0.5% on the supplied datasheet.

Figure 4-2; Photograph of experimental platform from a data collection session. Bike is mounted on the ergometer with the SRM cranks mounted on the bike. Motion capture markers have been placed on the bike and rider and the rider is wearing a breath analyser mask

One of the main calibration techniques used is motion capture. This is undertaken in a laboratory specifically equipped for motion capture, with the motion of the cyclist's lower body being tracked and recorded. The motion is then used to drive the model in a realistic manner for the

rider in question. The motion capture system used is the 12 Camera (6x T40 and 6x T160) Vicon MX T-series motion capture system. While exact tracking of the HJC such as the STD method, as discussed in the literature review, would prove to be useful in modelling a rider, its invasive nature makes it very unattractive to the author so the use of normal motion capture equipment will be used. This has the advantage of subjects being more likely to participate and involving less risk. The Helen Hayes marker system (Kadaba et al. 1990) gives an accuracy of +/- 3mm using a 5 camera system, and is widely used. Modification of this system should provide enough accuracy for motion capture. Markers are attached to the subject in a predefined manner (Helen Hayes(Kadaba et al. 1990) marker set plus markers for bicycle), to match with a model held in the system, these enable the system to track the markers and record their movements. When combined with the knowledge of what the markers are attached to, this means the lower body movement is captured and can be used in the cycling model. This movement data will then be used to drive the model, ensuring the model is moving in the same way that the test subject is. This improves the validity by making sure the model is not moving inaccurately and thereby using the muscles in a manner unlike that of the rider in reality. The system is used to capture only the lower body movement to keep time costs to a minimum.

The data logger allows storage of the data from the SRM cranks. The model used is the DL1 Data Logger (Race Technology Ltd, England) which allows for 13 external inputs and samples at 100Hz. Data is stored on a memory card.

To assess the rate the cyclist is performing at and to ensure performance below the riders lactate threshold, the cyclist wears a portable Vo2000 analyser (as used by Carey et al. (2005)). This monitors breath composition and allows for an assessment(Carey D.G., 2005) of the level to which the rider is performing. It will then be possible using the analyser to keep the rider below their lactate (or anaerobic) threshold so that the activity remains an aerobic activity. This is important as muscle behaviour is different during anaerobic exercise when compared with aerobic exercise. This breath analysis also enables data collection to be carried out in a physiological steady state fashion as data is collected once these readings have plateaued implying the body has adjusted to the new conditions.

4.2 Testing procedures

The data collection is divided into three segments; an initial torque data collection session for the initial torque model, a motion capture (and other data) collection session, and a tertiary session to collect the torque readings needed for the second torque model. The same

competitive male cyclist (regular participation in cyclo-cross events) was used for all sessions. Biodata for the rider was as follows:

- Age: 31
- Height: 185.42 cm
- Weight: 71.67 kg

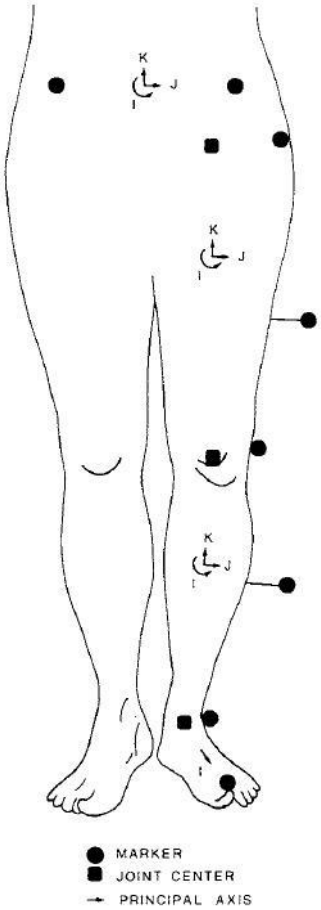

Figure 4-3; Helen Hayes marker set used as the basic for our motion capture session

The initial torque data collection was undertaken using the circular chainring that was supplied with the SRM system, to collect torque information for various power outputs and cadences. The data range investigated was cadences between 60 and 120 rpm at 10rpm intervals and the power range between 100W and 300W at 50W intervals. The collection was undertaken in a systematic method starting at 100W and 60 rpm and raising the cadence up to 120 rpm then raising the power output by 50W and working back down to 60rpm. This method was repeated until 300W and 90rpm at which point the collection was stopped at the cyclist's request. No data was collected for 300W at 100rpm, 110rpm or 120rpm.

The second data collection was carried out to gather information for more variables. Testing occurred in the biomechanics laboratory in building 45 of the University of Southampton. Ethical approval was provided by the School of Health Sciences Ethics Committee (SoHS-ETHICS-09-021) (University of Southampton).Torque, cadence, power, motion, EMG, and HR were collected. EMG markers were placed on the right and left vastus lateralis and medialis, making four sensors in total. A total of 23 markers are used to track the motion; 18 for the cyclist and 5 for the bicycle, based on a modified Helen Hayes marker set as specified earlier. The cyclist markers were placed so that both left and right sides had the same markers. These were as follows; tip of the big toe, heel, ankle, tibia, thigh, knee, iliac crest, posterior superior iliac spine, anterior superior iliac spine. The 5 bicycle markers were placed on the left and right pedals, the left and right sides of the bottom bracket and the saddle. Two chainrings were used in this part of the investigation; the standard chainring and the Rotor Q-Ring. The effects of varying saddle height, cadence, and crank arm length were also investigated. The standard chainring was used as an initial investigation before the tests using the Q-Ring were started. To this end a sampling plan, as described previously, was devised to give a good spread of data across the design space of the four variables (chainring orientation, cadence, saddle height, and crank arm length). The cranks are variable from 150mm to 190mm in 2.5mm intervals; this gives a plan size of 17 distinct points. Saddle height is varied between +20mm and -20mm in 2.5mm intervals as well, with 0 taken as the riders' original seat height which was in the position of most comfort. Cadence is varied between 70rpm and 110 rpm in 2.5rpm intervals. This covers the riders comfort range. Finally the symmetrical nature of the Q-Ring is exploited with holes 1 through 17 of 35 being used as the orientation. The orientations are based on the Q-Ring predefined orientations with holes 1 through 5 being marked and the remaining holes identified using the logical progression of the numbering. The sampling plan is split into two subsets (one 8 points and one 9 points) with both being individually space filling to minimise both random and systematic error. This means that either could be used as a standalone sampling plan. The sampling plan can be seen in Table 2.

This data collection session ran over two days with the standard chainring, test one, two, and three carried out on the first day and tests four to nine and twelve undertaken on the second day. Tests one, two and three were also repeated on this day. Tests ten, eleven, and thirteen through seventeen were not completed due to lack of time. All these tests were carried out at a power output of 250W. This value was selected as it represents a level which while requiring effort by the cyclist can be maintained for prolonged periods. It also matches up with the power level used several times in the literature(Kautz & Hull 1995).

Following the investigations detailed in chapter 6 the investigator believed that more torque data was required at and around the targeted optimisation point from both the circular chainring and the Q-Ring. The torque data previously corrected had suggested a relationship with how the chainring radius was varying and the torque being generated so it was desirable to collect more experimental data. A third session was carried out whereby more torque data was collected using the circular chainring and the Q-Ring. This was all carried out at 250W between 70rpm and 110rpm. The chainring orientations selected were zero, four, eight, twelve, and sixteen as this gave a good spread of the possible orientations. Testing occurred in the following order; circular, twelve, four, zero, eight, sixteen. In each instance the test started at 110rpm and was decreased by approximately 10rpm until at 70rpm, and then increasing by 10rpm until back to 110rpm. These data were for use in the second torque model which we will discuss later.

Saddle height (mm)	Crank arm length (mm)	Cadence (rpm)	Chainring orientation
-17.5	155.0	75.0	5
12.5	162.5	95.0	4
-2.5	172.5	72.5	1
-15	185.0	82.5	8
-7.5	175.0	102.5	17
0.0	152.5	107.5	13
-20.0	165.0	92.5	11
5.0	167.5	70.0	12
20.0	170.0	97.5	14
-12.5	160.0	110.0	6
17.5	150.0	85.0	10
7.5	190.0	90.0	3
-5.0	157.5	80.0	16
15.0	177.5	77.5	7
10.0	182.5	105.0	9
-10.0	180.0	100.0	2
2.5	187.5	87.5	15

Table 2; Data collection plan for the second data collection session. Saddle height is in mm and the rider's normal saddle position is taken as 0. Crank arm length is varied between 150 and 190 mm, cadence is in revolutions per minute. Chainring orientation refers to the mounting position of the Q-Ring, holes 1-5 are marked and other positions are worked out from these markings

4.3 Model Calibration

The data mentioned in the previous section is used for a mixture of model calibration and results validation. Torque, motion capture, and power output data is all used to calibrate the model. The calibration which has been used for each investigation will be outlined in those specific discussions. The EMG data collection had been intended to allow for validation of computational results from the biomechanical model. Unfortunately the data recorded from the EMG sensors was just noise and did not provide us with any useable information.

4.4 Summary

In this chapter we have looked at the equipment and procedures which have been used to gather the experimental data. Instrumented crank arms, and two different shaped chainrings are attached to an endurance road bicycle which is mounted on an ergometer allowing for data collection of torque, cadence, and power output. This equipment was supplemented in the second data collection session with motion capture equipment, EMG sensors, and breath analysis to provide more information for calibrating and validating the biomechanical models used in this study, and to ensure data collection was carried out with the rider in a steady state. These data are then used to carry out the investigation into optimising the chainring shape for the rider. Some processing of data is necessary and this will be discussed when it is utilised.

Chapter 5 Torque models

Along with the local cadence profiles we use to model the chainring shape, the other main input in to the musculoskeletal model is a torque model. This gives the musculoskeletal model data on how much force the legs are producing and allows for the muscle activity calculations to take this into account. We infer the torque profile for a given local cadence profile using a model based on a set of experimental data collected from different chainring shapes at varied cadences and power outputs, with the specifics of these variations defined in the relevant section. Torque data was acquired at 100Hz by the data logger described in chapter 4 (effectively 67 data points for a 90rpm revolution). During the course of this investigation two torque models were utilised, an initial model, and an improved model which we will now discuss. In both cases the models used the same inputs; a local cadence profile for the intended chainring, and a target power for the model. These inputs allowed the models to generate a torque profile for one revolution of the bicycle chainring.

5.1 Initial model

The initial torque model was created using the experimental data collected from the first session, as detailed in section 4.2 Testing procedures. These data of torque profiles for a circular chainring at varied cadences (60-120rpm in 10 rpm intervals) and varied powers (100-300W in 50W intervals) was used to create a surrogate torque model that was used in the initial investigations. With this raw data kriging was used to predict coefficients for a Fourier series, see section 3.4, which was used to describe the torque profile. Figure 5-1 shows an example torque profile generated for a circular chainring at 90rpm and 200W output. Following the acquisition of the Q-Ring and the decision to target the optimisation at the 250W mark this torque model was replaced with an improved version as detailed in the next section.

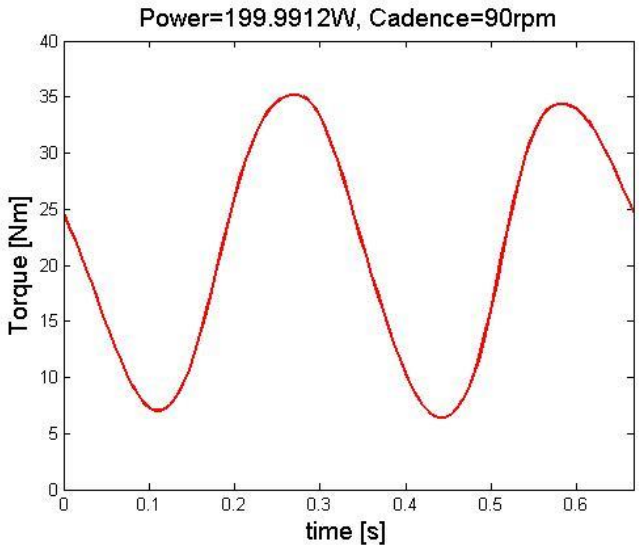

Figure 5-1; Torque prediction for a circular chainring from initial model

5.2 Improved model

After using the initial torque data for preliminary investigations another torque data collection session was carried out. This was used to collect torque data for varying cadences at the same power output (250W) and with different chainring shapes (circular and 5 different Q-Ring orientations). The aim of this was to record more torque data with which to make the surrogate torque model more accurate. Cadence and torque were stored using the data logger. Using the data collected from the second data session it was possible to identify the angle of the right crank arm when the cadence reading is taken (this is only read once per revolution). Data from the motion capture file and data logger were synced using a pulse on both files. The time between this pulse and the cadence reading was measured and then used to identify the marker coordinates for the right pedal at that time. This gave a value of ~55° clockwise from vertical. This was accurate for that specific revolution but it may be worth in future looking at angles for different rotations to see if there is any drift or variation in that data. Due to the cadence reading only being taken once per revolution the raw data for the cadence is stepped. Using these data the torque data for each revolution, with the right crank starting at 90^0, was processed. This start and end point was defined as 35/360 from the change in cadence.

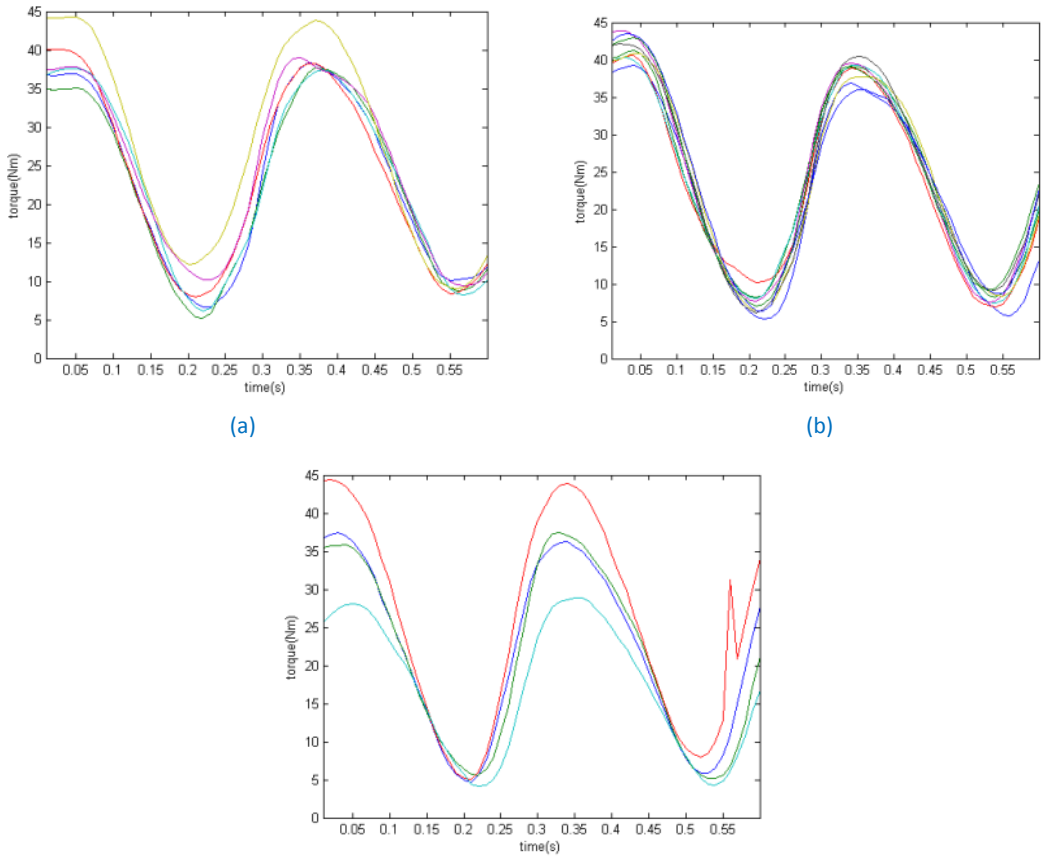

Figure 5-2; Example torque profiles from third data session. (a) torque profiles at 85 rpm (b) torque profiles at 90 rpm (c) torque profiles at 95 rpm

Each torque profile is stored with those of the same cadence (each value is rounded to the nearest whole number, in rpm). As shown in(c) Figure 5-2 again the torque profiles are a lot cleaner for 90 and start to vary more as you move away from this value. The method of determining the starting point of the revolution does however look to be robust as all torque profiles start in the same relative point. If the cadence reading is found to drift, possibly due to the cadence at that time, then this will need to be incorporated and will shift the torque profile accordingly.

With this torque data stored it was then possible to produce an improved torque model. This torque model takes the same inputs as the initial torque model and again returns an estimated torque profile for the chainring shape generated by the optimisation code.

1. With the local cadence profile for the whole chainring passed to the function the first stage is identification of the intended sample profile size.

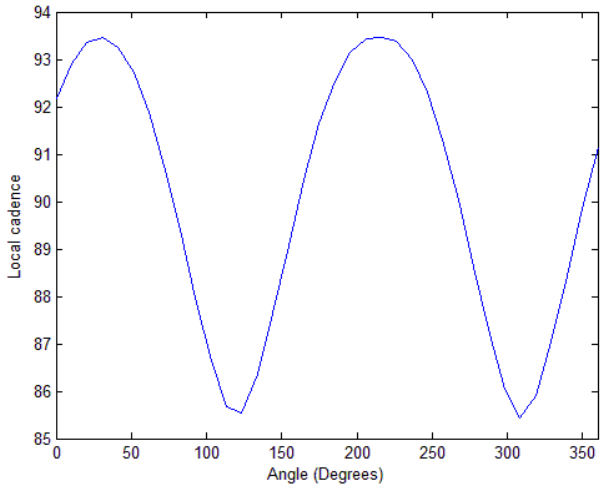

Figure 5-3; Initial cadence profile

a. Initially the mean local cadence is found (e.g. 90.0867 from Figure 5-3), this is then compared with the cadences of the circular chainring torque profiles and all profiles within 1 RPM of the mean local cadence are identified.

b. As the torque profiles have different data lengths depending on cadence so the mode of the torque profile lengths is then calculated.

Length of torque profile (in data points)	Number of profiles
66	1
67	9
68	12
69	3
70	1

Table 3; Examples of variation in torque profile length and distribution of profiles

c. We then scale the local cadence profile to match this size to reduce the amount of interpolation of the torque data required.

2. The local cadence profile is then stepped through to identify a torque value at each point along the rotation.

   a. At each point the gradient of the cadence profile is calculated (using first order central difference method) along with the gradients at the same point for each of the different Q-Ring rotations based on the local cadence profile found in section 6.2 Q-Ring investigation (the circular chainring has a constant 0 gradient as the local cadence is constant).

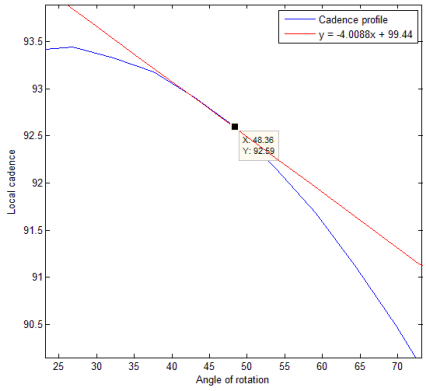

Figure 5-4; Gradient calculated at a step along the cadence profile of the shape being tested

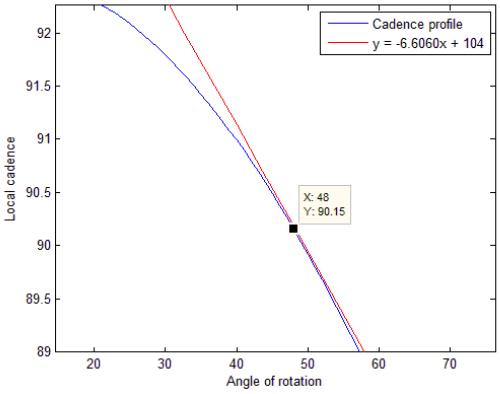

Figure 5-5; Gradient at same point along the cadence profile of the Q-Ring on hole zero

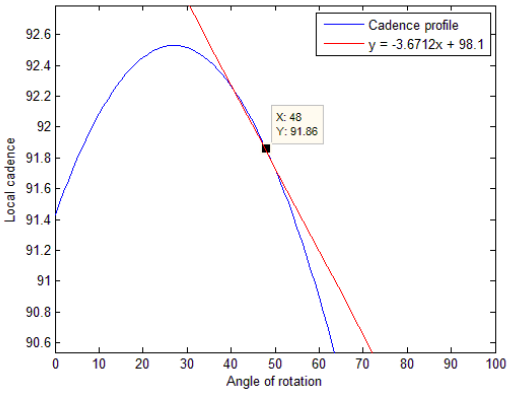

Figure 5-6; Gradient at same point along the cadence profile of the Q-Ring on hole 4

b. The gradients are then compared to assess which profiles would provide the best data to utilise.
    i. If there is a match in the gradient then that dataset is the only one utilised for that point, if there is not a match then the two closest profiles are used with a weighting used based on which is closer.

3. Again we compare the local cadence at the selected point with the datasets which have been identified to filter out the torque profiles of interest.
4. A polynomial is then fitted to the identified torque profiles and their associated powers allowing for a single value to be given at the stage in the rotation we desire.
5. With torque data generated for the entire rotation we then apply a fast Fourier transform to smooth the data, providing us with an expected torque profile for the local cadence profile that has been generated.

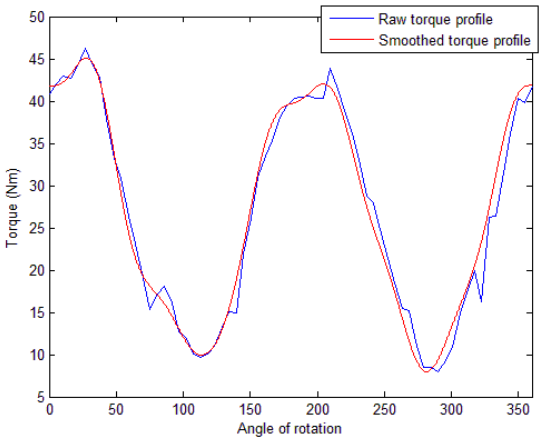

Figure 5-7; Predicted torque values and smoothed torque profile from improved torque model

5.3 Validation

To validate the torque profiles being generated by the second model we removed each of the torque datasets for the Q-Ring rotations in turn and carried out a prediction of a torque profile of the orientation that was removed. Figure 5-8 through Figure 5-12 show the results of these predictions versus the mean of the original datasets.

Chainring orientation	Mean squared error of prediction vs mean
Q0	7.2001
Q4	7.7661
Q8	9.2342
Q12	4.3993
Q16	13.8095

Table 4; Mean squared error of prediction torque profiles against actual data

The prediction for Q8, and Q12 seems to be a little out of phase on looking at the plots although the Q12 model gave the lowest mean squared error. Looking at the mean of the raw torque data we can see that for those configuration the peaks are slightly later in the rotation, probably caused by the rotation of the Q-Ring. The final configuration, Q16, looks to be in phase but has slightly higher peaks than the raw data mean. This is due to the lower peaks of this configuration; as the torque model is using the other rotations which has higher peaks it naturally predicts higher prediction for that rotation. By including torque profiles such as that for Q16 we give the torque model the ability to predict torque which doesn't "flow" quite as nicely as the other orientations, or profiles that are slightly out of sync such as Q8 and Q12.

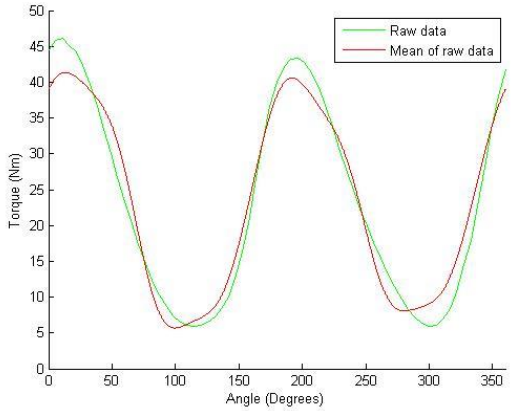

Figure 5-8; Q0 prediction versus actual torque data

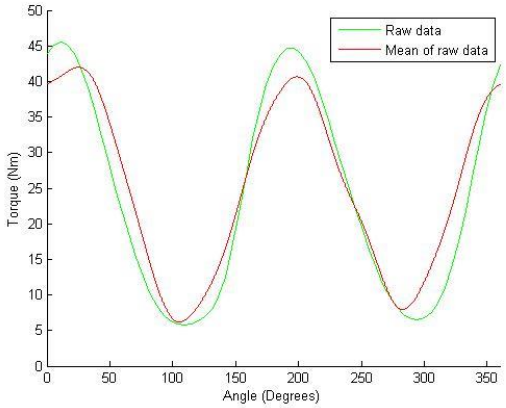

Figure 5-9; Q4 prediction versus actual torque data

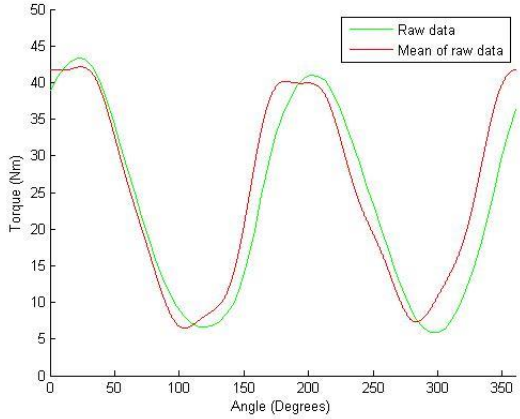

Figure 5-10; Q8 prediction versus actual torque data

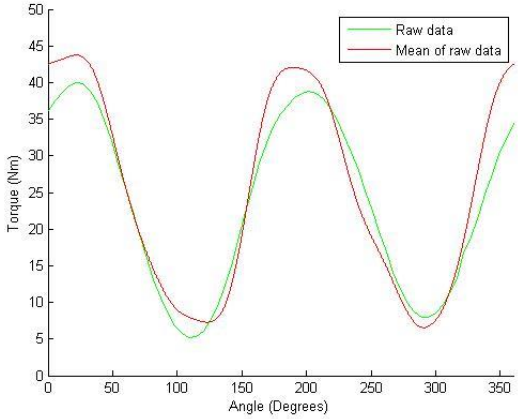

Figure 5-11; Q12 prediction versus actual torque data

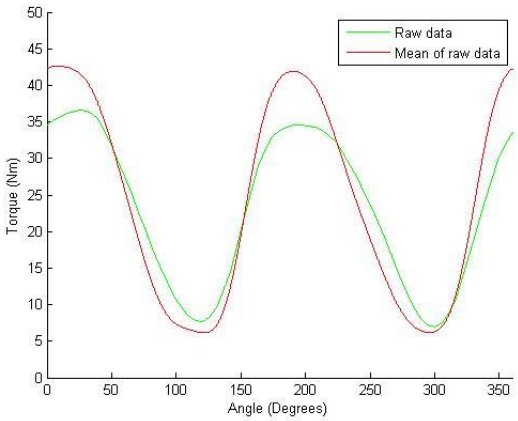

Figure 5-12; Q16 prediction versus actual torque data

5.4 Summary

In this chapter we have discussed the two torque models which have been used in this investigation. Both models take an input of a local cadence profile and use this to produce a

torque profile which the biomechanical model can utilise. An initial torque model was created based on data collected using a circular chainring at varying cadences and power outputs. These data were used to create a surrogate model to predict torque profiles from. After a decision was made to target a specific cadence (90rpm) and power output (250W) a second torque model was created using both a circular chainring and a Q-Ring. These data were combined with knowledge of the variation of the non-circular chainring to try and create a torque model which was more suited to predicting torque profiles for non-circular chainrings. This second model utilised comparisons with rate of change of radius to base its predictions on the most suitable source data. We have shown that it is necessary to have this source data to improve the ability of the torque model to more accurately predict results. Having detailed the general methods, data collection techniques and the torque models used we may now move on to discussing the results of the investigations undertaken as part of this study.

Chapter 6 Preliminary work

6.1 Results from basic models

This section will cover the work which was undertaken between the first and second test sessions. As such the only experimental data used here is torque data gathered at varying powers and cadences as set out in the last section.

6.1.1 Initial data collection

The first task that was undertaken with the collected torque data was to perform a visual inspection of the results.

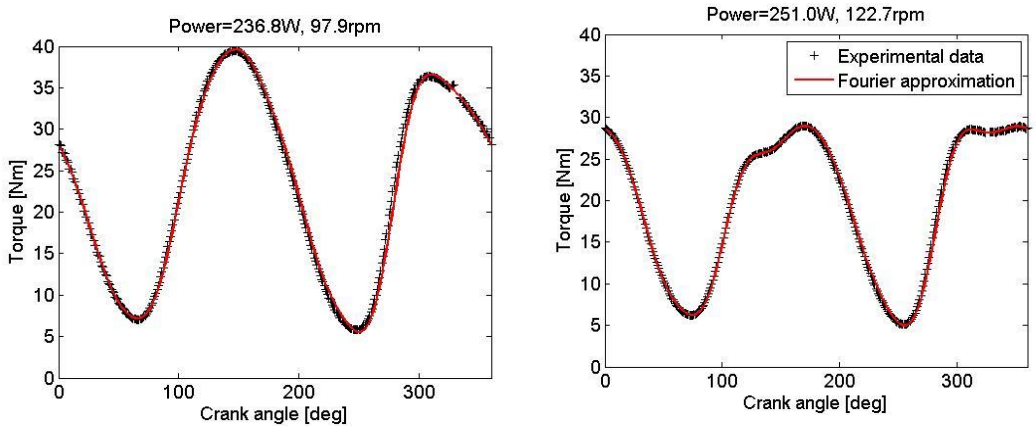

Figure 6-1; Example torque profiles at similar power outputs but differing cadences with 0 crank angle representing right crank arm in the horizontal position. Experimental data and the Fourier series approximation for that data is shown. The artefact at ~320 is due to magnetic cadence sensor

Figure 6-1 shows two plots of torque profiles collected. There is a noticeable artefact in both of these plots at approximately 320 degrees. This may be due to the point at which the magnet which is used to measure the cadence passes the wire inducing a change in the current properties of the wire and hence the reading. It should be noted, as shown in the section 5 of this document, that this artefact is not always present, but when present is always in the same location. As such it could be processed if it was found to be causing impacts on results. These plots are at similar power outputs but different cadences. These plots also show the Fourier series approximations (discussed earlier) used to train the surrogate model which was used to predict torque during the chainring optimisation. In both plots the left crank starts at the 3 o'clock position (90^{o} right of vertical) and rotates clockwise until it returns to its original position. These plots reveal the torque to be asymmetrical, they also appear to show a high cadence dependency. For cadences close to the optimum cadence the torque profile is "purer", in the sense that it is smoother and more sinusoidal. As the cadence is moved away from this optimum the "purity" decreases and the profile changes with reduced peak torque and the development

of non-distinct peaks. The asymmetry in particular is worth noting as it points towards any symmetrical chainring not being effective for this rider. These data should result in an asymmetrical chainring design being found.

6.1.2 Methodology implemented

The method used to modify the chainring shape has been discussed in the chapter 3 so this section will detail how the modification of the rotation speed was carried out for the results in section 6.1. The optimisation of a chainring shape required the use of a flexible method of description, so a Fourier series expansion as detailed in section 3.4 was used. This approach was also utilised to approximate the torque data allowing for a reduction in the size of data required in the torque surrogate model (initial torque model). The expansion is used to approximate the local cadence which is then converted into the driver for the crank in the AnyBody model in the form of the rotation speed as discussed earlier.

The optimisation of the chainring shape was undertaken in the following way; with the same method being used for both Model 1 and 2. The surrogate model of torque vs cadence is produced. A design of computer experiments is carried out, giving the initial points for the surrogate model of the activity. For each of these initial points the torque profile is calculated for the given chainring shape based on the torque surrogate model. The torque profile and local cadence profile are then passed to the musculoskeletal model. The normalised muscle force is then calculated for each of these starting points, thereby populating the surrogate model. Once the surrogate model has been populated it is explored by identifying a potential variable combination that will provide an improved result. Once the actual normalised muscle force for this point is calculated it is fed back into the surrogate model and the exploration continues until a given number of iterations has been carried out or the predicted improvement of the next point has dropped below a given threshold.

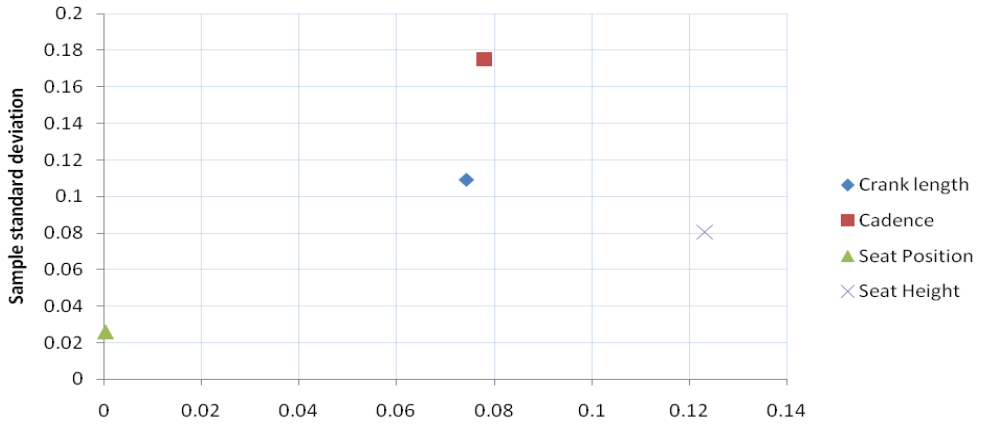

Figure 6-2; 4 variable parameter study results; proximity to the origin gives variable sensitivity in the overall function, crank length and seat height are shown to be the most important with seat position being the least.

6.1.3 Initial optimisation results

The first investigation carried out was a parameter study (similar to the sensitivity analysis of (Hull M.L, 1989)) of our own using the AnyBody software (version 3) and Model 1. The four variables modified were seat height, seat lateral position, cadence, and crank arm length. A (Morris) screening plan was created for four variables, this was then used to acquire normalised muscle forces for the different combinations. The standard deviations and means were then calculated for the sample allowing the variable sensitivity to be identified. The results can be seen in Figure 6-2. The proximity of the point to the origin displays the sensitivity of the target function (normalised muscle force) to the variable. The further away a variable is from the origin the more sensitive. This plot suggests that seat position (seat lateral position) is not an important variable with cadence and seat height being the most important. The next investigation was to optimise the chainring shape using the Fourier series expansion explained previously. Optimisation was carried out on both the Model 1 and Model 2. An initial sampling plan of 50 points was taken using the best Latin hypercube sampling method (Forrester A., 2008) which was the base for the surrogate model. The selected surrogate technique was Kriging, and 20 iterations were used to train the model whereby the areas of expected improvement were explored. To check the validity of the surrogate, a "leave one out" cross validation was carried out. The surrogate model, containing 70 points, has a point removed; the model must then predict the value that would occur at this point and this can be compared to the actual value.

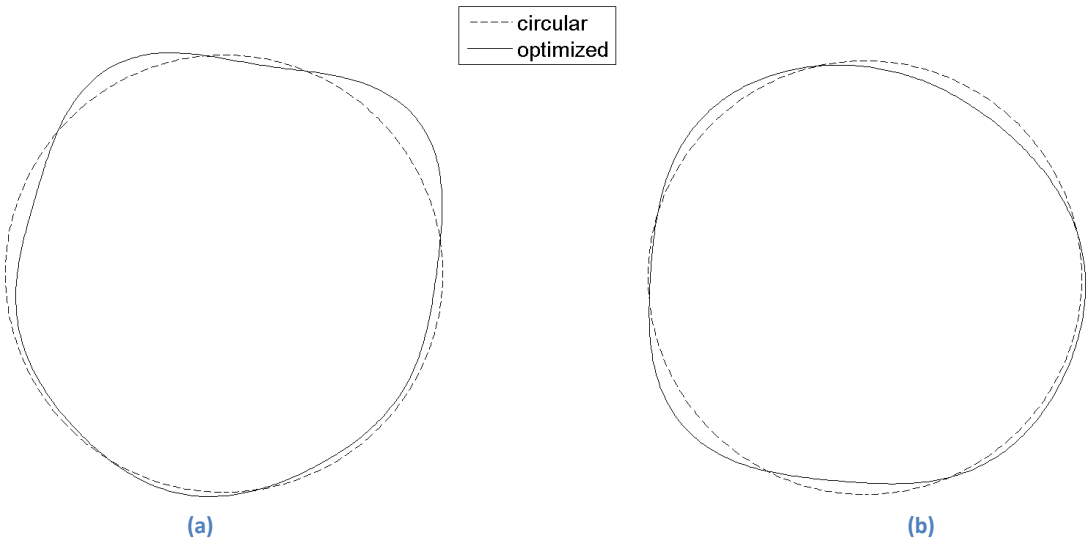

Figure 6-3; Optimised chainring shapes produced using the initial torque data. (a) is the shape produced using Model 1 (b) is the shape produced using Model 2

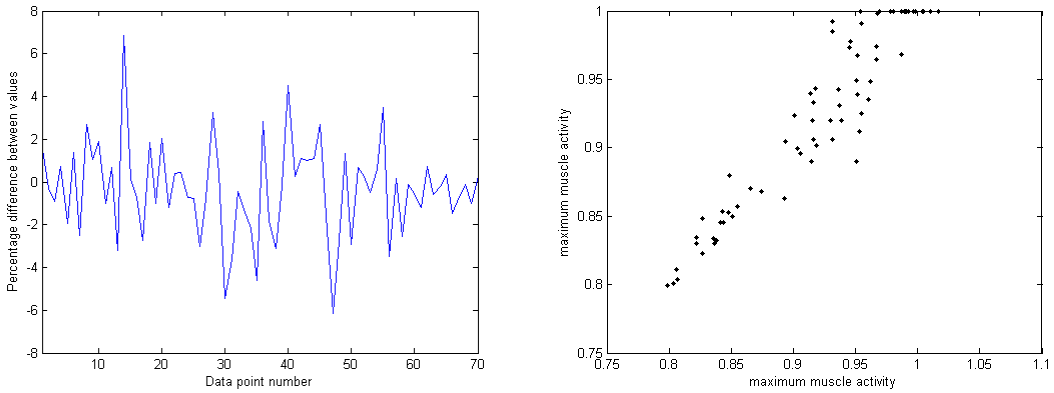

(a) (b)

Figure 6-4; Analysis from cross validation of the surrogate model. (a) shows the percentage error of predicted value against actual value for each of the values sampled. (b) shows the correlation between the predicted and actual values; this gave a correlation coefficient of 0.9472

Cross validation gave the following results; the model had an average error of 1.66% across the board along with a correlation coefficient of 0.9472. These results are very reasonable while the correlation plot shows that the data appears to correlate better at the minimum values. Due to the fact we are searching for the minimum this is useful as we are less concerned about values away from this. These results are presented in Figure 6-4; it should be noted that the axis labels on (b) of maximum muscle activity are the AnyBody software term for normalised muscle force. This should be remembered when viewing other maximum muscle activity plots in this chapter; in the text we will stick with using normalised muscle force.

(b)

Figure 6-3 shows the chainring shapes found by the optimization algorithm for both models. These are overlaid with a circular shape so that the differences between the circular and optimized shapes can be more easily assessed. The right crank arm is at the 3 o'clock position (90^{o} right of vertical). In the muscle activity plots the right crank arm also starts out at this position. Figure 6-5 shows the estimated normalised muscle forces for both circular and optimized chainrings in both models. The magnitude of the normalised muscle force is decreased by 17.92% on the Model 1 and 13.19% on the Model 2. Overall magnitude is much lower in the Model 1. In both cases the maximum peak decreases but this is paired with an increase in a minor peak alongside this main peak.

Table 5; Normalised muscle forces for circular and optimised designs for both Models 1 and 2

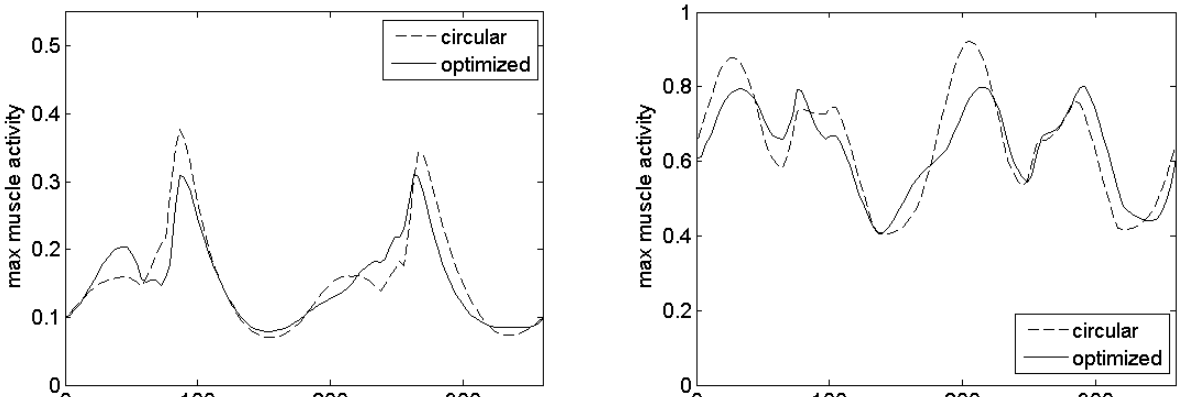

(a) (b)

Figure 6-5; Maximum muscle activity for optimised and circular chainrings (a) the results from the 2D model (b) the results from the 3D model

The two chainring shapes produced by the two different models are clearly different which matches up with the different normalised muscle force plots produced. Consideration must be given, however, to the more complex nature of the muscles in the Model 2 which detailed analysis would provide answers as to whether both are targeting the same primary muscles groups or not. This difference will also explain the large differences in the magnitudes of normalised muscle force; this could be due to some of the smaller muscle groups working at closer to their capacity most of the time, while the larger groups do not reach close to theirs as the exercise is not necessitating full strength from these muscles. Noticeably in Model 2 the iliopsoas muscle is identified as a one of the key muscles, as this is absent in the Model 1 this could explain the differences in shapes produced. The magnitude of the reductions achieved is very large and once further calibration with physical experiments is undertaken it is expected this value will fall.

All results in this section were peer reviewed and published in the proceedings of the 8th Conference of the International Sports Engineering Association. The author attended this conference and did an oral presentation of the paper(Purdue A.I., 2010, see Appendix B).

6.2 Q-Ring investigation

The Q-Ring is the most versatile of the production non-circular chainrings mentioned in section 1.1.4, with a possible 35 mounting positions in total. Due to this versatility we have purchased a Q-Ring so that we can acquire more data for non-circular chainrings to aid in the design of our own. This section will present the parameterisation of the Q-Ring shape and the computational results found using that shape. Comparison will also be shown with earlier results.

6.2.1 Q-Ring parameterisation

To enable use of the Q-Ring in the computational models, with the exception of those already being driven by the motion capture data, it was necessary to be able to describe the shape of this chainring. To this end the chainring was scanned so that the computer program GetDataGraphDigitizer (http://www.getdata-graph-digitizer.com/) could be employed to

produce a data set(X and Y coordinates for points manually placed on the perimeter of the Q-Ring) describing the shape. The base of each tooth valley was identified giving an outline of 53 points (the final point being a repeat of the first point). Once this dataset was acquired an investigation was carried out to try and define the shape as simply as possible. The following methods were used; Fourier series approximation, and description by both elliptical and superelliptical definition. To fit these definitions the same method was used for each: a genetic algorithm (the default one supplied in MatLab) with the fmincon function as a Hybrid Function (another minimisation function which is run once the genetic algorithm terminates). The target function which the GA was trying to minimise was:

$$val = sum\left(R_q - R_p\right)^2 \quad (2)$$

with val being the sum of the squared error, R_q being the local radii of the Q-Ring based on the aforementioned data set, and R_p being the local radii of the parameters being trialled. The local radius profile produced by those variables and the local radius profile of the Q-Ring is compared to find the difference. The sum of the difference squared was the given output for the function. Several methods were trialled to define the shape using the least number of parameters possible, to aid in later optimisation.

6.2.1.1 Using Fourier coefficients

The investigation using the Fourier coefficients was the logical starting point based on the system used to define the tailored chainrings laid out in the previous section. The parameterisation was trialled with ten coefficients and was then stepped down to four in intervals of two (due to the nature of the expansion). Each instance also includes the a_0 term along with the coefficients being searched so this provides us with 5, 7, 9, and 11 terms respectively. While the plots are similar closer inspection shows that the greater the number of terms that are used the closer the approximation is to the actual shape

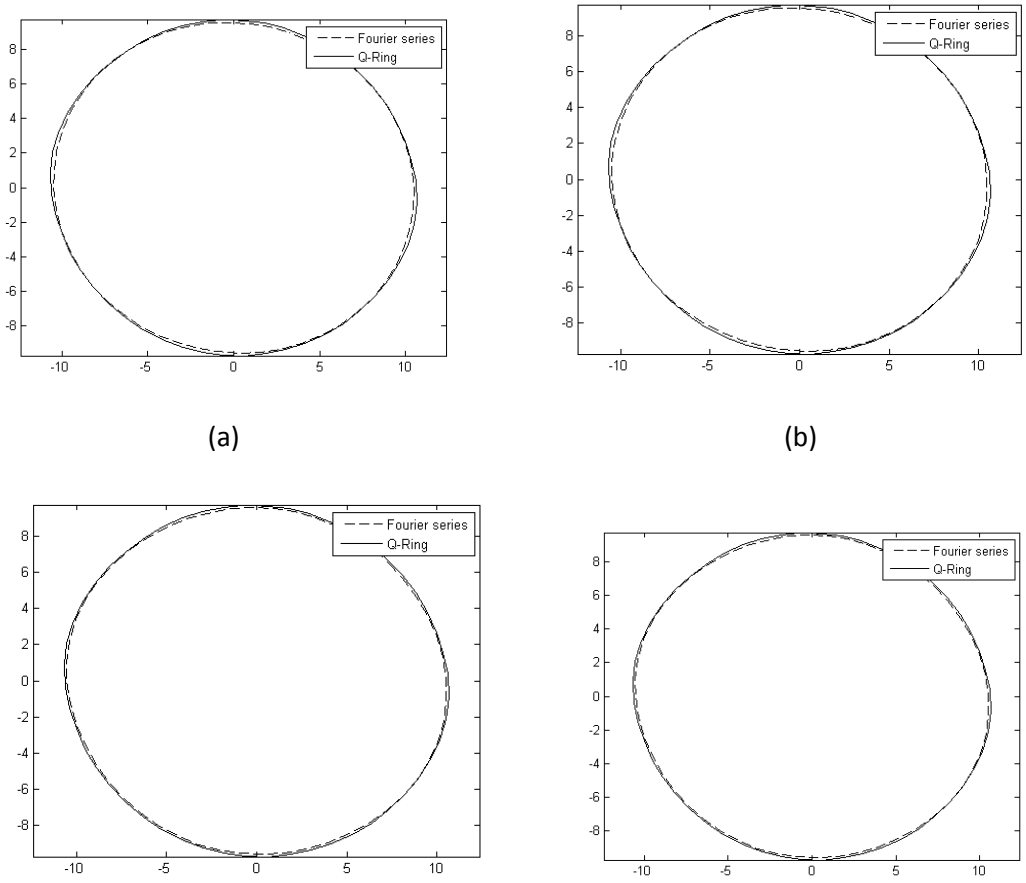

Figure 6-6; Plots of using Fourier series expansion to match Q-Ring shape
(a); using 5 terms (4 coefficients), (b); using 7 terms (6 coefficients), (c); using 9 terms(8 coefficients), (d); using 11 terms(10 coefficients)

6.2.1.2 Using an ellipse

The second method utilised was to fit an ellipse to the Q-Ring, which does look elliptical to the eye. The definition of the ellipse is relatively simple: the minor and major axis are defined along with a rotation. The equations which describe the locations of the points around the ellipse are as follows;

$$X(t) = a\cos(t)\cos(\varphi) - b\sin(t)\sin(\varphi) \quad (3)$$

$$Y(t) = a\cos(t)\sin(\varphi) + b\sin(t)\cos(\varphi) \quad (4)$$

Where t is the angle of the point from the X-axis (0 to 2π), a is the major axis and b is the minor axis. φ is the angle between the X-axis and the major axis of the ellipse.

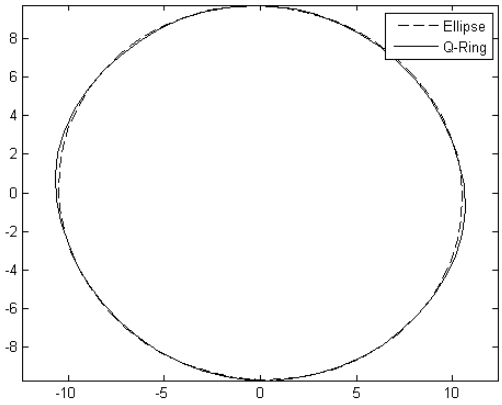

Figure 6-7; Q-Ring approximation using an ellipse

6.2.1.3 Using a superellipse

The third method was to fit a superellipse (or Lamé curve) to the shape. Superellipses are the family of curves between ellipses and rectangles. The superellipse has one more variable than the ellipse, with the variables defining the axes along with the curve of the shape between the axis points. The equations describing the point locations are as follows;

$$X(t) = a|\cos(t)|^{\frac{2}{m}}\text{sign}(\cos(t)) \quad (5)$$

$$Y(t) = b|\sin(t)|^{\frac{2}{n}}\text{sign}(\sin(\text{t})) \quad (6)$$

Where *t* is the angle, *a* and *b* define the axis lengths, and *m* and *n* control the curve between axes. With the x and y coordinates found a rotation was applied by converting to polar

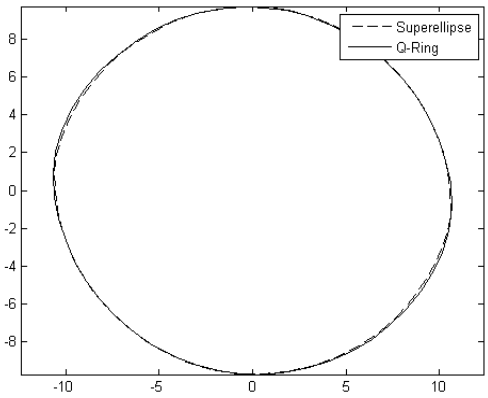

Figure 6-8; Q-Ring approximation using a superellipse

coordinates. This rotation was 0.9 times pi. This was done to neutralise the angle the Q-Ring was set at during scanning.

6.2.1.4 Selected parameterisations

Parameterisation method	Sum squared error	Max squared error	Mean squared error (MSE)
Fourier series (5 coef.)(F5)	0.7111	0.0452	0.0134
Fourier series (7 coef.)(F7)	0.7077	0.0464	0.0134
Fourier series (9 coef.)(F9)	0.5220	0.0187	0.0098
Fourier series (11 coef.)(F11)	0.5217	0.0195	0.0098
Ellipse	1.1860	0.0813	0.0224
Superellipse	0.1111	0.0097	0.0021

Table 6; Values for the sum squared error, maximum squared error, and mean squared error (MSE) for the different parameterisation options

The superellipse is a statistically the best fit for the Q-Ring shape, with the lowest error values. Compared to the 11 and 9 coefficient versions of the Fourier series (F11 and F9 respectively) the supereliipse has a sum squared error and mean squared error more than 4 times better. The max error for this method is also less than half that of the F11 and F9. These facts, combined with the low number of parameters necessary to define it, make it the optimum choice from the methods presented here.

6.2.2 Screening plot with Q-Ring orientation

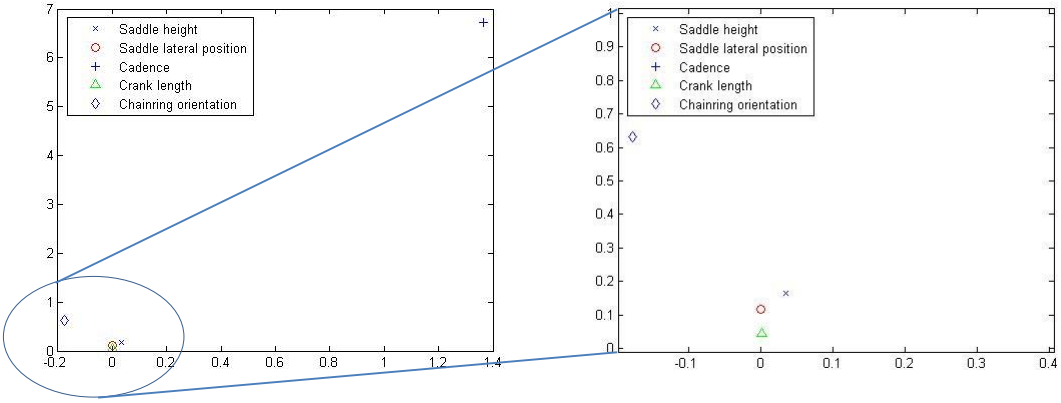

(a) **(b)**

Figure 6-9; Results from screening plot of variable effects on normalised muscle force (a) shows the overall plot (b) is a zoomed in view near the origin of plot (a). Chainring orientation means the orientation of the Q-Ring, saddle lateral position means forwards or backwards on the bike

Screening plans assess the importance of a given variable on their effect of a target function.

(b)

Figure 6-9 shows the results found when the screening plan was carried out with crank length, seat height, seat lateral position, chainring orientation (Q-Ring), and cadence being varied. Chainring orientation effectively means chainring shape in this assessment. The screening plan size was 300 configurations based on 50 random orientations, 35 steps per variable and 5 variables. The plot on the right is a zoomed in section of the left plot to show the detail for those

variables close to the origin in more detail. Similar to the results from the previous screening plot the cadence is identified as the most important variable, which, when the torque profile variation is considered stands to reason. It is significantly more important than the other variables. Assessing those closer to the origin shows that chainring orientation is the most important of these with the remaining three gathered close to the origin though the saddle height and position are more important than crank length. This identification of the importance of chainring shape points towards the work undertaken here as important. It also shows that multivariable optimisation may be required to find the optimum configuration for a rider. This screening plot used AnyBody v4.1 with the Model 2 so this could explain the variation when compared to the previous one.

6.2.3 Optimum Q-Ring rotation

While Rotor suggest that riders should start on hole 3 there is the ability to re-orientate the chainring to the orientation the rider finds the most comfortable or effective. An assessment of the effect this had on normalised muscle force, based on the Model 2 and the torque model used previously is displayed in (b)

Figure 6-10. Plot b displays how the maximum value of the normalised muscle force varied with the rotation. As would be expected for such a periodical shape the plot varies in a sinusoidal manner with two peaks and two troughs for the shape. There is a slight difference between the two peaks and also the two troughs though this is to be expected considering there is a possible 35 mounting positions. The optimum rotation (minimum normalised muscle force) was found at rotation 7, this equates to hole 28. This points to a rotation where the maximum radius is reached earlier in the pedal stroke than compared with the proposed mounting.

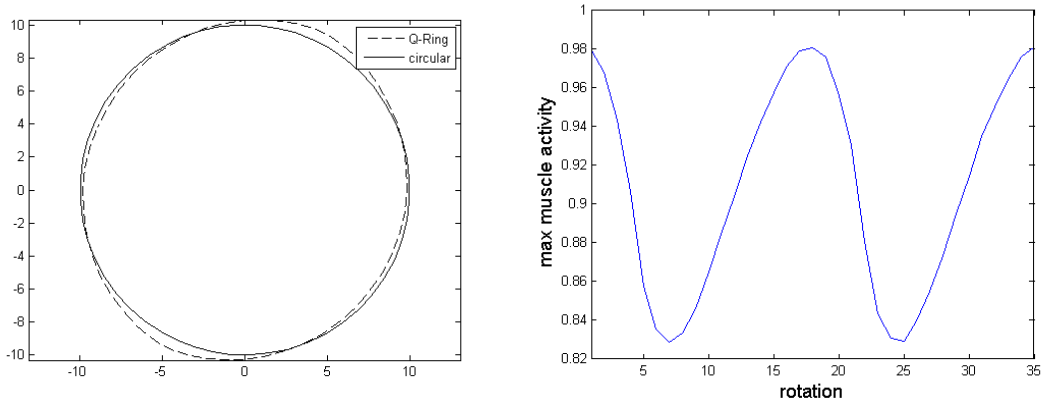

(a) (b)

Figure 6-10; Results from the Q-Ring orientation optimisation (a) shows the orientation which is best for the Q-Ring (the right crank arm is at the 3 o'clock mark) (b) shows the variation in values depending on the orientation

6.3 Initial comparisons

6.3.1 Q-Ring vs circular

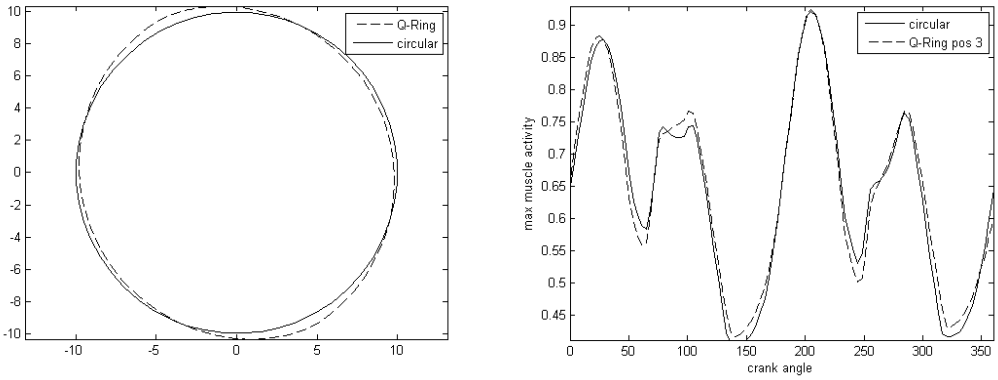

(a) (b)

Figure 6-11; Results from the comparison between the Q-Ring in the suggested rotation and the circular chainring (a) shows the shape comparison while (b) shows the maximum muscle activity comparison

Chainring	Normalised muscle force
Circular	0.9211
Q-Ring (suggested start point)	0.9250

Table 7; Normalised muscle force values for the circular chainring and the Q-Ring in the suggested orientation

The above plots show the comparison in the normalised muscle force plots and shape between the Q-Ring and the circular chainring as predicted by the Model 2. The Q-Ring is in the position suggested by Rotor as "a good start point" (hole 3). It identifies the iliopsoas as the major muscle (the highest peaks on both circular and Q-Ring). The iliopsoas is a muscle group made up of three muscles; the psoas major, the psoas minor, and the iliacus. The other major muscles identified by the model are the semimembranosus, biceps femoris, semitendinosus, and vastus lateralis. Interestingly the normalised muscle force for the Q-Ring in this rotation is actually higher (0.4%) than the circular chainring. The muscle plots produced by both are very similar. As this result seems to actually be worse than the circular chainring the optimum rotation found earlier is now compared. (b)

Figure 6-12 shows the rotation in comparison to a circular chainring followed by the muscle activities of both. A reduction of 10.02% in normalised muscle force is found when using the Q-Ring in this orientation.

Chainring	Normalised muscle force
Circular	0.9211
Q-Ring (optimum position)	0.8288

Table 8; Normalised muscle force results between the circular chainring and the Q-Ring in its optimum position

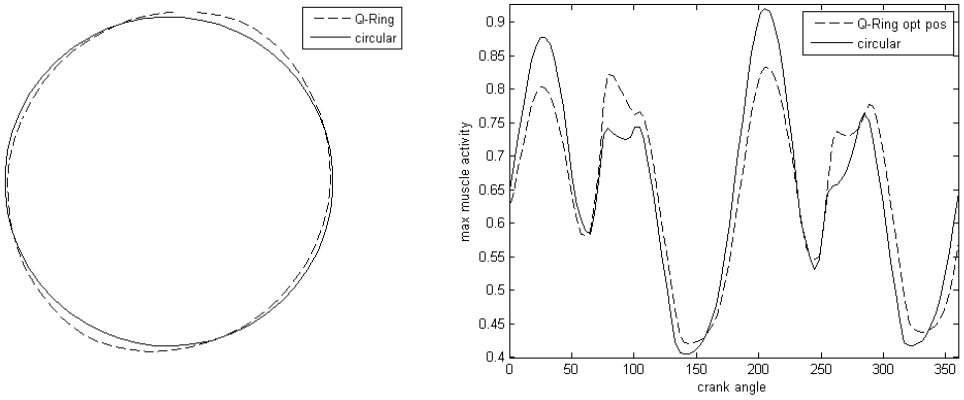

(a) (b)

Figure 6-12; Results from the comparison between the optimum Q-Ring rotation and the circular chainring (a) shows the shape comparison (b) shows the maximum muscle activity comparison

There is a noticeable drop in normalised muscle force for the Q-Ring on the higher peaks though there is also a noticeable rise in the less major peaks, particularly on the right leg. This suggests that as Rotor claim the Q-Ring is better than a normal circular chainring. The increase noticed however is quite large and it would be interesting to see if these predictions held with actual data, either immediate results or after acclimatisation, and how this affected fatigue.

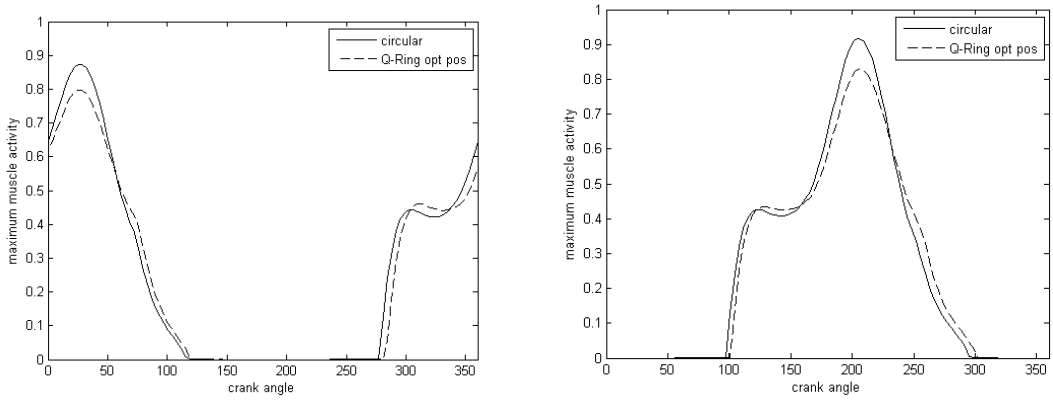

Figure 6-13; Maximum muscle activity for iliopsoas muscle in left and right leg respectively using the Q-Ring

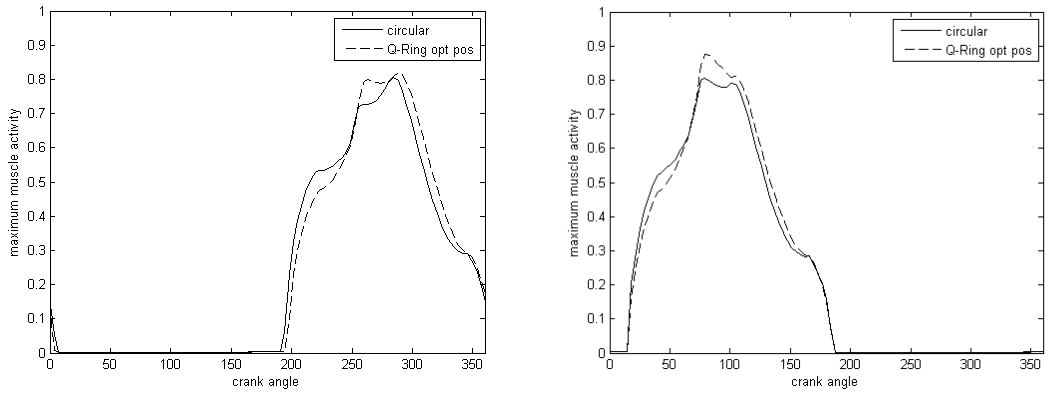

Figure 6-14; Maximum muscle activity for semimembranosus muscles in the left and right leg respectively using the Q-Ring

Figure 6-13 through Figure 6-17 show the normalised muscle force plots for the leg muscles identified as having the greatest normalised muscle force. All the muscles behave in a very similar way between the two which implies the changes are affecting these primary muscles. Their relative impact on previously less worked muscle has not been investigated yet.

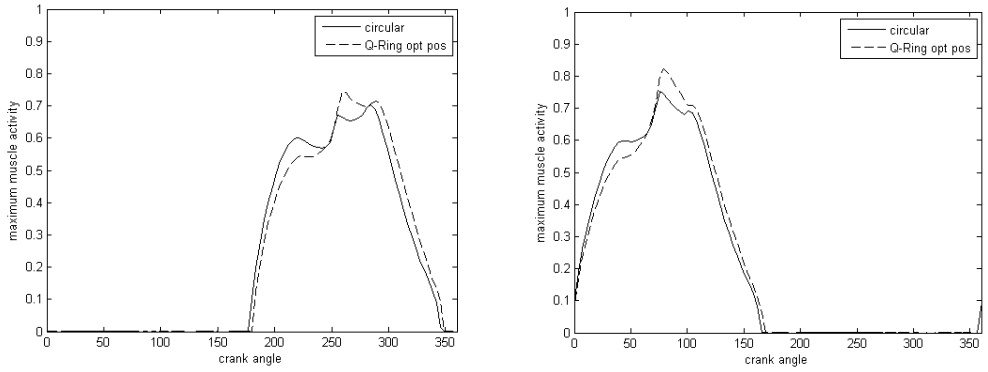

Figure 6-15; Maximum muscle activity for the biceps femoris caput longum muscles in left and right leg respectively using the Q-Ring

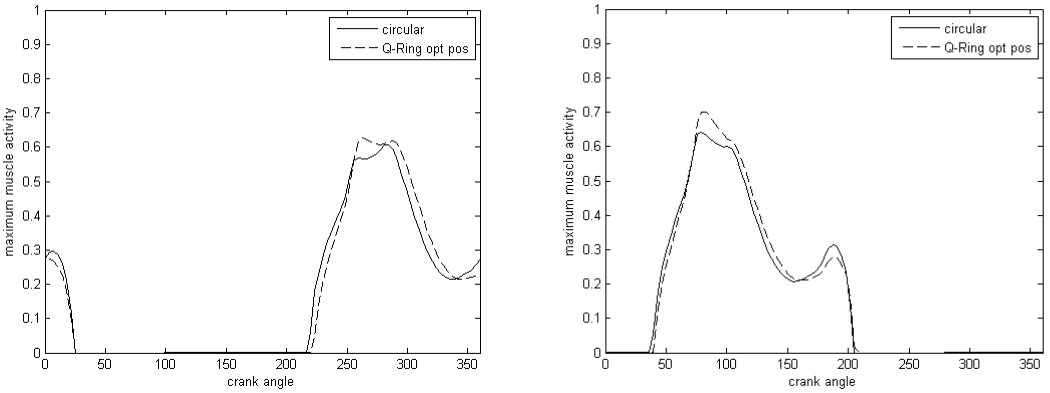

Figure 6-16; Maximum muscle activity for the semitendinosus muscles in the left and right leg respectively using the Q-Ring

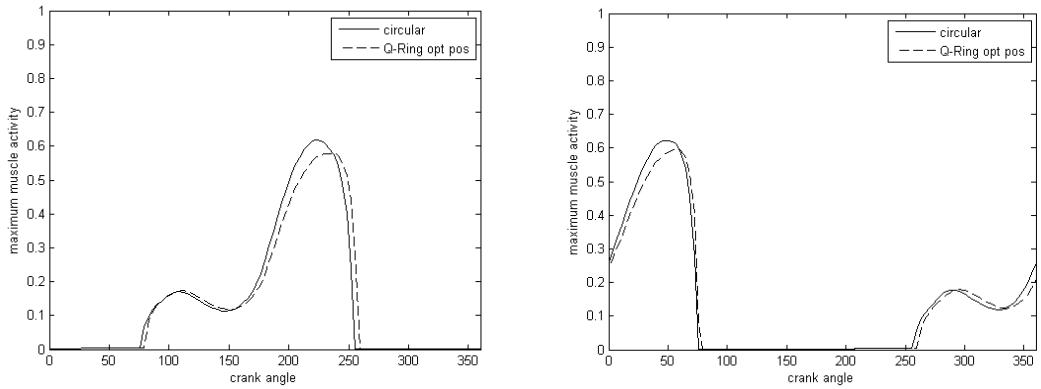

Figure 6-17; Maximum muscle activity for the vastus lateralis muscles in the left and right leg respectively using the Q-Ring

6.3.2 Q-Ring vs initial results

With a circular comparison complete we then consider how the Q-Ring matches up with our initial results found in the first section of this chapter. Again the Q-Ring is in the proposed optimum position. (b)

Figure 6-18 shows the shape and normalised muscle force comparisons between the two shapes. While the Q-Ring produced a large reduction in normalised muscle force compared to the circular chainring the difference between that and the initial results is still significant (our initial results give an improvement of 3.68% more than this Q-Ring orientation). Interestingly the primary peaks are about the same height for both chainrings with the secondary peaks appearing more varied between the two designs. Troughs are very similar as well in the profile.

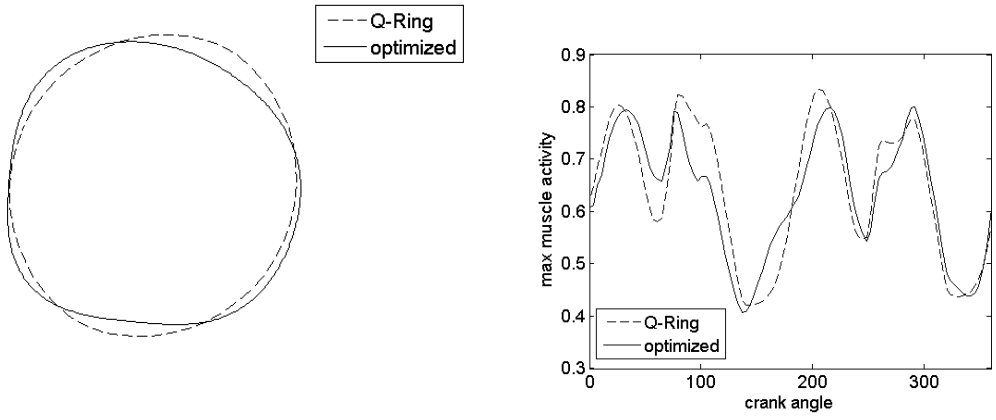

(a) **(b)**

Figure 6-18; Comparisons of the initial optimisation results (using the 3D model) and the optimum Q-Ring results.(a) shows the shape comparison between the two (b) shows the maximum muscle activity comparisons between the two

Chainring	Normalised muscle force
Initial optimisation	0.7996
Q-Ring (optimum position)	0.8288

Table 9; Maximum muscle activity values for both the initial optimisation (using the 3D model) and the Q-Ring in its optimum position

6.4 Chainring angular velocity

One of the main premises of this methodological study was the initial assumption that it was possible to model a non-circular chainring by modifying the local cadence and so the local angular velocity of the pedal during the rotation. This assumption had two parts; firstly that a circular chainring had a constant angular velocity, and secondly that a non-circular chainring had a non-constant angular velocity. With the data acquired from the motion capture laboratory it was possible to investigate if this assumption was a valid one. By isolating the marker attached to a pedal it was possible to calculate the angle of the pedal and the angular velocity at each data point and analyse both a circular and non-circular chainring. Firstly we will look at the circular chainring; Figure 6-19 shows the predicted angular velocity of the circular chainring along with the fast Fourier transform of the raw data. While there is some variation on the Fourier transform it does not go far from the predicted values and the general trend matches. Secondly we looked at the angular velocity when using the Q-Ring. Figure 6-20 shows the results of this analysis. A prediction of the mean angular velocity based on raw data from multiple rotations of the Q-Ring is plotted, as is the angular velocity of the Q-Ring as modelled by the Fourier series as covered in section 6.2.1.

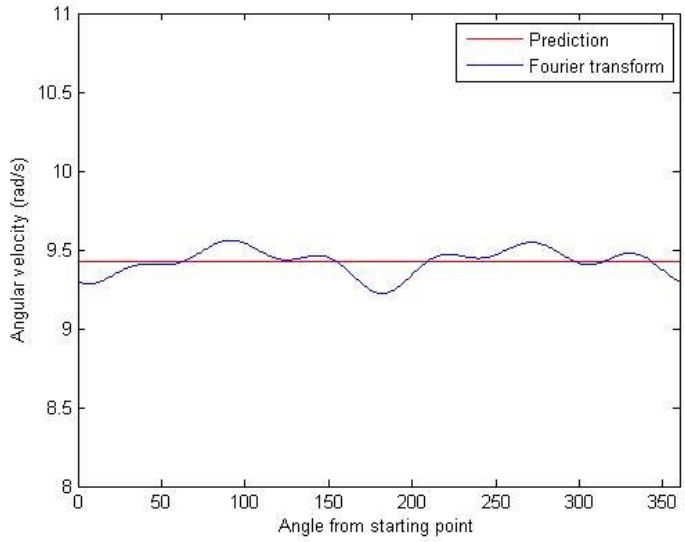

Figure 6-19; Comparison of predicted angular velocity and Fourier series transformation of raw data for circular chainring

While the prediction and Fourier series expansion do not match exactly, possibly due to too much variation in the raw data, the graph confirms the theory that non-circular chainrings alter the local cadence of the cyclist. There is a clear difference between the circular and Q-Ring plots so this information justifies the optimisation approach taken during this investigation.

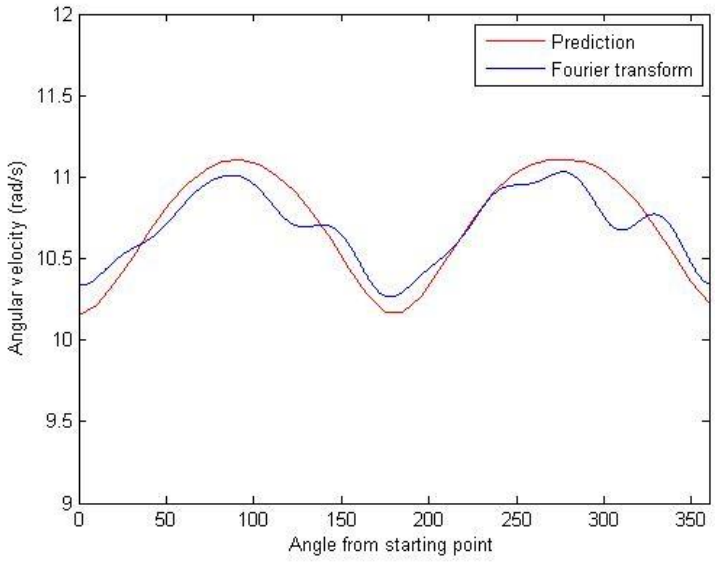

Figure 6-20; Comparison of predicted angular velocity and Fourier series transformation of raw data for a Q-Ring

6.5 Optimisations using improved torque model

The previous results that have been shown in this study have utilised the Models 1 and 2 described in section 3.3 Biomechanical Model development, the results which follow were produced using the final musculoskeletal model; the modified GaitLowerExtremity model (Model 3). This model was driven by motion capture data, so collected motion capture data was interpolated to give an expected cycling motion based on the chainring that was being tested. At this stage the development of the improved torque model had also been carried out, so this was also utilised. These two new models were the basis of the final optimisations and investigations of this project. Two optimisations were carried out as an initial test; one using a 3 variable offset ellipse, and one using a chainring shape defined by a Fourier series expansion with 10 coefficients as per section 3.4. The results of these two studies are shown here.

The first of these results is the 3 variable offset ellipse; with the three variables being axis length, rotation, and offset of the ellipse centre along the axis length being controlled. The limitations on the variables were as follows; axis length min: 0.8, max: 1.2, rotation min: 0, max: 2 Pi, offset min: -0.1, max: 0.1. Figure 6-21 through Figure 6-24 show the results for this. As you can see from the shape comparison against a circular chainring the algorithm has found an elliptical shape which has been rotated and also offset as optimum (subject to the limitations applied).

The chainring has been offset towards the drive phase of the right leg; due to the higher force production during this stage. The results of the optimisation were as follows; axis length 0.8154, rotation 0.6089 radians, offset 0.1000. These gave a normalised muscle force of 0.1449, a reduction of 14% on the normalised muscle force of 0.1685 given by the circular chainring.

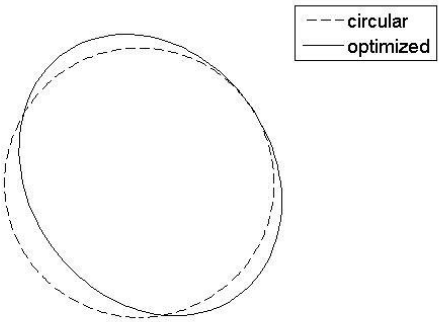

Figure 6-21; Chainring shape produced using optimisation of a 3 variable offset ellipse

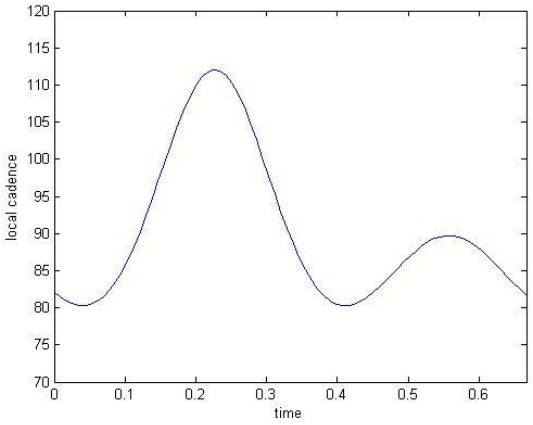

Figure 6-22; Local cadence profile for offset ellipse

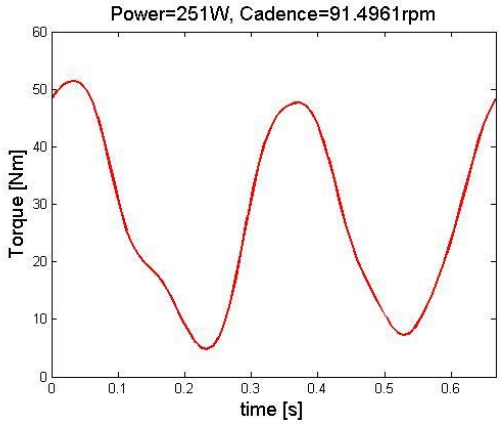

Figure 6-23; Torque profile for offset ellipse

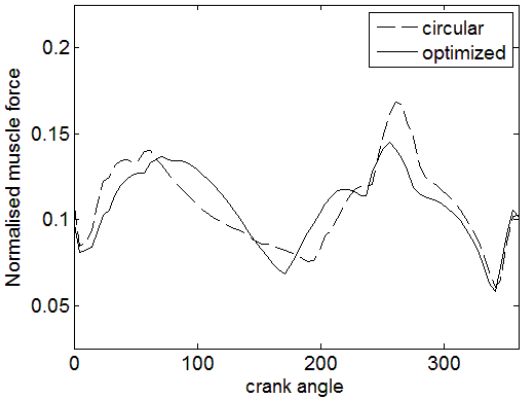

Figure 6-24; Normalised muscle force of offset ellipse against circular chainring

The second result is the chainring shape defined by the Fourier series expansion, defined by 10 variables with limitations of being a minimum of -3 and a maximum of 2. The results shown here were obtained after 20 iterations of the surrogate model exploration. Figure 6-25 through Figure 6-28 show the results of this study. In this case the chainring shape fluctuates around the outline of the circular chainring for approximately half the rotation but then has two noticeable protruding areas, one at 5 o'clock and a much larger one at 2 o'clock. Again this large increase in local radius (and subsequent decrease in local cadence) is in the drive phase of the right leg. So as with the offset ellipse the local cadence is being slowed in the right leg drive phase to

maximise that area of higher torque. The results given by this optimisation gave a normalised muscle force of 0.1436; a reduction of 14.8% on the circular chainring value (the ten coefficients were as follows; -1.9794, 1.9975, 1.9564, 1.9917, 1.9557, 1.6071, 1.9856, 1.9616, 1.9699, and 1.9859). Having found this result it was noted that actually this chainring shape would not deliver the intended local cadences if it was manufactured and produced due to the inclusion of concave sections. These sections would result in the chain not following the radius/skipping so modifications would be needed for the algorithm to produce a chainring that would work if physically made and used.

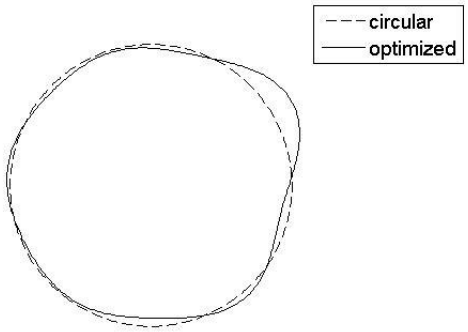

Figure 6-25; Chainring shape comparison of optimised Fourier chainring

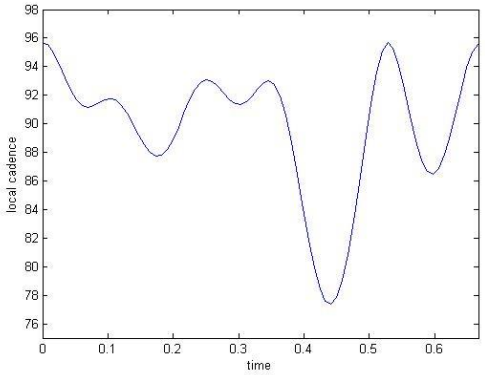

Figure 6-26; Local cadence profile for optimised Fourier chainring

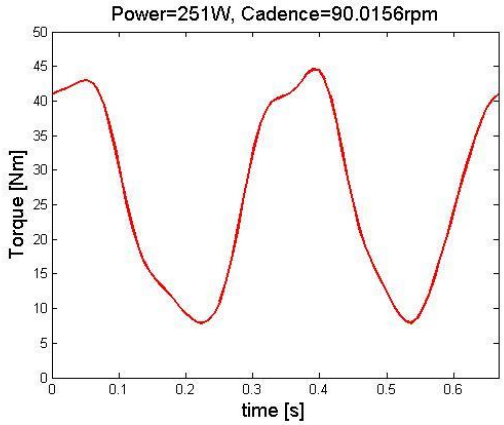

Figure 6-27; Torque profile for optimised Fourier chainring

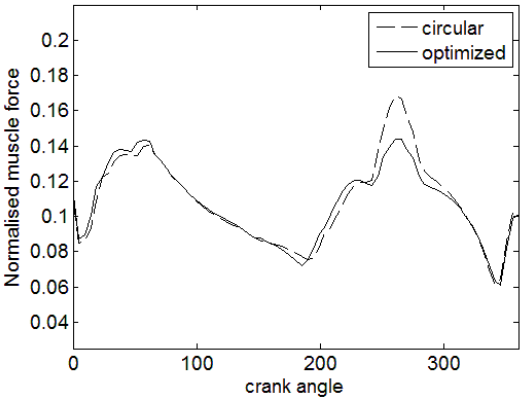

Figure 6-28; Normalised muscle force plots for optimised Fourier chainring and circular chainring

It should also be noted that due to the changing of the musculoskeletal model the results in this and later sections cannot be directly compared to earlier results which utilised different models. It is only possible to directly compare results found using the same model.

6.6 Investigations around the design space

While utilising the improved torque model and new musculoskeletal model (Model 3) as in the last section we also undertook investigations around the design space. In this section we will briefly look at these results; a 2 variable and a 3 variable exploration using an ellipse shape. The first of these (Figure 6-29) shows the results from the 2 variable investigation. One axis length was varied and the rotation of the shape was also varied; due to the variation of one axis length the other axis length was automatically varied to maintain the same total circumference. With the sample points taken the surface plot gives a good approximation of the maximum muscle activity across the whole sample area. A central area is seen matching the axis length of 1 which is around the midpoint of the range; this corresponds to a circular chainring hence rotation has no effect on the maximum muscle activity. We can also see that as expected the same normalised muscle force (max muscle activity) is generated by creating the same ellipse with a different combination of the variables; a rotated ellipse with a shorter axis length will be the same ellipse as one that has an axis length longer by the same amount.

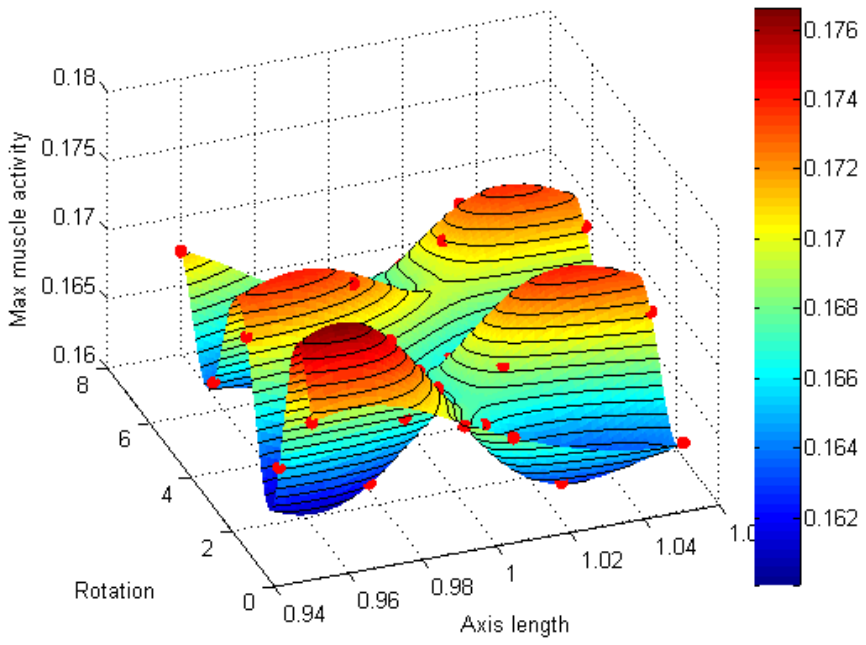

Figure 6-29; 3D plot of muscle activity for a 2 variable ellipse study

Figure 6-30 takes the previous study a step further and adds an offset to the variables. The ellipse centre can now be moved away from the centre of the rotation point by a small amount. This nested plot uses the same axes as the previous 2 variable plot; each plot is viewed straight down with the coloured contours showing normalised muscle force for a specific plot. Each plot then represents a different offset value. The central plot looks similar to a top down view of Figure 6-29 as there is no offset. As the chainring is offset the smaller hotspots merge until we end up

with less fluctuation due to axis length and the majority of variation due to rotation. The highs and lows are also more pronounced as the offset increases in either direction, though the lows are still higher than the maximum values found in the previous section.

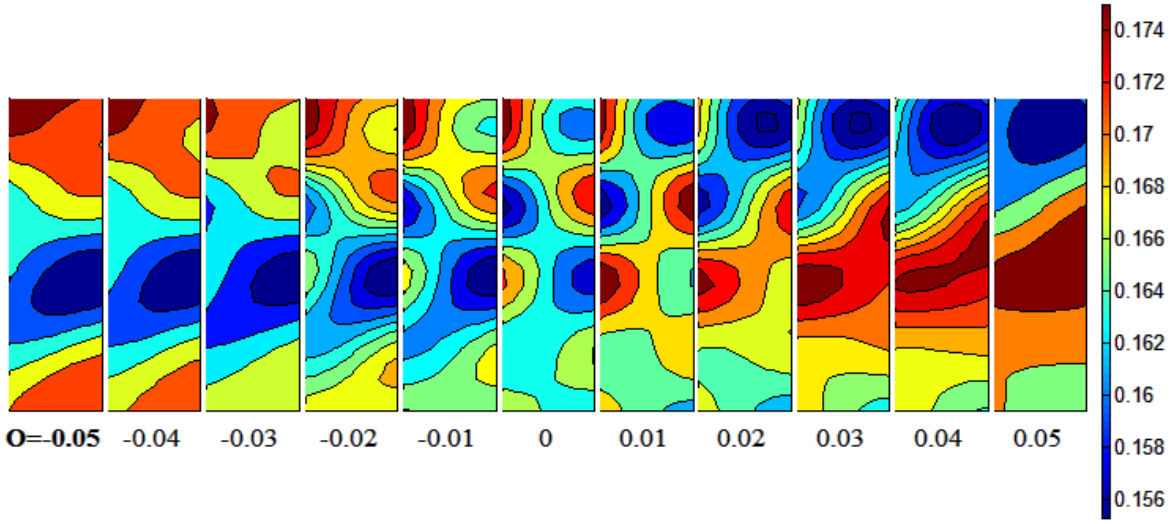

Figure 6-30; Nested plot of normalised muscle force for a 3 variable ellipse study

6.7 Summary

Having detailed the data collection, general methods, and the creation of the torque models this chapter has discussed the work which was carried out prior to acquiring our final optimised designs. Normalised muscle force plots and maximum muscle activity plots are presented, it is highlighted that these two terms are the same metric as maximum muscle activity is how the AnyBody software refers to the normalised muscle force.

We have presented the initial results utilising Model 1 and 2 and the initial torque model. A high cadence dependency is shown for torque "purity" while asymmetric torque profiles have hinted at the resultant chainring being asymmetrical as well. A four variable parameter study has shown cadence have the largest effect on target metric when changed, while seat position has the least. A Fourier series expansion is used to describe non-circular chainrings in both Models 1 and 2.Surrogate modelling (with a correlation coefficient of 0.9472) is carried out resulting in reductions in normalised muscle force of 17.92% using Model 1 and 13.19% with Model 2.

An investigation is undertaken using the shape of the Rotor Q-Ring; which is scanned and parameterised to decide on the best method of describing the shape. Fourier series expansion, an ellipse and a superellipse are all trialled with the superellipse having the best results in terms

of being the statistically best fit and also requiring a low number of parameters. A screening plot is carried out including the chainring shape (different rotations of the Q-Ring, which pointed that after cadence chainring shape had the next biggest effect on target metric output. An optimum Q-Ring rotation was found at hole 28 which gave a 10% reduction in normalised muscle force when compared with the circular chainring.

Chainring angular velocity has been assessed by using the motion capture data collected. The circular data shows some variation but fits the general trend of the expected constant angular velocity. The angular velocity of the Q-Ring again does not match exactly but has a much higher range from peak to trough than the circular chainring. This data backs up the assumption that a non-circular chainring will affect angular velocity and justifies the method of chainring shape description used in this study.

Using Model 3 and the improved torque model two optimised designs are found; one using an offset ellipse, and the other using the Fourier series expansion used previously. The offset ellipse gave a reduction of 14% in normalised muscle while the Fourier chainring gave a 14.8% reduction, however the Fourier chainring had some concave sections which a chain would not be able to follow so this design is not of use. Also the offset ellipse was right on the limit of one of its constraints. As such tweaks to these optimisations must be carried out.

Finally a two and three variable ellipse study of the design space are carried out to give a visualisation of how the normalised muscle force varies. For the two variable ellipse this shows the expected peaks and troughs which would be expected from the rotational symmetry of an ellipse. The three variable study adds offset to the ellipse and the nested plot shows that as an offset is added the peaks and troughs remain of a similar height/depth but become wider in shape, covering more of the design space.

The results from this chapter give a clear indication that normalised muscle force can be lowered by altering the chainring shape. We will now progress on to discussing the final chainring designs and the alterations to the optimisations which were necessary to discover them.

Chapter 7 Final designs

7.1 Design decisions

Following on from the results shown in section 6.5 we made some alterations to the optimisations to find our final results. In the case of the elliptical chainring this involved increasing the maximum size the axis could be extended to. In the case of the Fourier series expansion chainring the optimisation code was improved in two ways; firstly expected improvement was integrated into the code to aid in searching of the design space. Secondly code was added to prevent concave sections in the chainring shape as was seen in the previous set of results.

7.2 Elliptical chainring

With the initial optimisation for the offset ellipse being right on the limit of the offset limitation and very close to the axis limitation it was decided to re-run this optimisation with the limitations extended (axis length min: 0.7, max: 1.3, offset min: -0.2, max: 0.2). The results shown in Figure 7-1 through Figure 7-4 are the outcome of this optimisation. An axis length of 1.2986, a rotation of 2.570 radians and an offset of -0.0034 were the optimum combination of variables found. This gave a normalised muscle force of 0.1432, a reduction of 15% on the normalised muscle force of 0.1685 given by the circular chainring.

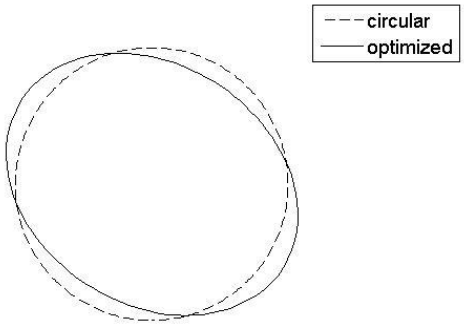

Figure 7-1; Chainring shape comparison of final optimised offset ellipse compared to a circular chainring

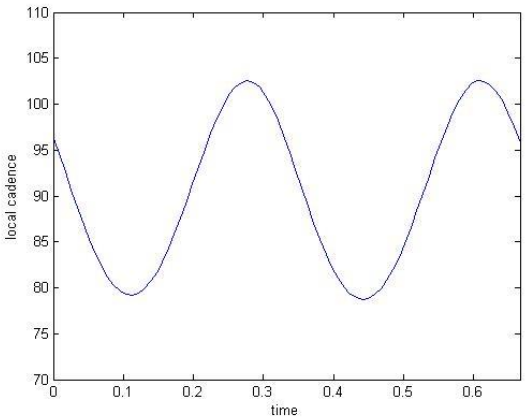

Figure 7-2; Local cadence profile for final optimised offset ellipse chainring

Interestingly as can be seen from Figure 7-1, in this case the chainring has not been shifted towards the top right quadrant as the last offset ellipse was, instead the chainring has a longer axis and has had more rotation applied. A larger reduction in normalised muscle force has been achieved though, and Figure 7-4 shows that the normalised muscle force has been lowered for both legs (each peak is lower than the corresponding circular peaks). The chainring is also of the same orientation as Hautz et al mentioned in section 2.6.1.

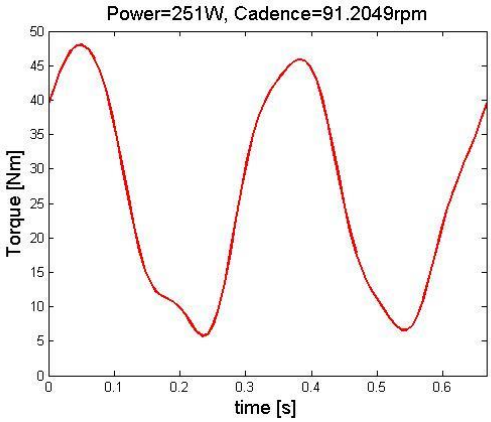

Figure 7-3; Torque profile for final optimised offset ellipse

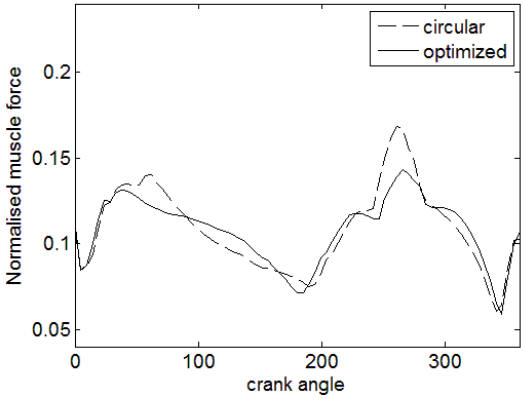

Figure 7-4; Normalised muscle force for final optimised offset ellipse and a circular chainring

7.3 Fourier series expansion chainring

As stated in the previous chapter the Fourier series expansion chainring shape that was produced suffered from a flaw in its design; while the computational model could deal with convex sections in the shape if the chainring had been manufactured and tested the chain would not have followed the whole shape so performance would not be as intended. Code was implemented to prevent concave sections occurring based on the change of the gradient. We also implemented expected improvement code to increase the efficiency of the surrogate model search due to the large (ten) number of variables that were being altered. Figure 7-5 through Figure 7-8 show the results of this optimisation. The results (-2.9995, -2.9643, -0.8805, 1.9555, 1.3757, 1.9922, 1.9860, 1.9860, 1.8929, 1.3343) give a final normalised muscle force of 0.1426; a reduction of 15.4% on the circular result and the largest reduction found during this study.

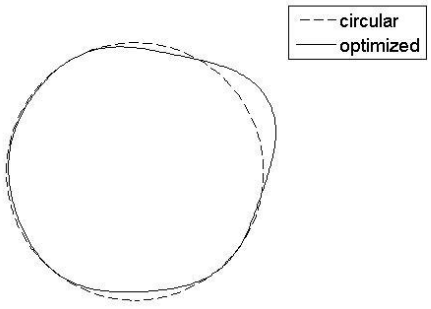

Figure 7-5; Chainring shape comparison between final Fourier chainring and circular chainring

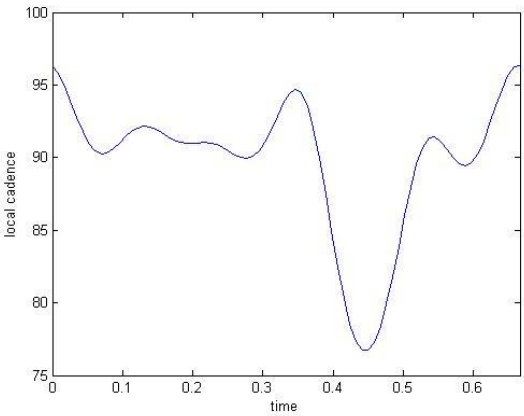

Figure 7-6; Local cadence profile for final optimised Fourier chainring

In this case the chainring shape produced is very similar to that found in section 6.5; the shape is very similar to the circular shape apart from a large protrusion in the top right quadrant. Due

to the constraints inhibiting concave sections this has resulted in three sections which look quite flat to the naked eye. To maintain the average rpm of 90 the radius has had to be reduced to allow for the radius increase in that section. Looking at Figure 7-8 shows that the profile is very similar on the left hand side and then much lower on the right hand side in the location of the main peak.

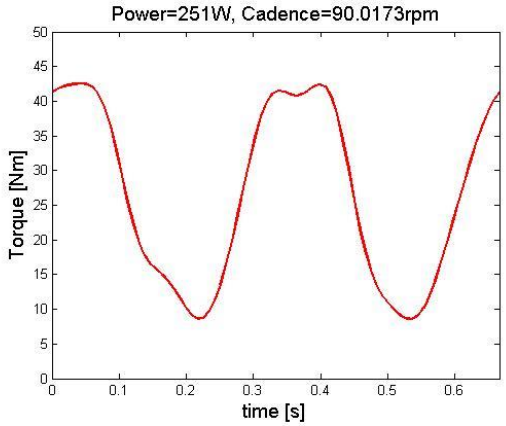

Figure 7-7; Torque profile for final optimised Fourier chainring

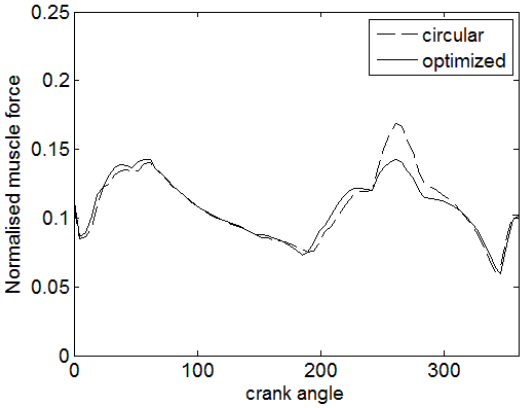

Figure 7-8; Normalised muscle force comparison between final optimised Fourier chainring and circular chainring

7.4 Motion capture differences

As detailed earlier in this thesis the motion capture data was interpolated to effectively modify the chainring shape. We will now take a brief look at the difference between the motion capture data for the circular chainring and the Fourier chainring to show how the data used to drive Model 3 differed. The ellipse motion capture data is not presented to keep the plots as clear as possible. For each marker we have an x, y, and z graph with both chainrings presented on the same plot. As the processing to create the new data accelerated and decelerated the movement that was already present we would expect to find the plots matching in shape but with gradients varying slightly and noticeable points shifting slightly within the revolution period.

First we will look at the left pedal marker. Figures 7-9 to 7-11 show the x, y, and z plots for this marker. As expected the shapes are the same, although the y graph is smoother but it should be noted the movement in this axis was very small so any smoothing that had occurred will be clearer on this plot. Also the Fourier plots do fluctuate away from the circular plot as expected but always hitting the same peaks and troughs.

Next we will look at the left ankle marker. These values are presented in Figures 7-12 to 7-14. Again we see the same transformation with these values as occurred with the left pedal marker. Figures 7-15 to 7-17 show the values for the left knee marker. These plots show again the same

transformation visible in the other plots with same basic shape being present but gradients being increased/decreased depending on the how the Fourier chainring was differing from the circular chainring.

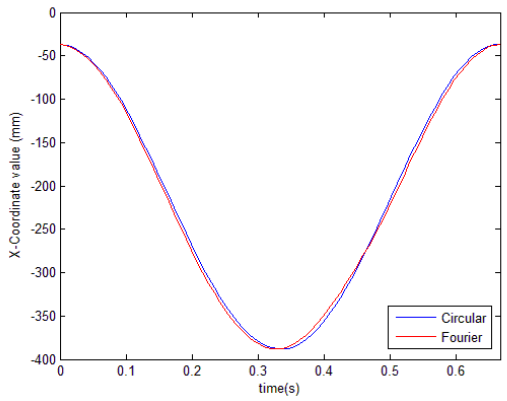

Figure 7-9; X coordinate values for left pedal marker for both circular and Fourier

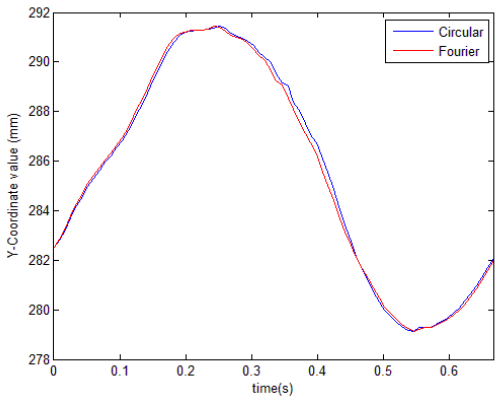

Figure 7-10; Y coordinate values for left pedal marker for both circular and Fourier

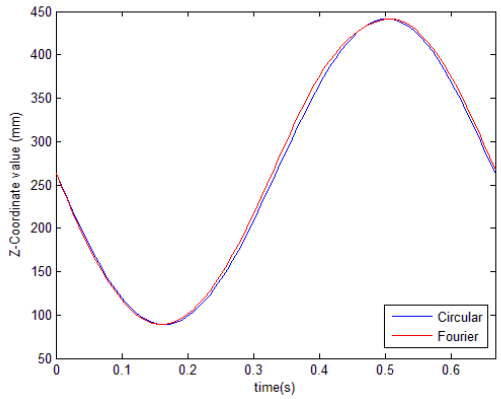

Figure 7-11; Z coordinate value for left pedal marker for both circular and Fourier

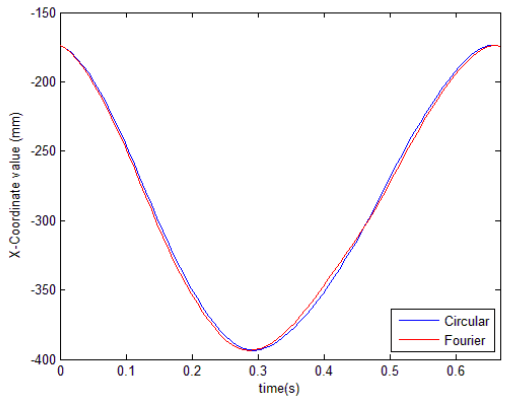

Figure 7-12; X coordinate values for left ankle marker for both circular and Fourier

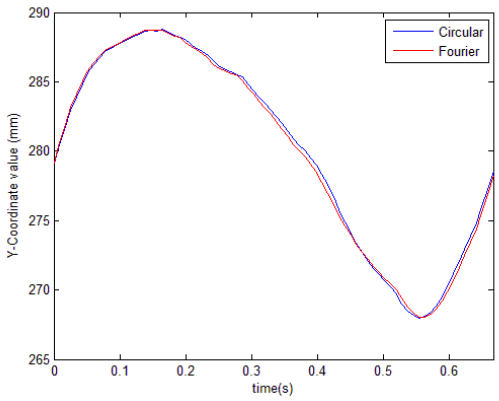

Figure 7-13; Y coordinate values for left ankle marker for both circular and Fourier

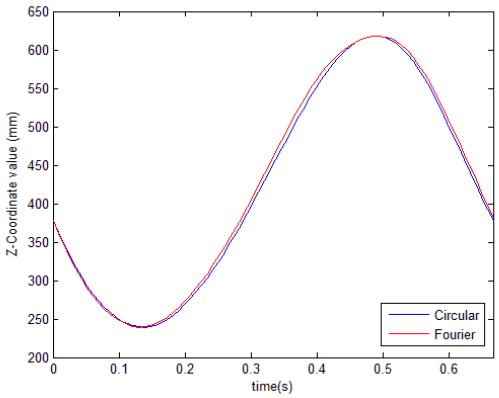

Figure 7-14; Z coordinate values for left ankle marker for both circular and Fourier

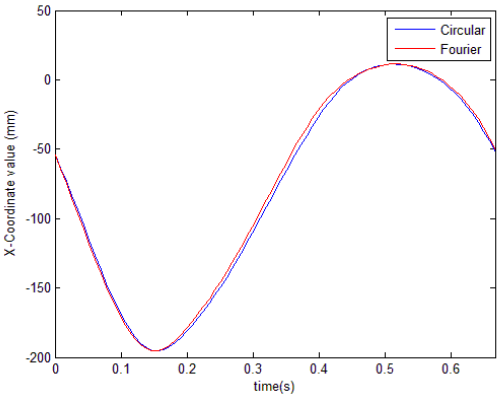

Figure 7-15; X coordinate values for left knee marker for both circular and Fourier

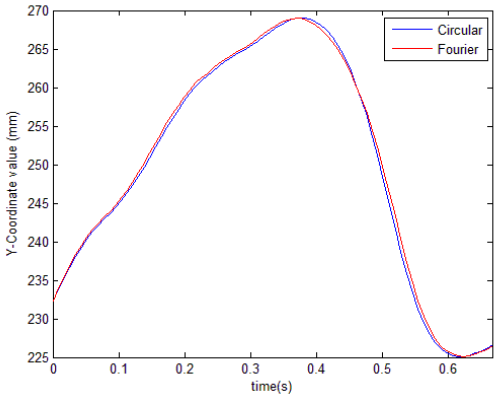

Figure 7-16; Y coordinate values for left knee marker for both circular and Fourier

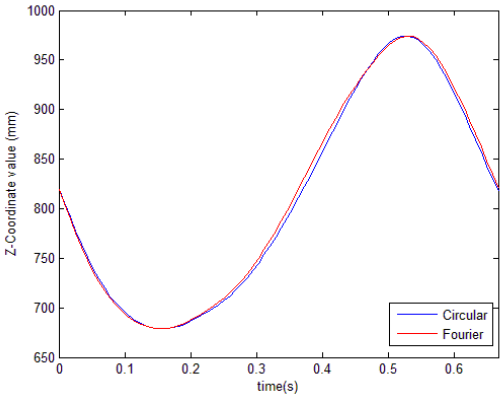

Figure 7-17; Z coordinate values for left knee marker for both circular and Fourier

Having looked at the left pedal, left ankle, and left knee markers we will now have a look at the two markers placed to track hip movement; the left anterior superior iliac spine and left posterior superior iliac spine. Figures 7-18 to 7-20 show the values for the left anterior superior iliac spine and Figures 7-21 to 7-23 show the left posterior superior iliac spine. Again we see the same transformation as before in the data from circular to Fourier but the other thing to note is how little movement there is on these markers (~20mm movement on y, ~10mm on x and z). This matches with Neptune & Hull (1995, 1996) who stated the hip movement could be set to a

fixed position for ~90rpm although interestingly this movement was measured above their power limit of 225W. It might be interesting to see if actually removing any movement from the hip made any difference to the outputs from AnyBody.

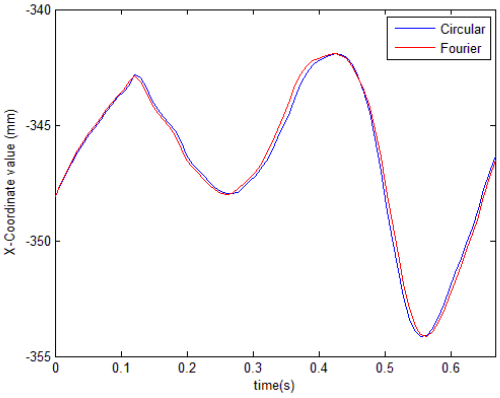

Figure 7-18; X coordinate values for left anterior superior iliac spine marker for both circular and Fourier

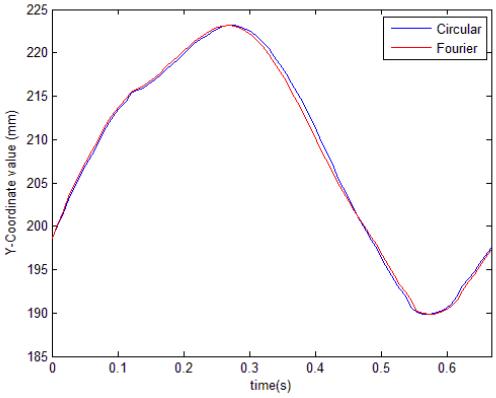

Figure 7-19; Y coordinate values for left anterior superior iliac spine marker for both circular and Fourier

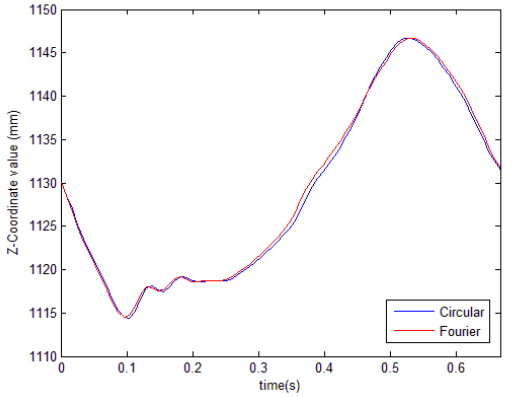

Figure 7-20; Z coordinate values for left anterior superior iliac spine marker for both circular and Fourier

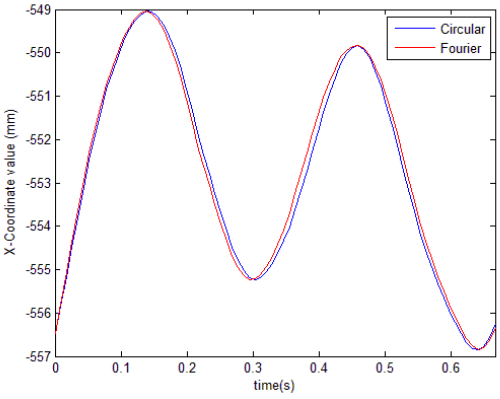

Figure 7-21; X coordinate values for left posterior superior iliac spine marker for circular and Fourier

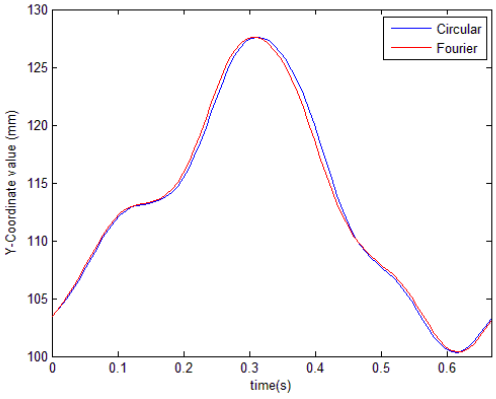

Figure 7-22; Y coordinate values for left posterior superior iliac spine marker for both circular and Fourier

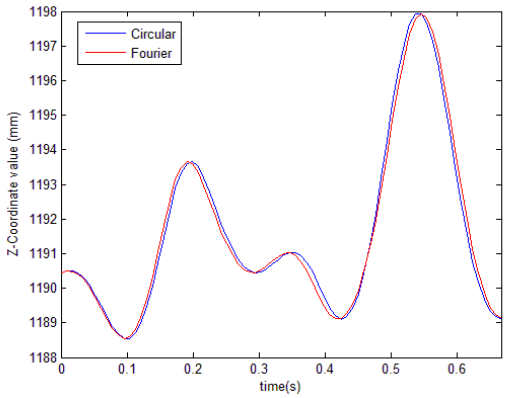

Figure 7-23; Z coordinate values for left posterior superior iliac spine for both circular and Fourier

7.5 Summary

In this chapter we have presented the final two chainring designs which were identified during this study by the optimisations undertaken. The ellipse design space used in the previous chapter was increased as the results were right on the limits set. Constraints were applied to the Fourier chainring to ensure that the design that was produced would function the same in real life if it was created as the computational model did; i.e. no concave sections which the chain would skip. A final ellipse (axis length: 1.2986, rotation: 2.570 radians, offset: -0.0034) gave a 15% reduction in the highest peak of normalised muscle force and achieves a reduction in both the left and right leg peaks, something the Fourier chainring does not achieve. The final Fourier design (with coefficient values of -2.9995, -2.9643, -0.8805, 1.9555, 1.3757, 1.9922, 1.9860, 1.9860, 1.8929, 1.3343) produced a reduction of 15.4% in normalised muscle force; the greatest reduction found in this study, although there is a slight increase in normalised muscle force on the right leg. Both designs deliver the lowered normalised muscle force we were aiming for and should result in lower lactate and delay the onset of fatigue physically created and tested. While earlier optimisations had given a consistent design idea of trying to maximise the right leg drive phase these two designs appear to offer slightly different methods with similar results. We have also displayed how these changes in chainring shape affected the motion capture data being used to drive Model 3 in AnyBody. As expected the shape remained the same but the gradients were increased or decreased as expected. In the next chapter we will look in detail at the specific muscles and how they were affected by these chainring designs.

Chapter 8 Computational results from final designs

8.1 Results and discussion

In this chapter we will present a muscle specific analysis of the musculoskeletal model outputs produced during the optimisation of the chainring shape. In each instance one muscle will be presented with the results of all three chainring shapes (Fourier, ellipse, and circle) shown on the same graph. Left and right legs will also be combined and shown as one plot. In doing so we will assess the impacts the change in chainring shape have had on the normalised muscle forces of the model. Again it should be noted that normalised muscle force is what the AnyBody software refers to as maximum muscle activity. As such plots of maximum muscle activity up to Chapter 7 are of normalised muscle force, not actual muscle activity.

The first thing to note is the number of muscles that produced plots that matched the normalised muscle force plot generated for the optimised designs in the last chapter. There were 17 different muscles with either an identical plot or a plot that only varied for the last 40 degrees of the revolution. Of these 17 muscles, 14 had identical plots and 3 varied in the last section. As the plot is identical for each of the muscles in the first group, and the same is true of each of the muscles in the second group only one graph is shown for each group. Figure 8-1 shows the plot for any of the muscles in the first group and Figure 8-2 shows the plot for any of the muscles in the second group. As can be seen in the final 40 degrees of the profiles the second graph deviates from matching Figure 8-1; it decreases faster, dips lower and then rises more sharply before finishing at the same point.

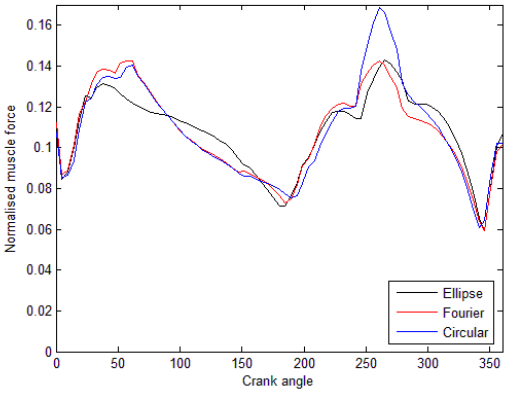

Figure 8-1; Normalised muscle force plots for ellipse, Fourier, and circular chainrings for the first group of muscles

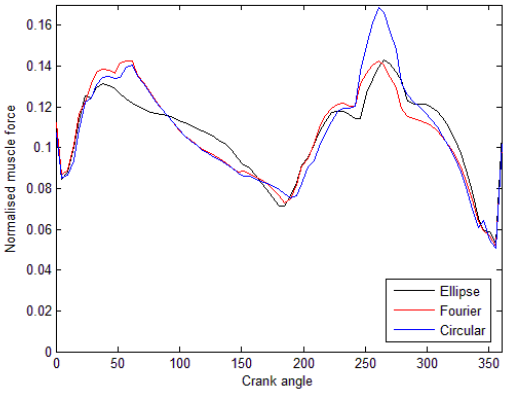

Figure 8-2; Normalised muscle force plots for ellipse, Fourier, and circular chainrings for the second group of muscles

The first group, containing the muscles whose normalised muscle force profiles matched exactly for the entire rotation, contained the following muscles:

- Quadratus femoris

- Obturator internus
- Obturator externus superior
- Gemellus inferior
- Tensor fasciae latae
- Gluteus maximus inferior
- Gluteus maximus superior
- Iliacus mid
- Iliacus lateralis
- Sartorius distal
- Sartorius proximal
- Biceps femoris caput breve
- Extensor hallucis longus
- Tibialis Anterior

The pelvis to femur area has the highest number of these muscles; the quadratus femoris, obturator internus, obturator externus superior, gemellus inferior, gluteus maximus, tensor fasciae latae, and Iliacus are all connecting the leg to the top of the femur and have the same plot. There were muscles in this region which had noticeable normalised muscle force but did not fit in with this identical plot. While the gluteus maximus gave a maximum normalised muscle force plot, the gluteus medius and gluteus minimus both gave high normalised muscle forces on the highest spike but variations around the rest of the rotation.

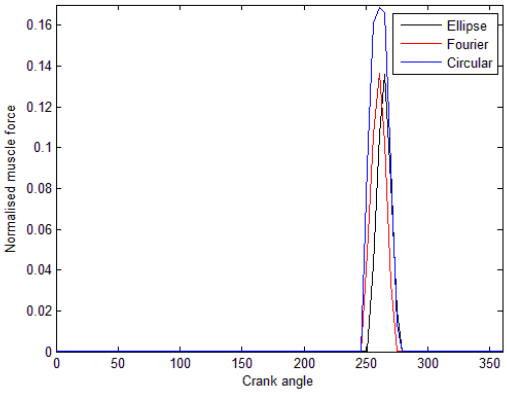

Figure 8-3;Normalised muscle force plots for ellipse, Fourier, and circular chainrings for the gluteus medius anterior muscles

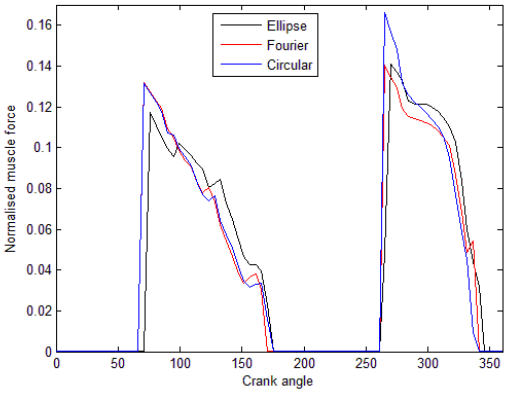

Figure 8-4;Normalised muscle force plots for ellipse, Fourier, and circular chainrings for the gluteus medius posterior muscles

Figure 8-3 and Figure 8-4 show the muscle plots for the gluteus medius muscles. Interestingly on the anterior muscle there is only a normalised muscle force on the left leg, and a very brief

one, no normalised muscle force occurs on the right leg. On the posterior muscles there is a sudden high normalised muscle force at the peak locations on both legs then a more gradual decrease in comparison.

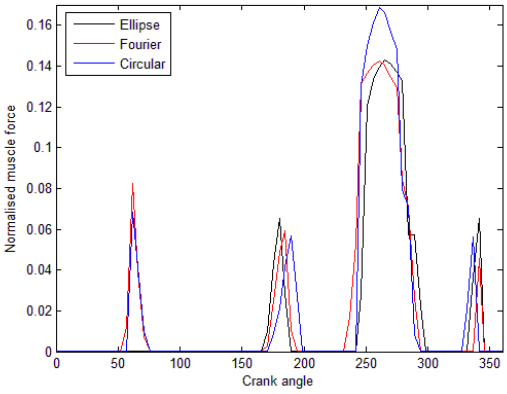

Figure 8-5; Normalised muscle force plots for ellipse, Fourier, and circular chainrings for the gluteus minimus anterior muscles

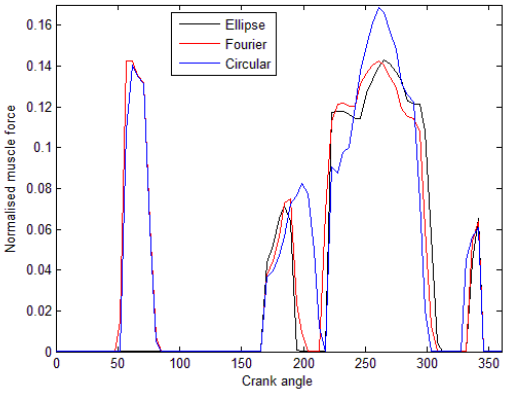

Figure 8-6; Normalised muscle force plots for ellipse, Fourier, and circular chainrings for the gluteus minimus mid muscles

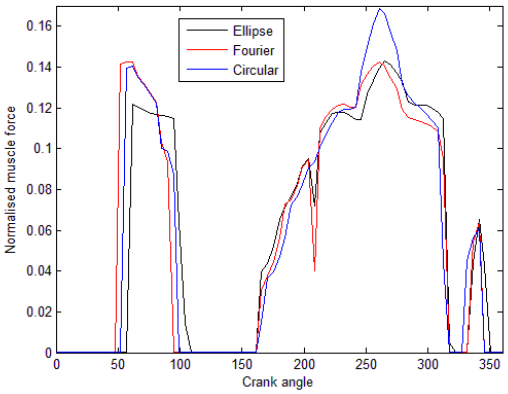

Figure 8-7;Normalised muscle force plots for ellipse, Fourier, and circular chainrings for the gluteus minimus posterior muscles

For the gluteus minimus (Figure 8-5 through Figure 8-7) we see varied activity again. As before the anterior muscle has a high normalised muscle force on the left leg but a much lower normalised muscle force on the right leg. The mid and posterior muscles have a longer normalised muscle force on the left leg but the size of the normalised muscle force is similar in size between each leg.

Going back to the discussion of the identical plots, the location of the other muscles listed are in the upper leg (sartorius distal, sartorius proximal, biceps femoris caput breve), lower leg (tibialis anterior) and foot (extensor hallucis longus). Unlike the pelvis to femur area we see that these three sections have far less muscles following that maximum normalised muscle force plot. While the extensor hallucis longus muscle in the foot follows that max plot, the flexor digitorum longus (Figure 8-8), flexor hallucis longus(Figure 8-9), and extensor digitorum

longus(Figure 8-10) all have high normalised muscle forces as well. The flexor digitorum longus and flexor hallucis longus muscles both have large troughs in the plot before the left leg spike. The extensor digitorum Longus on the other hand is very close to the max identical plots apart from some sharp drops in normalised muscle force on the right leg, with an additional large drop in normalised muscle force on the elliptical chainring.

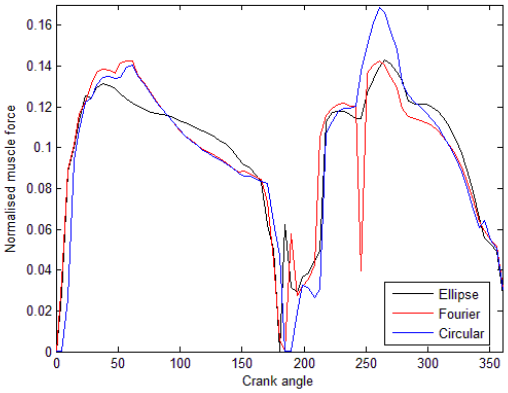

Figure 8-8; Normalised muscle force plots for ellipse, Fourier, and circular chainrings for the flexor digitorum longus muscles

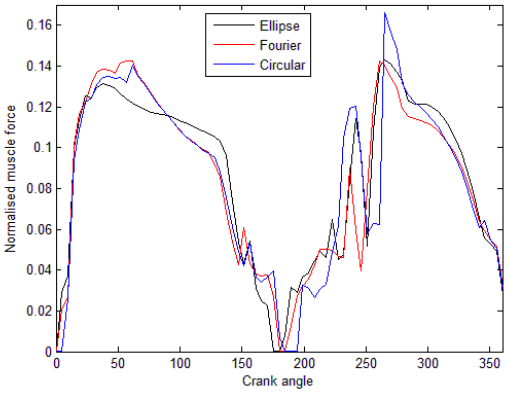

Figure 8-9; Normalised muscle force plots for ellipse, Fourier, and circular chainrings for the flexor hallucis longus muscles

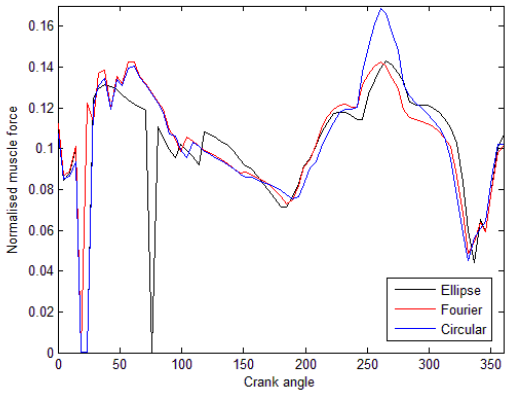

Figure 8-10; Normalised muscle force plots for ellipse, Fourier, and circular chainrings for the extensor digitorum longus muscles

The second group, with the deviation in the final 40 degrees of rotation contained the following three muscles:

- Pectineus
- Adductor brevis proximal
- Gracilis

As has been shown in the gluteus muscle plots the normalised muscle force can spike very sharply so this sharp alteration at the end of the rotation suggests a drop in muscle recruitment at that stage as the pedals approach the locations of top dead centre and bottom dead centre.

There were also two other muscles that produced normalised muscle force plots that were of interest due to the level of activity; the biceps femoris caput longum and the rectus femoris. Figure 8-11 and Figure 8-12 show the plots for these two muscles. As can be seen the biceps femoris caput longum has very similar peak shapes to the identical graphs above and the maximum normalised muscle force plots, but away from the peaks it drops off rapidly. Rectus Femoris on the other hand follows the same general path as the above graphs with larger fluctuations on the descent after each peak, as the pedals pass towards the end of the drive phase. Interestingly the ellipse normalised muscle force drops much lower than the other two designs for the rectus femoris.

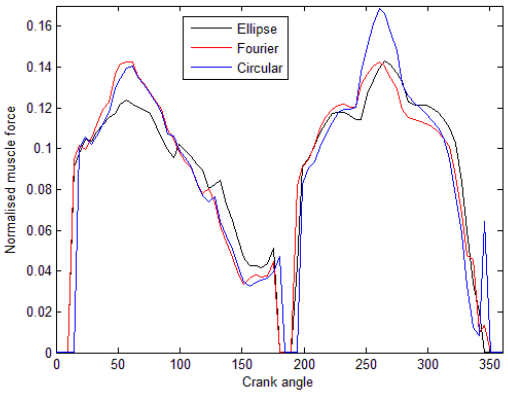

Figure 8-11; Normalised muscle force plots for ellipse, Fourier, and circular chainrings for the biceps femoris caput longum muscles

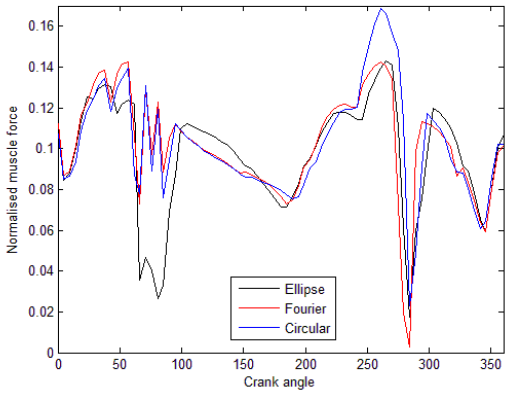

Figure 8-12; Normalised muscle force plots for ellipse, Fourier, and circular chainrings for the rectus femoris muscles

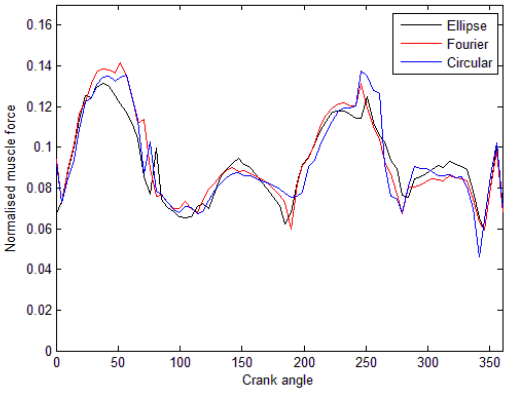

Figure 8-13; Normalised muscle force plots for ellipse, Fourier, and circular chainrings for the gastrocnemius medialis muscles

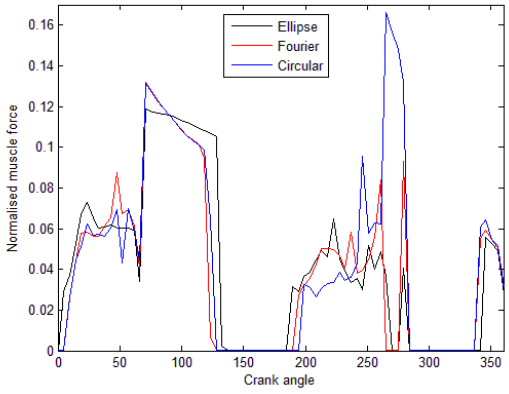

Figure 8-14; Normalised muscle force plots for ellipse, Fourier, and circular chainrings for the tibialis posterior lateralis muscles

Figure 8-13 through Figure 8-15 show the remaining plots of interest for the lower leg. Figure 8-13 shows the gastrocnemius medialis normalised muscle force, these muscles are active for

the whole rotation (right and left leg are on same plot). The right leg has a slightly higher normalised muscle force on this muscle unlike most of the others where the left leg gives a higher result. Figure 8-14 gives the normalised muscle force for the tibialis posterior lateralis muscles and is far sharper than the previous graph. The point of interest on this graph is that both the optimised chainrings have very low normalised muscle force in the space where the circular chainring has its highest normalised muscle force of the whole rotation. For the tibialis posterior medialis (Figure 8-15) is similar to the tibialis posterior lateralis although the Fourier and Ellipse chainrings have high normalised muscle force in this case.

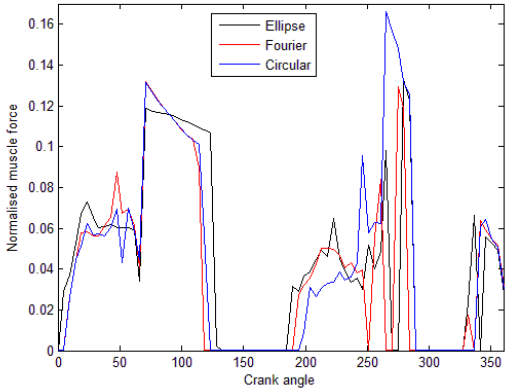

Figure 8-15; Normalised muscle force plots for ellipse, Fourier, and circular chainrings for the tibialis posterior medialis muscles

In the upper leg the vastus lateralis inferior, vastus lateralis superior, and vastus medialis inferior all gave the same results for normalised muscle force. Figure 8-16 shows the normalised muscle force for the vastus lateralis superior, this shows four definite peaks; two large, two small. On the right leg peak the Fourier and circular are noticeably higher than the ellipse, however on the two smaller peaks the ellipse is noticeably higher than the other two. On the left leg peak the ellipse and Fourier normalised muscle force is much lower than that of the circular, and also lower than the right leg which is not common in these results.

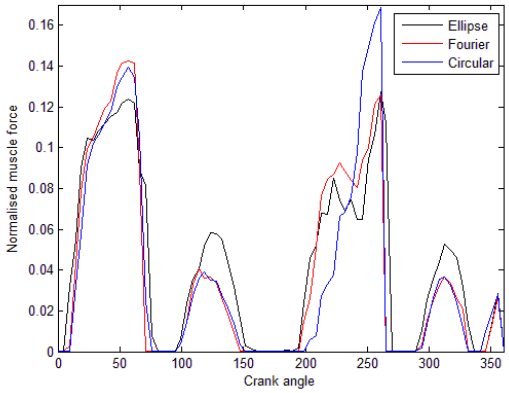

Figure 8-16; Normalised muscle force plots for ellipse, Fourier, and circular chainrings for the vastus lateralis superior muscles

Validation of some of these results using EMG could be carried out, to compare how the muscular predictions made by the musculoskeletal model compare with that of the cyclist when they are using the chainrings. Ultrasound could also possibly be used although this has been shown to detect muscle activity but not be able to discern level of activity (Hodges et al. 2003), so this could be used to detect activation periods but not size of activation. We can however compare how some of these results look to previously published data on muscle activations. Li & Caldwell (1998) published data on some of the muscles we have discussed in this chapter in the paper on muscle coordination in cycling. Some of their results can be seen in Figure 8-17; with these data being for the right leg. First we will compare our results for gluteus maximus and biceps femoris with those shown below. As the plots we have presented are for both legs it is worth noting that we will focus on the left half to make the comparison. Li & Caldwell show that activity of gluteus maximus and biceps femoris is very similar which backs up our findings of both muscles having the same normalised muscle force (Figure 8-1).

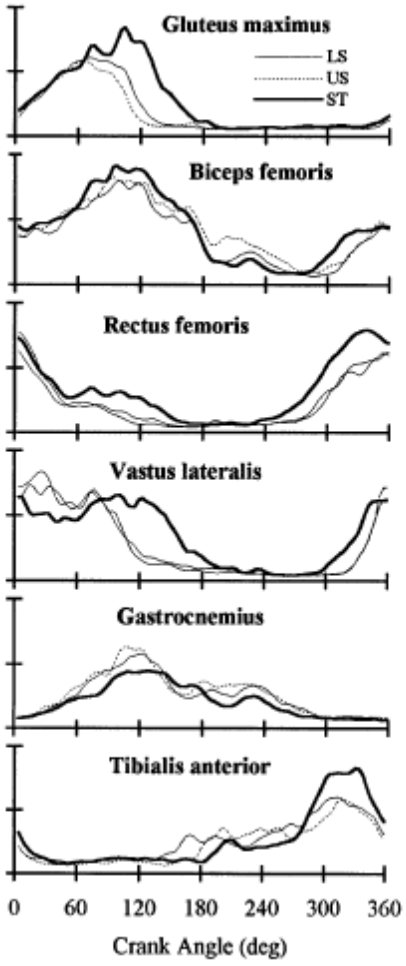

Figure 8-17; EMG data plots from Li & Caldwell (1998) for six right leg muscles starting at TDC. LS; level seated. US; uphill seated. ST; uphill standing.

Comparison between our rectus femoris plot (Figure 8-12) and the one shown in 8-17 however show a much different plot. In 8-12 the normalised muscle force has a similar plot to that of the gluteus maximus and biceps femoris however Li & Caldwell clearly show the activity being out of phase with those two muscles. The comparisons between vastus lateralis (Figure 8-16) are again much more like those presented in Figure 8-17 although the normalised muscle force plot for gastrocnemius (Figure 8-13) again does not quite match that as presented here. We have found a similar peak height whereas Li & Caldwell present a lower muscle activity. While it is not ideal that there are some discrepancies between the published data and those found by the AnyBody software the fact we are targeting the muscles with the highest output which do match up with the published data means the results from the optimisation should translate into real world effects if produced.

8.2 Summary

In this chapter we have presented a muscle specific analysis of the computational results which were obtained from the final designs described in Chapter 7. 14 muscles had the same normalised muscle force profile as the plot detailing the maximum of all muscles while three other muscles varied only in the last 40 degrees of the revolution. A concentration of these muscles was noted around the pelvis to femur area, while there were other muscles such as gluteus medius which had high normalised muscle forces but were not exerting force for the entire duration. Gluteus medius anterior showed no muscle force on the right leg. Gluteus minimus muscles show a much longer duration of force on the left leg than the right, with the right gluteus minimus anterior producing a very small peak in comparison to the left. The brevity of the gluteus muscle plots show a drop in muscle recruitment as the pedals approach the locations of top dead centre and bottom dead centre. Gastrocnemius medialis unlike the other muscles shows a higher normalised muscle force on the right leg than the left. A very large reduction in normalised muscle force is noted on the tibialis posterior lateralis with both the optimised chainrings while the circular provides the highest value at the same point. The vastus lateralis superior muscle shows an increase in normalised muscle force on the right leg for the optimised design, a trait that is not found on other muscle plots. Generally, large reductions have been seen on the left leg normalised muscle force, but this has in some cases resulted in an increase on the right leg normalised muscle force. The Fourier chainring while reducing the left leg peak by slightly more does result in a higher right leg activity. The elliptical chainring on the other hand reduces the right leg activity as well, in some muscles quite noticeable in comparison to the Fourier. It would be of interest to see which resulted in better physical performance. Finally we briefly discussed how these results matched up with published data on

muscle activation in cycling; this provides some validation of the AnyBody output and our optimisation results.

Having detailed the computational results from our final chainring designs we will now conclude this thesis with a summary of the work completed, some of the limitations of this study, and some areas of possible future work which may be carried out.

Chapter 9 Conclusion

This chapter will conclude this thesis, it will summarise the work that has been completed and then proceed to discuss limitations and possible avenues for future work that could be undertaken.

9.1 Summary of work completed

A parameter investigation has shown cadence and chainring shape to be important variables in the resultant normalised muscle forces of the rider. While cadence depends on what the rider is cycling on, what speed etc., the chainring shape can be modified to give an extra improvement of lower normalised muscle force not possible using a circular chainring. Torque profiles are shown to be asymmetrical and highly cadence dependent with this leading to non-symmetrical chainring designs.

Confirmation of the assumption made by the author that a circular chainring has a constant angular velocity has been displayed. Angular velocity data attained using motion capture and a production non-circular chainring has confirmed the theory that a non-circular chainring will have a non-constant angular velocity. These data backup the use of describing the chainring shape by using local cadences in this work.

Experimental motion capture and torque data has been successfully integrated with both the surrogate and musculoskeletal models to allow optimisation to be carried out. Various reductions in normalised muscle force have been obtained depending on the complexity of the musculoskeletal model being used. The model with the highest level of fidelity has shown a 15% reduction in normalised muscle force for two differently designed chainrings. This reduction was identified on the left leg which initially had a higher normalised muscle force than the right leg according to the musculoskeletal modelling software. Even if these reductions are found to be smaller in the physical world it is worth noting that at a competitive level every little bit can count, and make the difference between first and second. Therefore any reduction should be viewed as a success as it should slow the production of lactate and delay the onset of fatigue.

Consideration needs to be given to the chainring shapes produced though as some presented here would not be physically possible due to the derailleur not working for them etc. Shapes should not contain small concave sections as the chain will not actually follow these and just skip them thereby sticking to the same local radius as before and after. It would also be wise to consider the physical limitation of the human rider. Acclimatisation is sometimes required for

an improvement to be fully gained so testing may need to consider this. Large specific normalised muscle forces will need to be avoided as these may increase the risk of injury.

9.2 Limitations

We will now provide a brief discussion into the limitations of this study and the potential effects these limitations may have had or may have.

The first of these limitations is this study focussed on only one subject. While it gives an indication as to the feasibility of the procedures undertaken here to design a tailored chainring for a specific rider further studies with more riders would be necessary to attain an understanding of the applicability across more participants.

The next limitation is with the focussing on the muscles in the legs; while the legs were looked at in quite high detail the effects on other muscles such as the lower core muscles were not taken into account and may have been impacted by the change in chainring shape. A full body model with the same level of muscle fidelity would take longer to run test instances but would provide valuable information as to whether it was necessary to include more than just the legs.

As the chainring was designed for 250W power output and a cadence of 90rpm it is unknown how using this chainring in other conditions would affect the cycling performance. The reduction in normalised muscle force at the target conditions may result in an increase at lower or higher cadences. This may mean that for instance the chainring is ideal for level time trialling but of less use in other competitive conditions.

As the AnyBody modelling software is a commercial piece of software that is constantly being worked on and upgraded it was necessary to “freeze” the testing environment so that newer results could still be compared with older ones without the concern of changes to the software algorithms affecting the results. Due to this it was not possible to automate the optimisation process, while the surrogate modelling and optimisation was done automatically it was still necessary to manually run the AnyBody model for every instance of data collection that was required. This was quite a time consuming process and full automation would allow for more samples and for more complex design spaces to be investigated.

During discussion of the biomechanical model development we highlighted that the computational models did not take in to account any losses associated with the whole chaindrive. Losses such as frictional losses between chainring and chain, or the effect the derailleur would have on the results of using a non-circular chainring are not included in the models.

9.3 Possible future work

Robust design is used widely in industry allowing for engineering products to be produced which are both effective and robust with their operation. As it would be difficult to ensure that a cyclist was pedalling at the right cadence and with the right technique for which the chainring was designed it would be wise to design the shape so that it was effective for an acceptable range of variation. While this may result in a decrease in the peak reduction it will also lessen the sensitivity to cadence etc. which should make the product more useful to riders.

Production of optimised chainring designs would enable an experimental assessment of the real world effects of the new designs. This could lead to being able to predict the actual performance improvement achieved by using a chainring based on the computational results. It would also experimentally validate the models and optimisation process.

While we have utilised torque data from the Q-Ring in five different orientations, thereby giving us torque data for six different chainring shapes (five Q-Ring orientations, plus circular chainring), it would be good to gather torque data for more non-circular chainrings. If these data included torque for non-regular non-circular chainrings it would help on two fronts. Firstly it would allow for a better assessment of how the chainring shape impacts the torque profile, and secondly these data would help to improve the torque model.

In this study we have used torque data and motion capture data along with data on the riders' height to tailor the musculoskeletal model and surrogate model for optimisation of the chainring shape. It would be good to carry out an assessment of the importance of each of the different sets of data collected. This could potentially indicate if all the data collection carried out is necessary, or how reliant the final outcome is on the amount of each different data type.

Following on from the acclimatisation period recommended by Rotor on their Q-Ring and the acclimatisation period used in some of the studies covered in the literature review it would be interesting to see how the rider responded to the optimised design over time. Regular monitoring of the rider over time would allow for assessing if any performance improvement stayed/decreased/or increased. This would give an indication if the riders' body adapted to the changed normalised muscle forces.

As this study only utilised one participant it would be of interest to carry out the study with more participants. This would allow for assessment of if the procedure can optimise for any given cyclist or has limitations. It would also allow for a better assessment of how different participants' data affected the optimisation process. With multiple participants it would also be

possible to see if there were similar torque profile or cycling motion characteristics which could be utilised to build a larger dataset for the optimisation to source data from. Alternatively this could lead to less data needing to be collected for an optimisation to be carried out for a rider.

The optimisations carried out here minimised the peak maximum muscle activity (normalised muscle force) for the whole revolution. As was seen on the Fourier chainring this resulted in the reduction occurring on one leg while the other remained almost the same, although the peak that was reduced was significantly higher to begin with. Carrying out an assessment to see if it was possible to optimise for each leg and therefore achieve a reduction in the peaks for both legs could be an interesting way to take this research forward.

By selecting certain muscles it would be possible to check if the muscle activities being predicted by the musculoskeletal model were accurate for how the riders' body responded to the designed chainring shape. This would potentially allow for tweaks to the musculoskeletal model or validation of its predictions.

It would be possible to get the optimisation to target specific muscles and raise/lower their normalised muscle force depending on requirements. This could be of use in injury recovery, moving effort away from muscles in the early stages of injury recovery, and then being able to target a specific muscle to work it harder to regain lost strength in that muscle.

Appendix A

Proposed experimental protocol for testing designed chainrings.

Materials

-Bicycle: Specialized S-Works Roubaix

-Ergometer: Tacx Cycleforce i-magic

-Instrumented crank arms: Part of SRM Science power meter system: Octalink Shimano

-Breath analyser: portable Vo2000 breath analyser

-Laptops: 2 laptops, one to run ergometer software, the other to show crank arm and breath analysis results.

-EMG: Aurion 'Zerowire' 16 channel telemetered system

-Motion capture: 12 camera MX T-series system

-Blood lactate analyser: Lactate Pro system

-Blood lactate consumables: measurement strips and lancets

-Water bottle: Suitable for rider to use while cycling.

-Chainrings: 3 custom made chainrings for testing, plus one "standard" circular chainring

-Tools: Allen keys for changing chainrings

-Paper towels: For wiping oil from hands after handling chainrings

Procedure

The participant will arrive and be asked for consent and then will be asked to change into suitable cycling clothing in a private changing area. They will then mount the bicycle and adjust it so that it is comfortable. They will then be asked to perform a 15 minute warm up. Once this is complete they will dismount the bicycle and the researcher will mount the chainring that is being tested at that instance. The researcher will then attach the EMG electrodes and reflective markers (for motion capture system) to the participants' legs. The participant will then be asked to remount the bicycle. A card shield will prevent the participant viewing the chainring until they have mounted the bicycle. They will then be asked to cycle at 90rpm with a 250W power output for two hours (or until they cannot maintain that level, whichever is shorter), there will be visual information as to current rpm and power output so the rider can keep as close to these target values as possible. During this period perceived exertion values will be recorded every ten minutes. They will also be asked to wear a breath analysis mask for 30 seconds every 10 minutes. Blood lactate will be measured every 15 minutes. The participant will then be asked to dismount the bicycle. The EMG electrodes and reflective markers will then be removed and the standard chainring will be remounted by the investigator. They will then be asked to mount the bicycle again and do 4 maximum effort sprints for 20 seconds with 40 seconds recovery in between. A final blood lactate measurement will then be taken. They will then be allowed to warm down for as long as necessary (estimated at 15 minutes). Each test session should be no more than four hours in length, and there will be four sessions; one pilot session to familiarise the participant with the protocol, one for the circular chainring, and one for each of the optimised

chainrings. Each test will be carried out at the same time of day and on the same day of the week, with a week's gap between.

Statistical analysis

Breath composition and blood lactate values will be assessed across the two hour period for each of the three chainrings. Perceived exertion values and their inter and intra variability will also be assessed. Peak and average power output from maximal sprints will be compared as will the variability of the power output from the different maximal sprints. The EMG data will be used to compare to the musculoskeletal model muscle activation predictions. Motion capture data will be compared with predicted movement.

Ethical issues

The activity will result in the participant becoming more dehydrated then they were at the start of each test. Water will be available throughout each test and after each test so the rider can rehydrate themselves whenever they need to. There is also the potential that the rider will push themselves too hard in the maximal testing to "get the right results". During the maximal testing the power, cadence and torque readings will be hidden from the participant and the participant will not be told the results from each test until the completion of all tests to ensure there is no "trying to beat the last result" occurring. This testing would be challenging to a non-competitive cyclist but by using a cyclist who regularly competes they will be used to the physical demands of a test such as this. Very small amounts of blood will need to be taken for blood lactate analysis, this will involve lancing the ear each time. The participants' body should naturally heal these quickly.

Appendix B

Available online at www.sciencedirect.com

ScienceDirect

Procedia Engineering 00 (2009) 000–000

Procedia Engineering

www.elsevier.com/locate/procedia

8th Conference of the International Sports Engineering Association (ISEA)

Efficient human force transmission tailored for the individual cyclist

Purdue A.I.[a]1*, Forrester A.I.J.[a], Taylor M.[a], Stokes M.J.[a], Hansen E.A.[b], Rasmussen J.[b]

[a]*University of Southampton, University Road, Southampton, SO171BJ, United Kingdom*
[b]*Aalborg University, Pontoppidanstræde 101, DK – 9220Aalborg East, Denmark*

Received 31 January 2010; revised 7 March 2010; accepted 21 March 2010

Abstract

The paper investigates the possibility of improving the efficiency of force transmission for the individual cyclist. Musculoskeletal modelling using commercial software (AnyBody) is utilised to assess variations in the bicycle configuration. Rider-specific data were collected to enable an assessment of seat position, cadence, crank arm length, and chainring shape. Optimisation of these parameters is carried out to minimise normalised muscular force, with the aim of delaying the onset of fatigue. Reductions of 13% and 18% were found in peak values. Chainring shapes were noticeably altered with significant differences between the two results due to differing musculoskeletal model fidelity.

Keywords: Cycling; Optimization; Rider specific; Chainring

1. Introduction

A cyclist's bicycle is set up in the configuration which they find the most comfortable, with it being generally assumed that this yields the most efficient position. The actual physical effects of changing this setup will be considered here in terms of the effect of variation in performance. Multivariable optimization of cycling biomechanics has been done before[1] with similar variables being explored, with the exception of chainring shape, however the present study utilized the more advanced mechanism of specific muscle force resolution provided by a detailed musculoskeletal model.

A bicycle drive train is extremely efficient (~ 98%)[2] although the rider interface is subject to noticeable losses , partly due to the "one size fits all" nature of the circular chainring. Commercial non-circular chainrings have been produced before with two notable ones being the Biopace chainring from Shimano and the Q-Ring from Rotor. These were both designed with differing design mentalities with the Biopace designed to lower the rate of change of direction of the legs at the upper and lower limits of the pedal stroke. This is achieved by having the chainring at its largest radius at the two "dead spots" (the points at which the torque is lowest). The Q-Ring on the other hand, was designed so that the rider could control when the maximum equivalent chainring size was

* Corresponding author. Tel.: +442380-594-643; fax: +442380-594-813.
E-mail address: alex.purdue@soton.ac.uk.

doi: 10.1016/j.proeng.2010.04.029

placed in the cycle. This means it is more flexible, and can be mounted in the same orientation as the Biopace if the rider so wishes, though Rotor suggest it should be mounted with the smallest radius at the dead spots. The Q-Ring is more noticeably non-circular than the Biopace, which in passing appears to be circular. The failure of wide spread uptake of these chainrings suggest that while they work for some people, they do not work for others so the ability to design a rider-specific chainring would assist those still using the circular rings due to ineffectiveness of commercial products. Here a computational model will be used to assess the effects of varying the local radius to improve the total efficiency for a specific athlete. This study investigates the effect of configuration on efficiency of force transmission from cyclist to road and numerically optimizes the set up using a detailed musculoskeletal model processed in the AnyBody Modeling System[3].

Chainring shape analysis and modification have been carried out by previous authors[4], though the analysis and modification were purely theoretical, and analysis undertaken on non-circular designs has been based on non-rider specific chainrings[5].

2. Method

One competitive male cyclist took part in this study, which took the form of an observational case study during data collection. The participant volunteered and gave written consent for involvement in the study once ethical approval had been acquired from the local committee (School of Health Sciences Ethics Committee, University of Southampton).

To obtain the torque characteristics of the cyclist several sets of torque profiles were collected for varying cadences and power levels. Design of experiments were undertaken for both physical and computer experiments. These provide sampling positions in the design space for data to be collected from. Data collection took place, based on these sampling points, on an electromagnetically braked bicycle ergometer (Tacx Cycleforce i-magic, Wassenaar, The Netherlands). The bicycle (a Specialized S-Works Roubaix with Shimano Dura-Ace components, Morgan Hill, California, United States of America) is mounted with instrumented crank arms (SRM track power meter system, Germany) which enable torque data to be collected.

From the physical data a surrogate torque model was produced. A surrogate (or meta) model[6] is a low cost replacement of an original function. They enable educated guesses as to the appearance of an engineering function based upon a few affordable measuring points. Meta models can give results many orders of magnitude faster than the original source while still being useful at predicting away from known points. A surrogate model of the torque was produced to enable realistic prediction of torque profiles produced for the local cadences which represent the variations in the local chainring radius.

Musculoskeletal modeling, using the commercial software AnyBody Modeling System v4.1 (AnyBody Technology, Aalborg, Denmark), was used to predict muscle activity during the movement. The software utilises inverse dynamics along with a muscle recruitment algorithm[7] to predict which muscles would be used and how much they would be made to work. The recruitment algorithm is based on the assumption that the body recruits muscles efficiently; as such the software effectively carries out the motion using the least muscular effort. The output selected as the target for minimization, during the optimization, was, what the software refers to as, the maximum muscle activity; this is the normalised muscle force (the actual force divided by the total force possible). Two models were used for this study; a simplistic model and a more complex model, both containing Hill-type muscles[8]. The simplistic model contains eight muscles per leg with motion being prescribed by attachments at the saddle and pedals, and constraints implemented on the knee and heel motions. This was used for both a parameter study and for initial optimization of the chainring shape. The more complex model utilizes the same motion prescription but has approximately 42 muscles per leg; this was used solely for the chainring shape optimization.

A parameter study was carried out by altering the stated variables with the exception of chainring shape and recording the highest value for the maximum muscle activity for the whole movement. A full factorial sampling plan was used for this part. This type of sampling plan covers the design space in a uniform distribution of data collection points; it gives a good overview of the design space though can be computationally expensive due to the number of points sampled. Actual torque data was used to calibrate the model. The results from this study allow for identification of optimal values (or locations) and analysis of how the objective function varied as variables were altered. A screening plan was also undertaken using the same setup to assess the relative importance of the variables being changed.

To enable the chainring to be optimized, its shape is represented by variations in the local cadence; a slower local cadence representing an increase in local radius and a faster local cadence representing a decrease. This shape is described by 10 Fourier coefficients which prescribe the local cadence profile with zero values representing 90rpm. Values which are above or below zero represent an increase or decrease in local cadence respectively. Using the results from an initial design of computer experiments a surrogate model is then created for the muscle activity. By modifying models provided in the supplied repository and implementing a system for

interfacing between these models and the optimization code it was possible to modify the models automatically based on the surrogate muscle activity model. A mapping of how the muscle activity varies within the design space enables possible areas to be identified which would produce an improved result. The model is then run with the configuration identified by this process and the results from these runs are then fed back into the surrogate model to improve the prediction (see figure 1). A convergence criterion is set so that once the predicted improvement for a non-measured configuration compared to the best measured configuration falls below a certain value the optimization is stopped.

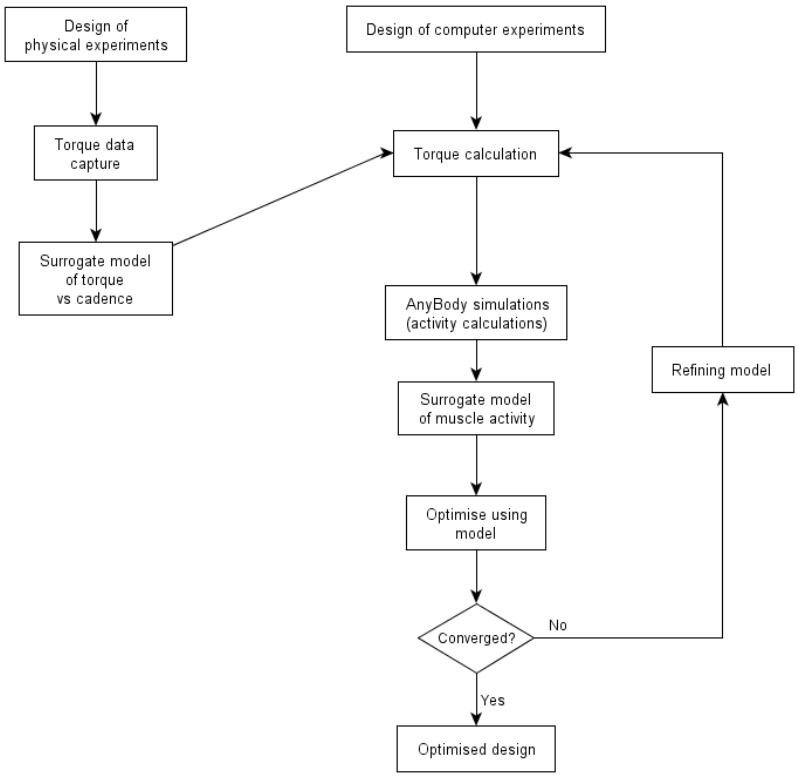

Fig. 1. Chainring optimization work-flow

3. Results

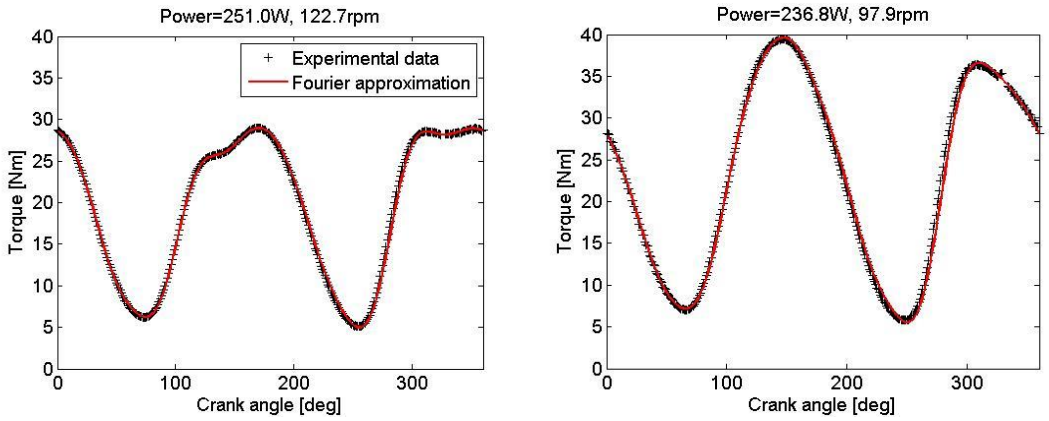

Fig. 2. (a)torque profile at ~120rpm; (b)torque profile at ~100rpm

Fig. 3. Sampling plot, showing effects of variation in setup, produced using the basic model

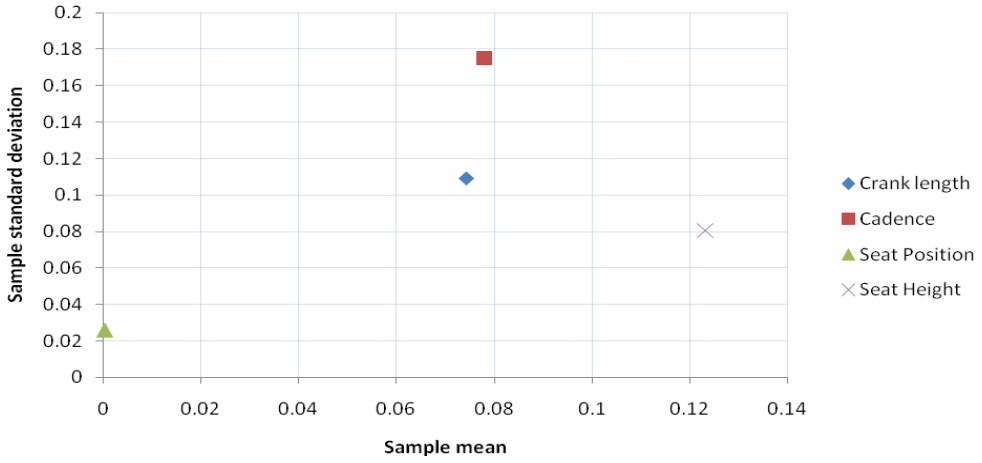

Figure 2 shows the sample torque profile data collected from the instrumented crank arms. The two plots are at similar power outputs but different cadences. These plots also show the Fourier approximations used to train the surrogate model, which is used to predict torque during the chainring optimization. Figure 3 shows a sampling plot for the basic model results. This plot enables an assessment of the effects of changing a variable on the objective function (in this case the maximum muscle activity). Variables which are close to the origin on this plot do not have a large impact when changed, with the variables further away having a greater effect. On this plot, seat lateral position is the only variable close to the origin with seat height and cadence being the furthest away. Figure 4 shows the chainring shapes found by the optimization algorithm for both models. These are overlaid with a circular shape so that the differences between the circular and optimized shapes can be more easily assessed. The right crank arm is at the 3 o'clock position (90° right of vertical). In both torque profiles and muscle activity the right crank arm also starts out at this position and rotates clockwise returning to its original position at the right hand side of these figures.

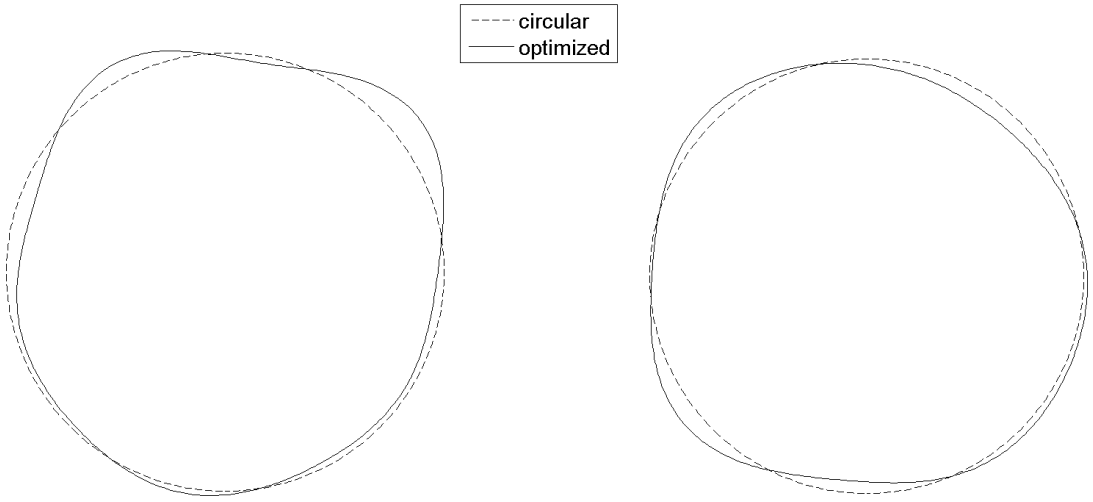

Fig. 4. (a) circular and optimized chainring shape from basic model; (b) circular and optimized chainring shape from complex model

Figure 5 shows the estimated muscle activities for both circular and optimized chainrings in both models. The magnitude of the maximum muscle activity is decreased by approximately 18% on the basic model and 13% on the complex model. Overall magnitude is much lower in the basic model. In both cases the maximum peak decreases but this is paired with an increase in a minor peak alongside this main peak.

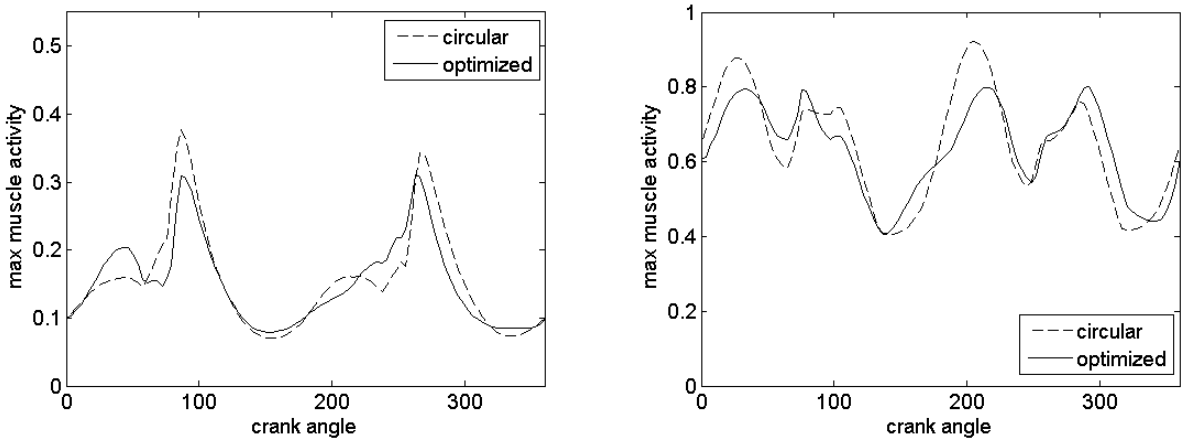

Fig. 5. (a) circular and optimized muscle activities using basic model; (b) circular and optimized muscle activities using complex model

4. Discussion and Future work

The torque data reveals that the profiles are asymmetrical and appear to have a high cadence dependency. For cadences close to the optimum cadence the torque profile is “purer”, in the sense that it is smoother and sinusoidal. As the cadence is moved away from this optimum the “purity” decreases and the profile changes with reduced peak torque, and each peak torque is non-distinct.

The results of the parameter study show that seat longitudinal position is not an important variable and changing it has a very small impact on muscle activity. The remaining three variables have a significant impact. Results gave optimum values of 90 rpm for cadence and 0.17m for crank arm length, which agree with general cycling knowledge.

The two chainring shapes produced by the two different models are clearly different which matches up with the different muscle activity plots produced. Consideration must be given, however, to the more complex nature of the muscles in the second model which detailed analysis would provide answers as to whether both are targeting the same primary muscles groups or not. This difference will also explain the large differences in the magnitudes of maximum muscle activity; this could be due to some of the smaller muscle groups working at closer to their capacity most of the time, while the larger groups do not reach close to theirs as the exercise is not necessitating full strength from these muscles. Noticeably in the more complex model the iliopsoas muscle is identified as a

one of the key muscles, as this is absent in the simplistic model this could explain the differences in shapes produced. The magnitude of the reductions achieved is very large and once further calibration with physical experiments is undertaken it is expected this value will fall.

Recreational cyclists perform negative work[9] when cycling; the leg not pushing down is being pushed back up by the other leg. It is unclear in these models as to whether negative work is being done and if so the amount of impact this is having. This will need to be calibrated against measurements taken from the rider to assess the extent of negative work, if any, taking place. This should mean that when actual testing is undertaken muscles will work differently unless the rider has learned to lift the non-driving leg.

In future work, more accurate movement prescription will be given to the model as another calibration step. Chainrings will be produced to enable comparison between theoretical and experimental results.

Acknowledgements

Martin Warner for assistance with data collection. Peter Worsley for assistance with troubleshooting the code.

References

[1] Hull M.L., Gonzalez H. Multivariable optimisation of cycling biomechanics, *J Biomechanics* 1989;**22**:1151-1161

[2]Spicer J.B., Richardson C.J.K., Ehrlich M.J., Bernstein J.R. Fukuda M., Terada M. Effects of frictional loss on bicycle chain drive efficiency, *J Mechanical Design* 2001;**123**:598-605

[3] Damsgaard M., Rasmussen J., Christensen S.T., Surma E., de Zee M. Analysis of Musculoskeletal Systems in the AnyBody Modeling System, *Simulation Modelling Practice and Theory* 2006:**14**; 1100-1111

[4] Rankin J.W., Neptune R.R. A theoretical analysis of an optimal chainring shape to maximise crank power during isokinetic pedalling, *J Biomechanics* 2008:**41**;1494-1502

[5] Hue O., Chamari K., Damiani M., Blonc S., Hertogh C. The use of an eccentric chainring during an outdoor 1km all-out cycling test, *J Science and Medicine in Sport* 2007:**10**;180-186

[6] Forrester A., Sóbester A., Keane A. Engineering Design via Surrogate Modelling, 2008 ISBN 978-0-470-06068-1

[7] Rasmussen J., Damsgaard M., Voigt M. Muscle recruitment by the min/max criterion – a comparative numerical study, *J Biomechanics* 2001:**34**; 409-415

[8]Winters J.M., Woo S.L.-Y. Multiple muscle systems, 2008 ISBN 0-387-9730-9

[9] Neptune R.R., Herzog W. The association between negative muscle work and pedalling rate, *J Biomechanics* 1999:**32**; 1021-1026

Glossary

AT; Anaerobic threshold.

Angular velocity; (in this context) a measure of the rate of rotation of a chainring.

BDC; bottom dead centre; when the crank arm is at its lowest point during the revolution.

Cadence; the number of revolutions per minute a cyclist is making the chainring complete.

Computationally expensive; a process which requires a large amount of time/processing to complete.

History dependence; the effect of a muscles history on its performance.

Isometric force; force created without contraction of the muscle.

Lactate; a by-product of anaerobic respiration.

Local cadence; the instantaneous cadence at a given point during the chainring rotation.

MAP; Maximal aerobic power.

Maximum muscle activity; the main measurement metric used by this study from the AnyBody software. This is actually the normalised muscle force that has been calculated.

Model 1; the “2D” bicycle biomechanical model provided with the AnyBody software.

Model 2: the “3D” bicycle biomechanical model provided with the AnyBody software.

Model 3: the modified Gait model driven by motion capture data used in the later studies.

Muscle activity; when a muscle is creating force by tensioning or contracting, caused by electrical impulses.

Negative work; (in this context) the effect of the non-driving foot resting on the pedal reducing the torque being generated by the driving foot.

Normalised muscle force; the amount of force a muscle is generating divided by the maximum amount of force a muscle can generate.

RPM; revolutions per minute.

TDC; top dead centre; when the crank arm is at the peak of its revolution.

References

ACSM, 2005. *ACSM's Advanced Exercise Physiology*, Lippincott Williams and Wilkins.

Abbott, B.Y.B.C. & Louvain, X.M.A., 1952. The force exerted by active striated muscle during and after change of length. *Journal of Physiology*, 117, pp.77–86.

Amann, M. et al., 2004. An evaluation of the predictive variability and reliability of ventilatory threshold. *Medicine & Science in Sports & Exercise*, 36, pp.1716–1722.

Anon, 1996. *The Oxford Compact English Dictionary*, Oxford University Press.

Aunola, S. & Rusko, H., 1992. Does anaerobic threshold correlate with maximal lactate steady state? *Journal of Sports Sciences*, 10, pp.309–323.

Berto, F., Shepherd, R. & Henry, R., 2005. *The dancing chain: history and development of the Derailleur bicycle*, Van der Plas Publications.

Bertucci, W. et al., 2005. Effects on the crank torque profile when changing pedalling cadence in level ground and uphill road cycling. *Journal of Biomechanics*, 38(5), pp.1003–10.

Bertucci, W., Grappe, F. & Groslambert, A., 2007. Laboratory versus outdoor cycling conditions: differences in pedaling biomechanics. *Journal of Applied Biomechanics*, 23(2), pp.87–92.

Billat, V.L. et al., 2003. The concept of maximal lactate steady state: a bridge between biochemistry, physiology and sport science. *Sports medicine (Auckland, N.Z.)*, 33(6), pp.407–26.

Borg, G., 1998. *Borg's perceived exertion and pain scales*,

Box, George E P, 1957. Evolutionary operation: a method for increasing industrial productivity. *Journal of the Royal Statistical Society*, 6(2), pp.81–101.

Box, George E.P. & Draper, N.R., 1987. *Empirical model-building and response surfaces*,

Böhm, H., Siebert, S. & Walsh, M., 2008. Effects of short-term training using SmartCranks on cycle work distribution and power output during cycling. *European Journal of Applied Physiology*, 103(2), pp.225–32.

Caldwell, G.E. et al., 1998. Pedal and crank kinetics in uphill cycling. *Journal of Applied Biomechanics*, 14, pp.245–259.

Carey, D.G. et al., 2005. Respiratory rate is a valid and reliable marker for the anaerobic threshold: implications for measuring change in fitness. *Journal of Sports Science and Medicine*, 4, pp.482–488.

Cordova Martinez, D.A. et al., 2004. Preliminary report on Q-Rings. , pp.1–14.

Damsgaard, Michael et al., 2006. Analysis of musculoskeletal systems in the AnyBody Modeling System. *Simulation Modelling Practice and Theory*, 14(8), pp.1100–1111.

Ettema, G., Lorås, H. & Leirdal, S., 2009. The effects of cycling cadence on the phases of joint power, crank power, force and force effectiveness. *Journal of Electromyography and Kinesiology*, 19(2), pp.94–101.

Forrester, A., Sóbester, A. & Keane, A., 2008. *Engineering design via surrogate modelling*, John Wiley & Sons.

Fregly, Benjamin J & Zajac, Felix E, 1996. A state-space analysis of mechanical energy generation, absorption, and transfer during pedaling. *Journal of Biomechanics*, 29(1), pp.81–90.

Goffe, W.L., Ferrier, G.D. & Rogers, J., 1994. Global optimization of statistical functions with simulated annealing. *Journal of Econometrics*, 60(1-2), pp.65–99.

Gregor, R.J. & Abelew, T.A., 1994. Tendon force measurements and movement control: a review. *Medicine & Science in Sports & Exercise*, 26(11), pp.1359–1372.

Hansen, Ernst A & Smith, G., 2009. Factors affecting cadence choice during submaximal cycling and cadence influence on performance. *International Journal of Sports Physiology and Performance*, 4, pp.3–17.

Hansen, Ernst Albin et al., 2002. Crank inertial load affects freely chosen pedal rate during cycling. *Journal of Biomechanics*, 35(2), pp.277–85.

Hansen, Ernst Albin et al., 2009. Effect of chain wheel shape on crank torque, freely chosen pedal rate, and physiological responses during submaximal cycling. *Journal of Physiological Anthropology*, 28(6), pp.261–267.

Hastie, T., Tibshirani, R. & Friedman, J., 2009. *The elements of statistical learning* Second edi., Springer.

Hatze, H., 1977. A myocybernetic control model of skeletal muscle. *Biological Cybernetics*, 119, pp.103–119.

Herzog, Walter, 2004. History dependence of skeletal muscle force production: implications for movement control. *Human Movement Science*, 23(5), pp.591–604.

Hill, A.V., 1970. *First and last experiments in muscle mechanics*, Cambridge University Press.

Hodges, P.. et al., 2003. Measurement of muscle contraction with ultrasound imaging. *Muscle & Nerve*, 27(6), pp.682–692.

Hue, O et al., 2001. Enhancing cycling performance using an eccentric chainring. *Medicine & Science in Sports and Exercise*, 33(6), pp.1006–10.

Hue, Olivier et al., 2007. The use of an eccentric chainring during an outdoor 1 km all-out cycling test. *Journal of Science and Medicine in Sport*, 10(3), pp.180–6.

Hull, M L & Gonzalez, H., 1989. Multivariable optimization of cycling biomechanics. *Journal of Biomechanics*, 22(11-12), pp.1151–1161.

Huxley, A.F., 1957. Muscle structure and theories of contraction. *Progress in Biophysics and Biophysical Chemistry*, 7, pp.255–318.

Kadaba, M.P., Ramakrishnan, H.K. & Wootten, M.E., 1990. Measurement of lower extremity kinematics during level walking. *Journal of Orthopaedic Research*, 8(3), pp.383–92.

Kautz, S.A. & Hull, M L, 1995. Dynamic optimization analysis for equipment setup problems in endurance cycling. *Journal of Biomechanics*, 28(11), pp.1391–1401.

Klein Horsman, M.D. et al., 2007. Morphological muscle and joint parameters for musculoskeletal modelling of the lower extremity. *Clinical Biomechanics*, 22(2), pp.239–47.

Kohler, G. & Boutellier, U., 2005. The generalized force-velocity relationship explains why the preferred pedaling rate of cyclists exceeds the most efficient one. *European Journal of Applied Physiology*, 94(1-2), pp.188–95.

Komi, P.V., 1990. Relevance of in vivo force measurements to human biomechanics. *Journal of Biomechanics*, 23, pp.23–25,27–34.

Krige, D.G., 1951. A statistical approach to some basic mine valuation problems on the witwatersrand. *Journal of the Chemical, Metallurgical and Mining Engineering Society of South Africa*, 52, pp.119–139.

Li, L.I. & Caldwell, G.E., 1998. Muscle coordination in cycling : effect of surface incline and posture. *Journal of Applied Physiology*, 85(3), pp.927–934.

Morris, M.D. & Mitchell, T.J., 1995. Exploratory designs for computational experiments. *Journal of Statistical Planning and Inference*, 43, pp.381–402.

Nakashima, M. et al., 2012. Optimizing Simulation of the Arm Stroke in Crawl Swimming Considering Muscle Strength Characteristics of Athlete Swimmers. *Journal of Biomechanical Science and Engineering*, 7(2), pp.102–117.

Neptune, R R & van den Bogert, A.J., 1998. Standard mechanical energy analyses do not correlate with muscle work in cycling. *Journal of Biomechanics*, 31(3), pp.239–45.

Neptune, R R & Herzog, W, 1999. The association between negative muscle work and pedaling rate. *Journal of Biomechanics*, 32(10), pp.1021–6.

Neptune, R R & Hull, M L, 1995. Accuracy assessment of methods for determining hip movement in seated cycling. *Journal of Biomechanics*, 28(4), pp.423–437.

Neptune, Richard R & Hull, Maury L, 1996. Methods for determining hip movement in seated cycling and their effect on kinematics and kinetics. *Journal of Applied Biomechanics*, 12, pp.493–507.

O'Hara, C.R. et al., 2012. Effects of chainring type (circular vs . Rotor Q-Ring) on 1km time trial performance over six weeks in competitive cyclists and triathletes. *International Journal of Sports Science and Engineering*, 06(01), pp.25–40.

Pandy, M.G., 2001. Computer modeling and simulation of human movement. *Annual Review of Biomedical Engineering*, 3, pp.245–273.

Raasch, C.C. et al., 1997. Muscle coordination of maximum-speed pedaling. *Journal of Biomechanics*, 30(6), pp.595–602.

Rankin, J.W. & Neptune, Richard R, 2008. A theoretical analysis of an optimal chainring shape to maximize crank power during isokinetic pedaling. *Journal of biomechanics*, 41(7), pp.1494–502.

Rasmussen, J, Damsgaard, M & Christensen, S T, 2001. Simulation of tendon energy storage in pedaling. In *9th Mediterranean Conference on Medical and Biological Engineering and Computing*. pp. 1–4.

Rasmussen, J, Damsgaard, M & Voigt, M., 2001. Muscle recruitment by the min/max criterion - a comparative numerical study. *Journal of Biomechanics*, 34(3), pp.409–15.

Rasmussen, J. et al., 2004. Design optimization of a pedaling mechanism for paraplegics. *Structural and Multidisciplinary Optimization*, 26(1-2), pp.132–138.

Rasmussen, J. et al., 2002. Design optimization with respect to ergonomic properties. *Structural and Multidisciplinary Optimization*, 24(2), pp.89–97.

Rasmussen, John et al., 2005. Ergonomic optimization of a bicycle crank based on musculoskeletal modeling. In *2005 International Symposium on Computer Simulation in Biomechanics*. pp. 3–4.

Ratel, S. et al., 2004. Physiological responses during cycling with noncircular "Harmonic" and circular chainrings. *European Journal of Applied Physiology*, 91, pp.100–4.

Rejeski, W.J., 1981. The perception of exertion; a social psychophysiological integration. *Journal of Sport Psychology*, 3(4), pp.305–320.

Sacks, J. et al., 1989. Design and analysis of computer experiments. *Statistical Science*, 4(4), pp.409–423.

Sanderson, D.J. et al., 2006. Gastrocnemius and soleus muscle length, velocity, and EMG responses to changes in pedalling cadence. *Journal of Electromyography and Kinesiology*, 16(6), pp.642–9.

Scheuer, J. & Tipton, C.M., 1977. Cardiov ascular adaptations to physical training. *Annual Review of Physiology*, 39, pp.221–251.

Solberg, G. et al., 2005. Respiratory gas exchange indices for estimating the anaerobic threshold. *Journal of Sports Science and Medicine*, 4, pp.29–36.

Spicer, J.B. et al., 2001. Effects of frictional loss on bicycle chain drive efficiency. *Journal of Mechanical Design*, 123(4), pp.598–605.

UCI, 2012. UCI Rules. Available at: http://www.uci.ch/templates/UCI/UCI2/layout.asp?MenuId=MTkzNg&LangId=1 [Accessed July 15, 2012].

Umberger, B.R. & Martin, Philip E, 2001. Testing the planar assumption during ergometer cycling. *Journal of Applied Biomechanics*, 17, pp.55–62.

Yamamoto, Y. et al., 1991. The ventilatory threshold gives maximal lactate steady state. *European Journal of Applied Physiology*, 63, pp.55–59.

Zajac, F.E., 1989. Muscle and tendon: properties, models, scaling, and application to biomechanics and motor control. *Critical Reviews in Biomedical Engineering*, 17, pp.359–411.

Zamparo, P., Minetti, A. & di Prampero, P., 2002. Mechanical efficiency of cycling with a new developed pedal-crank. *Journal of Biomechanics*, 35(10), pp.1387–98.

Álvarez, G. & Vinyolas, J., 1996. A new bicycle pedal design for on-road measurements of cycling forces. *Journal of Applied Biomechanics*, 12(1), pp.130–142.